

---

Theses and Dissertations

---

Fall 2017

## Characterizing occupational instabilities induced by a four-DOF all-terrain vehicle simulator

John Stuart Michael  
*University of Iowa*

Follow this and additional works at: <https://ir.uiowa.edu/etd>

 Part of the [Biomedical Engineering and Bioengineering Commons](#)

Copyright © 2017 John Stuart Michael

This thesis is available at Iowa Research Online: <https://ir.uiowa.edu/etd/5969>


---

### Recommended Citation

Michael, John Stuart. "Characterizing occupational instabilities induced by a four-DOF all-terrain vehicle simulator." MS (Master of Science) thesis, University of Iowa, 2017.  
<https://doi.org/10.17077/etd.xxb6nsg>

---

Follow this and additional works at: <https://ir.uiowa.edu/etd>

 Part of the [Biomedical Engineering and Bioengineering Commons](#)

Characterizing Occupational Instabilities Induced  
By a Four-DOF All-Terrain Vehicle Simulator

by

John Stuart Michael

A thesis submitted in partial fulfillment  
of the requirements for the Master of Science  
degree in Biomedical Engineering in the  
Graduate College of  
The University of Iowa

December 2017

Thesis Supervisor: Associate Professor Salam Rahmatalla

Copyright by

JOHN STUART MICHAEL

2017

All Rights Reserved

Graduate College  
The University of Iowa  
Iowa City, Iowa

CERTIFICATE OF APPROVAL

---

MASTER'S THESIS

---

This is to certify that the Master's thesis of

John Stuart Michael

has been approved by the Examining Committee for the thesis requirement for the  
Master of Science degree in Biomedical Engineering at the December 2017 graduation.

Thesis Committee:

\_\_\_\_\_  
Salam Rahmatalla, Thesis Supervisor

\_\_\_\_\_  
David Wilder

\_\_\_\_\_  
Nathan Fethke

\_\_\_\_\_  
Charles Jennissen

## ACKNOWLEDGEMENTS

I would like to thank my parents, Rodney and Cynthia Michael, and my grandparents, Kay and Stu Moiles, for their support and encouragement throughout my undergraduate and graduate studies and beyond. Thank you to my fiancé, Lauren Roskos, for her love and support, for being a sounding board through the excitement and stress, and for her endless encouragement and calming hand. I thank my advisor, Salam Rahmatalla, for his support, trust, and encouragement to explore the new and the challenging. I would like to thank Dr. Charles Jennissen and Dr. Gerene Denning for the assistance in experimentation and SAFER-SIM for their grant funding. I thank Kyle Losik for his friendship, his honesty, his unmatched ability as a Swiss Army Human, and his assistance during experimentation; Dr. Jonathan DeShaw for his guidance during my undergraduate years and his insights during my graduate research; Ulysses Grant for assisting in the experimentation; Tony for assistance programming the simulation table; and Jeff for developing the physical electronic components of the ATV controller.

## ABSTRACT

All-terrain vehicles (ATVs) are used widely throughout the United States both for recreational activities, such as hunting and riding, and in occupational settings, such as agriculture. In both such activities, ATVs can pose a risk of injury and death resulting from a number of factors, including operator error, operating in an altered state, and misuse. In a study by Milosavljevic et al. (2011), a survey of agricultural workers in New Zealand displayed that roughly 60% of workers who operated an ATV experienced a loss of control event. The same study showed that nearly 50% of those occurred while riding on a steep slope. Despite these high levels of incidence, little research has been performed to understand the mechanisms that lead to loss of control or instability.

In order to study loss of control and instability, a four-degree-of-freedom human-in-the-loop ATV simulator was developed and integrated with a shaking table in a real-time interaction. The simulator allowed for operators to approach conditions by their own means and to study mechanisms of each individual's approach to traversing a terrain. Inertial measurement units were used to measure the acceleration and angular velocity of each subject at the S1, T10, C7, and head. Inertial measurement units were also mounted on the ATV and table. The ATV was instrumented with 32 force sensors to sense reaction forces applied to the machine at the feet, hands, saddle, and seat. A five-camera motion capture system was used to capture posture throughout the time series of each terrain. Data were reviewed and analyzed at a finer resolution of roughly three seconds in select subjects at moments when there were peaks in both force and acceleration.

Analysis showed that a cycle of instability and stability existed as moments of sudden input accelerations caused reactions in the spine and head. Further, component accelerations were analyzed to identify the acceleration of the subject relative to the ATV. The cycle and the time from input acceleration to bracing on the ATV to regain stability serve as a baseline for the subject's reaction to input acceleration and the time between input acceleration and regaining stability.

## PUBLIC ABSTRACT

Every year, thousands of individuals suffer injuries or worse while riding all-terrain vehicles (ATVs) during both occupational and recreational activities. Additionally, a substantial number of Americans live in a home with access to an ATV. Surveys of agriculture workers in New Zealand observed that nearly half of those who use ATVs in their work experience a loss of control or instability. Despite all of this, little research has been performed to study the cause of loss of control and instability in ATV operators. To address this gap, a human-controlled ATV simulator capable of moving in the front-to-back and up-and-down directions, as well as rotating up and down and side to side, was developed. Further, the simulator was instrumented to measure forces exerted on the ATV and the accelerations of the operator's body. Through experimentation, a cycle of instability was identified comprising a sudden input acceleration and subsequent stabilization by bracing the ATV. The results and identification of this cycle and its timing from input event to stabilizing event serves as a baseline for future studies into operators that are in sub-prime conditions.

## TABLE OF CONTENTS

List of Figures .....	vi
Chapter 1: Introduction and Motivation .....	1
Introduction .....	1
Literature Review of Factors Relating to ATV Accidents .....	1
Chapter 2: Development of the ATV Simulator.....	4
Introduction .....	4
ATV Simulator Description .....	4
Unreal Engine 4 .....	5
Oculus VR DK2 head mounted display .....	9
Experimental Setup .....	10
Chapter 3: ATV Simulator Characterization .....	12
Introduction and Methodology .....	12
Static Testing .....	12
Dynamic Testing .....	12
Results .....	13
Discussion.....	15
Static Testing .....	15
Dynamic Testing .....	16
Conclusion .....	16
Chapter 4: Characterization of Subject Perception and Simulator Sickness .....	18
Introduction .....	18
Methodology.....	18
Results .....	19
Discussion.....	19
Conclusion .....	21
Chapter 5: Characterization of Human Instability and Loss of Control .....	22
Introduction .....	22
Methodology.....	23
Data Collection Systems.....	23



Data Processing .....	26
Experimental Protocol.....	28
Chapter 6: Results and Discussion.....	32
Results .....	32
Subject 1.....	33
Subject 2.....	35
Subject 3.....	36
Subject 4.....	37
Subject 6.....	39
Discussion.....	40
Chapter 7: Conclusion .....	42
Chapter 8: Future Work .....	44
References.....	45
Appendices.....	46
Appendix A: Force Calibration Figures .....	46
Appendix B: Trial Time series Force Data .....	62
Subject 1.....	62
Subject 2.....	65
Subject 3.....	68
Subject 4.....	71
Subject 5.....	74
Subject 6.....	76
Appendix C: Trial Time series Acceleration Data.....	79
Subject 2.....	79
Subject 3.....	82
Subject 4.....	84
Subject 5.....	86
Subject 6.....	89
Appendix D: Wellness Survey.....	93
Appendix E: List of Motion Capture Markers .....	94

## List of Figures

Figure 1: Workflow of human in the loop simulation. The user controls the ATV, which changes analog inputs to the Arduino. The Arduino in turn controls the simulated ATV. The roll and pitch angles and the speed of the simulated ATV then control simulation table, which gives input to the subject. ....	5
Figure 2: Potentiometers mounted on the rear disk brake used for controlling both the simulators rear brake and trigger for shifting into reverse. ....	6
Figure 3: Potentiometer mounted on right handlebar used for controlling the simulator's front brake. ....	6
Figure 4: Potentiometer mounted on right handle bar for controlling the simulator's throttle.....	6
Figure 5: Potentiometer mounter to the ATV steering column for controlling the simulator's steering. ....	7
Figure 6: Example of a greyscale heat map used for creating Unreal Engine Terrains. After terrains are created, artistic detailing is needed to create a realistic environment. Lighter tones are representative of peaks and high altitude while darker tones are representative of lower altitudes and valleys. ....	9
Figure 7: ATV seen in its safety restraints. The orange tire chocks are seen under the tires. The large tire wedges restrict the rotation of the rear tires. The global coordinate system is shown in the right corner. ....	11
Figure 8: Harness system is seen hanging freely from ceiling. ....	11

Figure 9: Roll Orientation Validation of the physical orientation versus the simulated orientation. A perfect match would yield a  $y=x$  regression line..... 13

Figure 10: Pitch Orientation Validation of the physical orientation versus the simulated orientation. A perfect match would yield a  $y=x$  regression line..... 14

Figure 11: Dynamic Roll Orientation Validation showing the matching of the physical orientation to the simulated orientation over a time history of driving the simulator through numerous terrains. The physical orientation is seen in blue, while the simulated orientation is in red. .... 14

Figure 12: Dynamic Pitch Orientation Validation showing the matching of the physical orientation to the simulated orientation over a time history of driving the simulator through numerous terrains. The physical orientation is seen in blue, while the simulated orientation is in red. .... 15

Figure 13: Average wellness scores from each survey taken throughout the experiment. Subject three did not report results for the Post HMD survey due to a system failure..... 19

Figure 14: A projection screen was used during testing to reduce simulator sickness and improve subject well being. .... 20

Figure 15: Placement of MVN MTw IMU sensors. (A) C7 (B) T12 and S1 (C) ATV (D) Simulation Table. Not Pictured: Head Sensor Mounted to Helmet. .... 23

Figure 16: An MTS Machine was used with compression protocol to load the force sensors. Not pictured, pucks were used in final calibration to concentrate the load on each sensor. Sensors were tuned during maximum compression..... 24

Figure 17: Location of each of the 48 force sensors placed on the ATV. The 8 sensors placed under the handle bars are not pictured. .... 25

Figure 18: Tekscan FlexiForce Sensors placed on ATV Simulator. Double Sided Tape was used to adhere the sensors to the simulator. The sensor's linear behavior was consistent even when bent allowing placement on a variety of surfaces..... 26

Figure 19: Comparison of component accelerations (a) and magnitude acceleration (b)..... 27

Figure 20: Marker placement can be seen on the anterior and posterior of the subject's upper body. Lower body markers were not used due to occlusion from the ATV. .... 29

Figure 21: Flat Map seen from above. This map was considered the least extreme condition and exposed subjects to conditions found on flat terrain. Subjects traversed this map back and forth. .... 30

Figure 22: "Up and Down" Map seen from above. This was considered a moderate difficulty condition featuring mild up hill and down hill traverses as well as sloped turns seen primarily in the upper section of the figure. This map was performed both forwards and backwards. .... 30

Figure 23: "Quick Up and Down" Map seen from above. This was considered the most difficult map for subjects to perform. It featured steep, fast ascents and descent as well as tight sloped turns and a hidden deer that subjects were to avoid as it was expected they would maintain full control of the machine the entire time. This map was performed both forwards and backwards. .... 31

Figure 24: Acceleration at the table, ATV, S1, T10, C7, and the head of Subject 1. The peak acceleration is seen in the center of the plot. It is most evident for body accelerations. .... 33

Figure 25: Reaction forces at the left hand, right hand, left foot, right foot, left thigh, and seat for Subject 1. The second peak is identified as the reaction the subject had as a result of instability. Time in seconds is on the x-axis. .... 33

Figure 26: Subject 1's component accelerations during the instability event. Of note is the positive x and z direction accelerations at the input moment in 25 (a) and the resulting positive x and negative z accelerations seen across the rest of the figures..... 34

Figure 27: Acceleration at the table, ATV, S1, T10, C7, and the head of Subject 2. The peak acceleration is seen in the center of the plot. It is most evident for body and ATV accelerations. .... 35

Figure 28: Reaction forces at the left hand, right hand, left foot, right foot, left thigh, and seat for Subject 2. The force reaction is evident at roughly 19 seconds across the system. Time in seconds is on the x-axis. .... 35

Figure 29: Acceleration at the table, ATV, S1, T10, C7, and the head of Subject 3. The peak acceleration is seen in the center of the plot. It is most evident for body and ATV accelerations. .... 36

Figure 30: Acceleration at the table, ATV, S1, T10, C7, and the head of Subject 4. The peak acceleration is seen in the center of the plot. It is most evident for body and ATV accelerations. .... 37

Figure 31: Reaction forces at the left hand, right hand, left foot, right foot, left thigh, and seat for Subject 4. The force reaction is evident at roughly 87 seconds across the system and sustained throughout the instability event. Time in seconds is on the x-axis. .... 37

Figure 32: Subject 4's component accelerations during the instability event. S1 and T10 accelerations show an increase relative to the table and ATV with components in the X, Y, and Z directions. Inputs were substantial in the positive X- Direction..... 38

Figure 33: Acceleration at the table, ATV, S1, T10, C7, and the head of Subject 6. The peak acceleration is seen in the center of the plot. It is most evident for body and ATV accelerations. .... 39

Figure 34: Reaction forces at the left hand, right hand, left foot, right foot, left thigh, and seat for Subject 6. The force peak is seen across the system at roughly 112 seconds. Time in seconds is on the x-axis. .... 39

## Chapter 1: Introduction and Motivation

### Introduction

Off-road vehicles are used widely across the United States for both recreational and occupational purposes. A variety of vehicles are available to the public, including dirt bikes, utility vehicles, and all-terrain vehicles (henceforth referred to as ATVs). In particular, roughly 11.2 million Americans over the age of 18 live in a home that owns at least one ATV (Scarborough, 2015). In addition, roughly 2.62 million Americans over the age of 18 live in a home that plans on owning one or more ATVs in the next twelve months (Scarborough, 2015). Even with the substantial ownership of ATVs in private households, this still fails to include the number owned by corporations and the government. Although use of off-road vehicles is very popular in the United States, injury rates to users remain high, often due to loss of control of the machine. The narrow wheel base and high center of gravity of the vehicle further increase the likelihood for instability of the vehicle and its operator. The Consumer Product Safety Commission estimates that 99,600 emergency department treated injuries were a result of riding an ATV. Amongst those 99,600 accidents that resulted in injury, 426 resulted in death, with more expected unreported (Topping & Garland, 2015). In order to further understand the mechanisms that lead to these risky loss-of-control events, a four-degree-of-freedom (four-DOF) simulator was designed to mimic the experience of riding an ATV in varied terrains. The development of this unique simulator offered a controlled environment in which to study subjects' response to potentially unsafe riding scenarios. The lab setting of these experiments permitted strict safety measures to ensure that extreme conditions could safely be achieved. Using force sensors and inertial measurement unit (IMU) motion sensors, high-risk moments were identified and studied to determine how subjects compensated and regained control in the moment.

### Literature Review of Factors Relating to ATV Accidents

Despite the aforementioned prevalence of injuries and deaths among ATV riders in the United States, little research has been carried out to understand the mechanisms of how and why such events occur. Furthermore, the existence of lab-controlled studies investigating such mechanisms is limited even further. In a lab-based study designed to study an ATV rider's dynamic response while riding, a simulation table was driven by lab-generated roll and pitch motion files. The subject's response was then evaluated by analyzing the joint angles of the torso and pelvis.

(Jennissen, et al., 2014). The study confirmed the hypothesis that active rider compensation for gross roll and pitch motions would occur as the subject was exposed to unexpected motion.

Stephen Milosavljevic, a researcher based in New Zealand, has done extensive work studying loss of control and injury in the field, working with farmers who have experience with riding ATVs. In one cross-sectional study of mixed-stock farm workers in New Zealand, it was found that 60.8% of the subjects had reported a loss-of-control event. Of those events reported by the subject population, 48.7% occurred while driving up or down steep slopes (11.7% due to turning on such a slope); 27.8% occurred due to striking a tree, animal, or fence; 12% occurred while driving on a wet or slippery surface; and 7.6% occurred due to high-velocity driving (Milosavljevic, et al., 2011). The same paper showed statistical significance ( $p < .05$ ) that daily distance traveled, mean velocity, and daily vibration dose value (VDV) were greater in the group that had experienced a loss-of-control event than in the group that had not experienced a loss-of-control event.

Carman et al. (2010) explored the ATV riding behaviors that may have influence over the operator experiencing a loss-of-control event. The study focused on the roll, pitch, and velocity of the ATV in different terrains and scenarios to identify how the technique of those with a reported loss-of-control event varied from the technique of those had not experienced a loss-of-control event. The study consisted of 30 New Zealand farmers, 63% of whom had experienced a loss-of-control event. The subjects were asked to drive a course that exposed them to uphill driving, downhill driving, driving across a slope, and driving on flat ground. The study analyzed the velocity of the ATV at different pitch and roll ranges, as well as the combination of the pitch and roll angles in different ranges. Despite the study's many metrics, only two yielded a statistically different result between the loss-of-control group and the non-loss-of-control group, subject age and the pitch angle when the operator reached their maximum roll angle.

Due to the large prevalence of injury while riding ATVs and the size of the population with access to them, research into the safety and operation of these machines is crucial. Field studies are a good base to begin from, but they are also hard to control for potentially confounding variables. Additionally, field studies can prove difficult when trying to control the environment for subject safety. To isolate variables, further study key metrics such as body joint angles or input forces, and ensure subject safety, we must be able to recreate the experience from the field in the laboratory. In the laboratory, numerous approaches can be taken, including prerecorded ride



files and multiple levels of simulation. A human-in-the-loop simulation, where the subject controls the result, offers the most favorable simulation method when studying operator tendencies and error because it allows for riders to approach similar scenarios with their own methodologies. Thus, a four-DOF human-in-the-loop ATV was created to study operator instability when traversing a variety of different riding conditions.

This thesis will cover a range of topics regarding the development and testing of a user-controlled ATV simulator and the subsequent subject testing, exploring the ATV simulator's ability to capture ATV operator instability and loss of control. In Chapter 2, the components making up the parts of the simulator will be described and their integration will be explained. Chapter 3 describes testing the efficacy of the simulator in both static and dynamic cases in order to ensure it was performing as expected. Chapter 4 explores the effect of using a head-mounted display in motion simulation studies using today's technologies and discusses whether a head-mounted display is advantageous in comparison to a traditional projection screen. In Chapter 5, a description of the experimental setup, data collection methods, and results will be discussed for subject experimentation, exploring the ability of the simulator to induce and capture instability and loss of control. The thesis ends with Chapter 6, where future work is outlined.

## Chapter 2: Development of the ATV Simulator

### Introduction

In order to study user instability while riding an ATV, we had to create an environment that placed the subjects in scenarios that could potentially cause such instabilities. In vibration experimentation, accelerations are often recorded in the field using accelerometers and then recreated on a motion simulator. Such methodology allows for studying human vibration, and in some cases have been used for creating basic field simulations (Jennissen, et al., 2014). Additionally, the simulator had to be designed to allow for limited rolling of the ATV to identify moments of full loss of control. Most simulators, such as the National Advanced Driving Simulator at the University of Iowa (UI), rigidly fix the chassis of the vehicle to a simulation table with actuators to simulate the suspension and road noise. For this case, the ATV's wheels and suspension were kept intact and were not fixed to the simulation table, allowing semi-free motion of the ATV with respect to the table.

The simulator developed for this project allows for full human control of the machine, also known as human in the loop. While in past lab studies the subjects have been exposed to recorded and lab-generated motion files, a human-in-the-loop simulator permits the subjects to control their exposure to simulator inputs. This allows for an inspection of the human-machine interaction of each subject in each condition uniquely, and it gives insight into how each subject is responding to the situation and environment they are exposed to under their own control.

### ATV Simulator Description

The simulator was designed using a MOOG six-DOF simulation table, Unreal Engine 4, an Arduino Leonardo, and an Oculus VR DK2 head-mounted display. Figure 1 shows the different components of the ATV simulator.

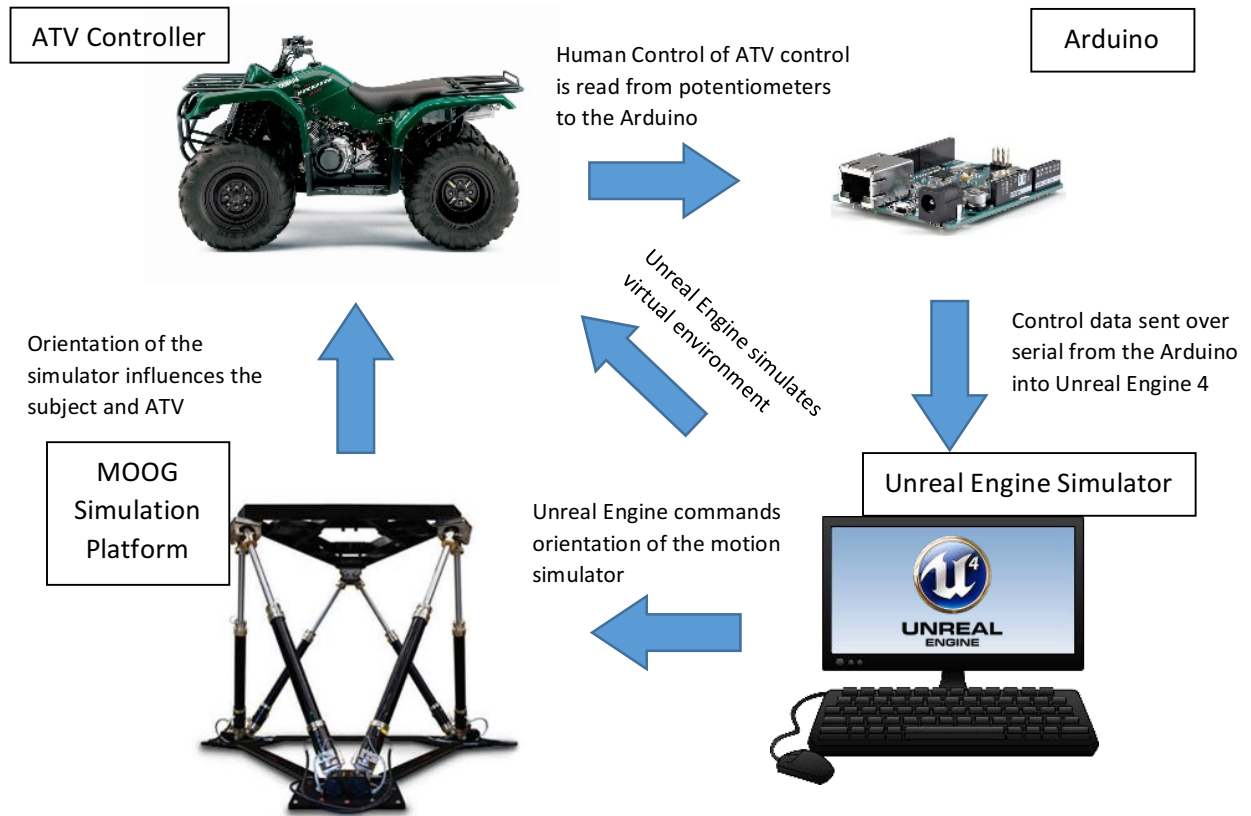
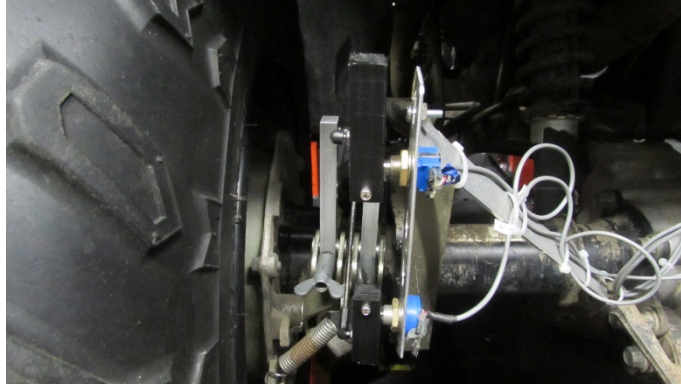


Figure 1: Workflow of human-in-the-loop simulation. The user controls the ATV, which changes analog inputs to the Arduino. The Arduino in turn controls the simulated ATV. The roll and pitch angles and the speed of the simulated ATV then control the simulation table, which gives input to the subject.

#### Unreal Engine 4

Unreal Engine 4 is a video game development platform built in C++, allowing for users of the software to develop their own scripts and code to run in the background. Using Unreal Engine and an Arduino Leonardo, the virtual world of the simulator was created. The Arduino was wired to potentiometers, which were mounted on the ATV. The potentiometers measured the rotation of components on the ATV including the right and left hand brakes, the foot brake, the throttle, and the steering column, by associating the voltage input to boundary voltage values. These values were then normalized onto a scale from 0 to 1000 and sent to Unreal Engine using the UE4duino plug-in that allows Unreal Engine to read values being transmitted to the computer's serial port. Once in Unreal Engine, the values were bound to vehicle controls built into the video game platform and allowed for control of the virtual ATV using real controls from a physical ATV.



*Figure 2: Potentiometers mounted on the rear disk brake used for controlling both the simulator's rear brake and trigger for shifting into reverse.*

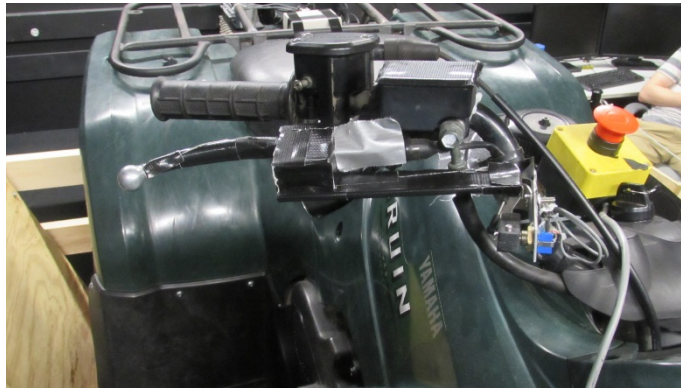


*Figure 3: Potentiometer mounted on right handlebar used for controlling the simulator's front brake.*

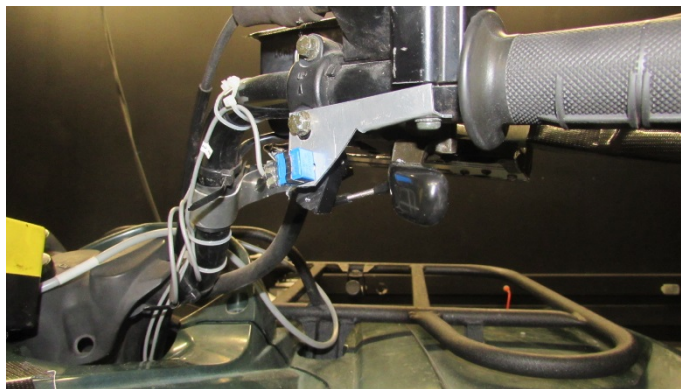


*Figure 4: Potentiometer mounted on right handlebar for controlling the simulator's throttle.*



*Figure 5: Potentiometer mounted to the ATV steering column for controlling the simulator's steering.*

In Unreal Engine 4, the orientation of the ATV was obtained from the root bone of the vehicle skeleton. The root bone is the skeletal joint that each part of the model is built out from. To draw a comparison, a biomechanical model may consider the pelvis to be its root bone with the other appendages growing out from it. In the ATV, the chassis has a similar point from which the wheels and suspension all branch out. The yaw portion of the orientation was considered to be zero at all times due to limitations of the simulation table. Similarly, the pitch and roll were limited to 20 degrees of rotation about the x and y axes. This control was put in place to prevent emergency table stops from being engaged during trials due to the kinematic constraints of the table. To provide road noise to the system, x-direction and z-direction accelerations ( $a_{x,z}$ ) were added to the simulator. The acceleration values were calculated by generating a random number from a Gaussian distribution between -5 and 5 m/s<sup>2</sup>. That value was then multiplied by the ratio of the current speed ( $v_n$ ) to the vehicle's maximum speed ( $v_{max}$ ) to produce vertical and fore-aft accelerations dependent on vehicle speed.

$$a_{x,z} = \text{RandomNumber}(n) * \frac{v_n}{v_{max}}$$

*Equation 1: Calculation of random acceleration value used to create a white noise vibration profile.*

In order to close the human-in-the-loop control loop, a plugin was developed in house to allow communication between the simulation table and Unreal Engine 4. This plugin used UDP packet communication carried between the Unreal Engine simulation and the MOOG motion simulation controller on a local area network via Ethernet. Each packet carried information about

the pitch and roll orientations of the simulated ATV and random vertical and fore-aft accelerations to the motion simulation table. The random accelerations were built by utilizing a random Gaussian distribution that was scaled by the ground velocity of the ATV, as described in equation 1. The packets carried to the controller were then buffered, and the simulation table created physical motion to best match the motion of the simulation. The packets were sent every time the screen refreshed, which was roughly 60 Hz.

Unreal Engine 4 offers a full physics simulation module for recreating real-world physics in the ATV video game engine. This module works by supplying values such as the maximum RPMs, the number of gears, and the gear ratios, in addition to creating torque curves, to control the acceleration and top speed of the vehicle. Other aspects of the ATV were also considered when developing the simulator, such as the friction between the tires and the ground, the stiffness properties of the tires, the damping and travel properties of the suspension, and a number of other inputs. Unreal Engine considers all of these inputs to create a physical simulation of the vehicle behavior. The behaviors in Unreal Engine's physical simulation engine include acceleration and velocity of the vehicle, lateral tire slip, suspension damping and travel, the ability of the vehicle to leave the ground, rollover, etc.

Unreal Engine also allowed for rapid development of environments for subjects to be tested in. This was important because subjects need to be exposed to many different terrains in order to understand responses and instabilities across many different scenarios. Unreal Engine provided tools for synthetically generating terrains and also allowed for black and white topographic images to be converted into terrains. For the purpose of this project, a set of maps simulating a basin and range environment were purchased as they allowed for the widest variety of terrain to be used in map development. The trails were then designed in those maps to expose subjects to flat, medium, and steep grades.

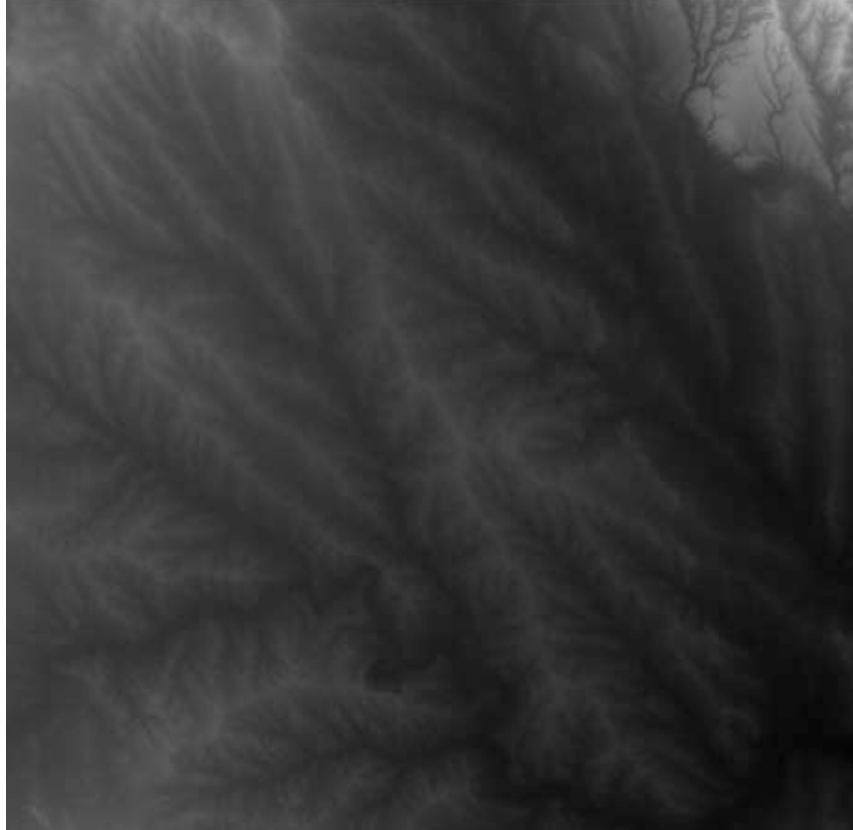


*Figure 6: Example of a greyscale heat map used for creating Unreal Engine Terrains. After terrains are created, artistic detailing is needed to create a realistic environment. Lighter tones are representative of peaks and high altitude, while darker tones are representative of lower altitudes and valleys.*

Oculus VR DK2 head-mounted display

Using the Oculus VR Development Kit 2 (DK2) head-mounted display allowed us to complete our virtual reality simulation. The Oculus DK2 is one of the most cutting-edge head-mounted displays available, and Unreal Engine 4 has a built-in setting to run the simulation using an Oculus DK2 seamlessly. The DK2 works by projecting two images, one on each eye, in order for the user to perceive depth in the virtual world they are experiencing. The screen uses low-latency, high-persistence video to create crisp imagery and reduce motion blur and simulator sickness. Additionally, the Oculus DK2 uses an accelerometer and gyroscope to estimate the orientation of the user's head and recreate that orientation of the camera in the simulation. Use of the Oculus Rift HMD resulted in a sub-study of test trials for its potential use and its effect across the subject population. Due to mixed reception in protocol trials, its use was limited during experiment trials in consideration of subject comfort and wellness. The head-mounted display was not utilized



during final subject testing, which will be addressed later in this thesis. The final model used a projection screen placed close enough to the subject to allow for parts of the screen to lie in the peripheral vision of the subject. Each of these systems interacted with one another in order to give the most immersive experience of riding an ATV.

#### Experimental Setup

Figure 7 shows the experimental setup of the ATV simulator at the 3D Bio-Motion Research Lab (3DBMRL) at the Center for Computer-Aided Design (CCAD) at the UI. Safety was heavily considered when designing a simulator that allowed for free motion of the ATV. Tire chocks were used under all four tires to reduce the amount that the ATV's tires could translate. They also served the purpose of opposing gravitational forces under large-magnitude pitching conditions. Large wedges were built to contain the rotational freedom of the rear tires to 20 degrees of roll in either direction. This permitted a maximum allowed roll of 40 degrees when combined with maximum table roll. The wedges also effectively reduced the sliding translation of the tires in more severe motions. Under the ATV chassis, braided steel cables rated for 4,000 lbs of load were attached to the table as a last-resort measure for containing the ATV upon failure of another system. Human safety was also considered as there was inherent risk in performing tests for loss of control and human instability. A four-point harness system was installed from the ceiling to catch a subject if they were thrown from the ATV and to protect them from surrounding hazards such as the simulation table and the ATV. A "rip-away" kill switch was installed on the handlebars of the ATV, similar to a jet ski, so that in the event of a full loss of control the table would suspend its motion and enter its reset protocol.





Figure 7: ATV seen in its safety restraints. The orange tire chocks are seen under the tires. The large tire wedges restrict the rotation of the rear tires. The global coordinate system is shown in the right corner.



Figure 8: Harness system is seen hanging freely from ceiling.

## Chapter 3: ATV Simulator Characterization

### Introduction and Methodology

A simulator's value is based on its ability to accurately recreate scenarios that would otherwise be expensive or dangerous to perform. Thus, the simulator needs to be characterized for several aspects, including its ability to recreate the expected orientations within its boundaries, its ability to behave virtually as it would be expected to perform in the real-life condition, and the ability to reduce simulator sickness amongst the subject population. To confirm the simulator was physically behaving as we expected it to, its orientation was confirmed by comparing simulated orientation generated from the Unreal Engine simulation and measured orientation from an Xsens MTw IMU, which was mounted rigidly to the simulation table. The IMU produces a quaternion of the sensor orientation, which can then be converted to roll, pitch, and yaw Euler angles.

#### Static Testing

The orientation of the sensor and motion simulation table were compared in two situations. The first situation was a static comparison of the orientations. This was accomplished by placing the simulated ATV in random orientations for long periods of time and comparing the results with the motion simulator's orientation over that time period. To quantify how well the physical system matched the simulated system, the percent error was calculated between the expected curve,  $y = x$ , and the curve produced by the gathered data.

$$\text{Percent Error} = \left( \frac{\text{measured} - \text{expected}}{\text{expected}} \right) * 100$$

*Equation 2: Percent error; used for measuring the difference between the commanded orientation and the actual orientation in static testing.*

#### Dynamic Testing

The second part of this characterization was a dynamic orientation matching. In dynamic orientation matching, the simulation traversed numerous terrains. Once again, the orientation of the simulation table was recorded using an IMU and was then compared to the values produced by the Unreal Engine 4 simulation. Data from the Unreal Engine 4 simulator were synced with the IMU simulator using a series of bumps to start the course, which were seen in each orientation dataset.

## Results

The figures presented below demonstrate the simulator's ability to match the orientations that were commanded to it. In the static orientation validations (Figures 9-10), a perfect match would pass through (0, 0) and have a fit equation of  $y=x$ . The dynamic validation was performed on a qualitative scale comparing the commanded orientation to the achieved orientation over time (Figures 11-12). A perfect match would be representative of perfect achievement of the simulator. The results from both of these validations were well within an acceptable range.

### *Static Orientation Matching Validation*

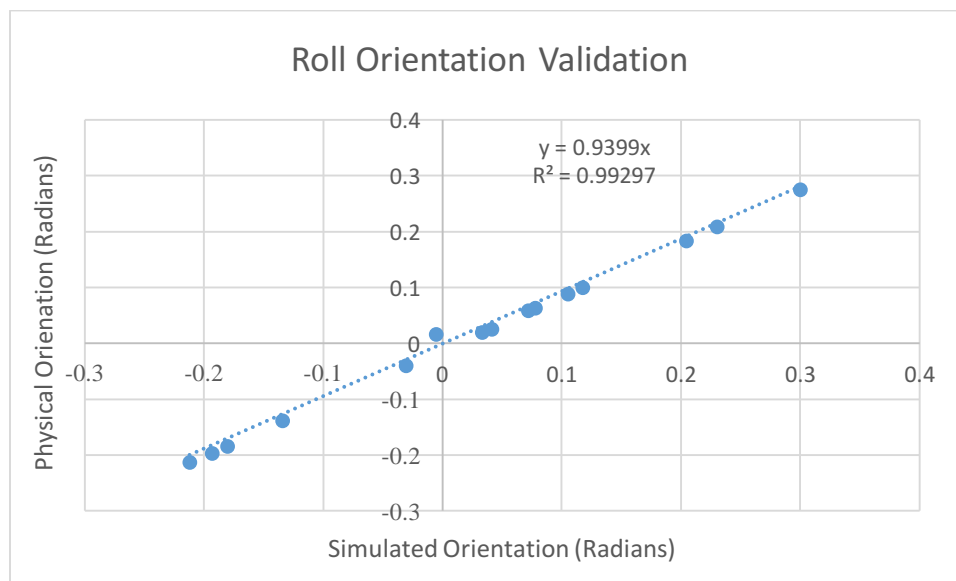


*Figure 9: Roll orientation validation of the physical orientation versus the simulated orientation. A perfect match would yield a  $y=x$  regression line.*

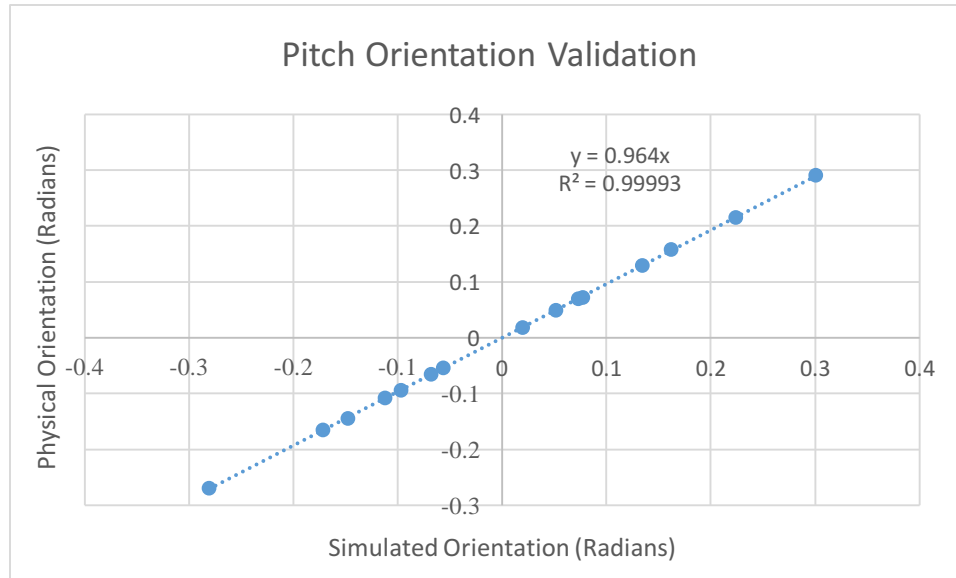


Figure 10: Pitch orientation validation of the physical orientation versus the simulated orientation. A perfect match would yield a  $y=x$  regression line.

#### Dynamic Orientation Matching Validation

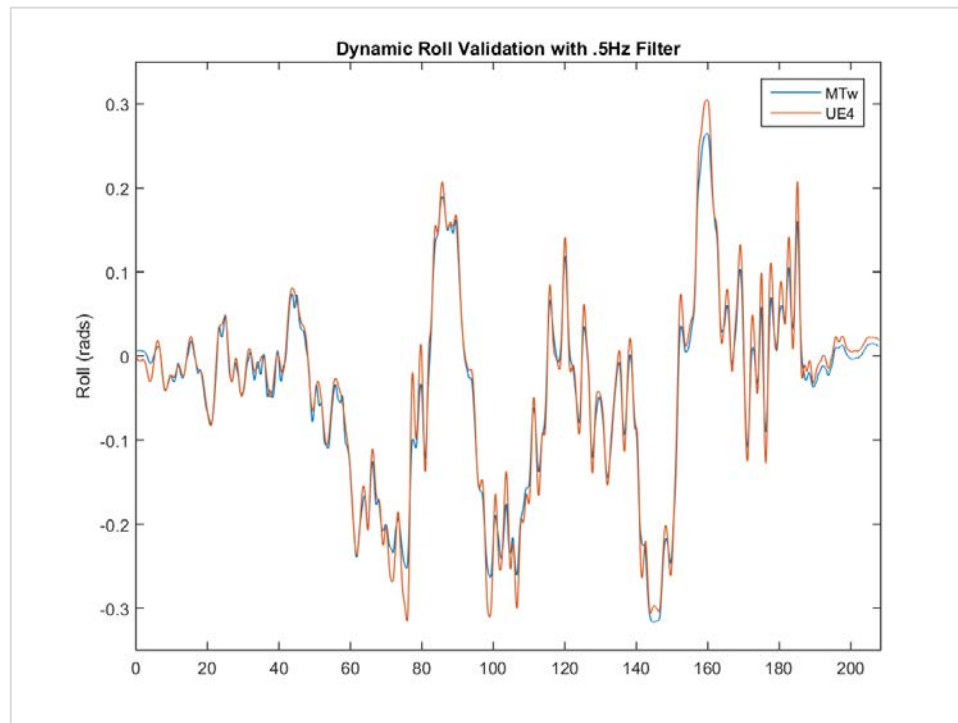


Figure 11: Dynamic roll orientation validation showing the matching of the physical orientation to the simulated orientation over a time history of driving the simulator through numerous terrains. The physical orientation is seen in blue, while the simulated orientation is in red.

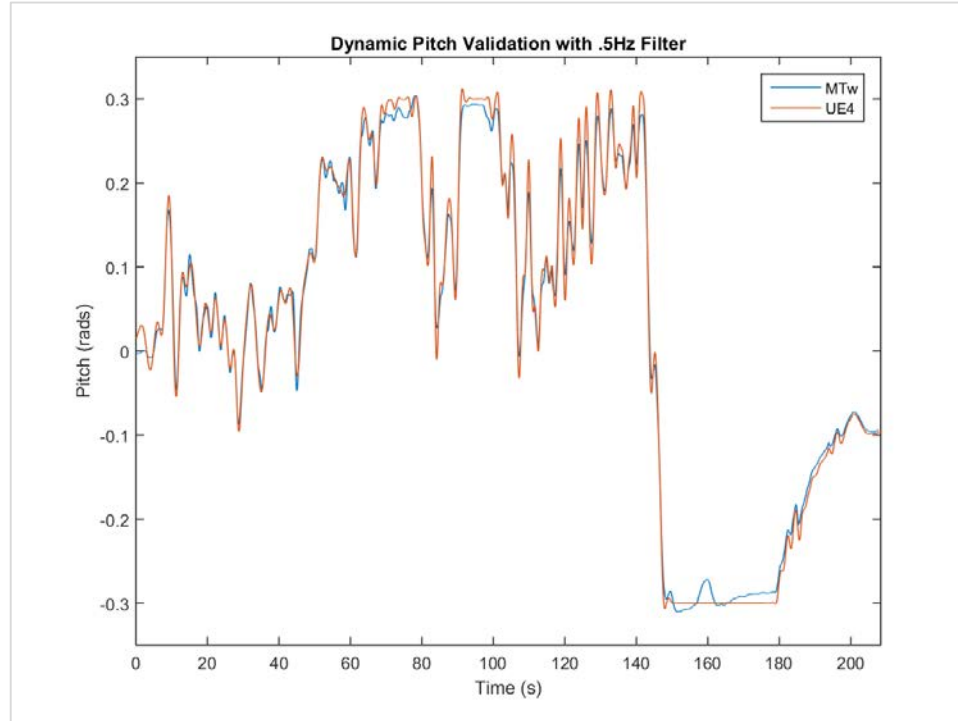


Figure 12: Dynamic pitch orientation validation showing the matching of the physical orientation to the simulated orientation over a time history of driving the simulator through numerous terrains. The physical orientation is seen in blue, while the simulated orientation is in red.

## Discussion

### Static Testing

The validation of orientations between the virtual and physical simulators showed promising results that the physical simulator was able to recreate high amplitude, low frequency motions. The static orientation validation was performed by placing each system in an orientation for an extended period time and recording the pitch and roll at each position. In a perfect matching situation, it would be expected that the best fit curve would produce a  $y=x$  curve. In the gathered results, the best fit curve was  $y=.9339x$  in the roll and  $y=.964x$  in the pitch. The static orientation matching for the roll produced a 6.61% error, and the static orientation matching for the pitch produced a 3.6% error. The error range of the sensor used to measure the orientation is 5%, which places the error of the pitch angle within that range. The roll angle, however, fell outside of this 5% measurement range. This could be due to the error of the table matching the simulator, or it could be due to the strong magnetic field produced by the steel simulation table, which could affect the sensor's ability to accurately measure orientation. This sensor error is a result of the manner in which the position of the sensor is measured. In MTw IMUs, position is

measured using the accelerometer, gyroscope, and magnetometer passed through a Kalman Filter, which can lead to error when placed in a strong magnetic field.

#### Dynamic Testing

The dynamic orientation validation was performed by comparing the roll and pitch angles throughout a time series of data. During that time series, the simulator was driven through many different terrains in order to test the dynamic ability at the ends of the motion range. As seen in Figures 10 and 11, the two systems matched each other well over the time history. The physical system did have some issues during dynamic testing. Due to the simulation table's internal system buffering commands to predict its future positions, it sometimes did not fully reach the amplitudes commanded by the Unreal Engine 4 simulator in order to better match future positions.

That being said, general trends of motion were well matched by the physical simulator, and undershooting occurred only during high-frequency, high-amplitude motions. The simulator is also limited by its ability to match high-frequency motion. In order to further understand this limitation, the data was filtered at many different frequencies until a best match was found. It appears the high-amplitude motion of the table is limited to a roughly .5 Hz -1 Hz motion. This could be the result of the motion controller filtering out data that it is not capable of matching, or it could be a limitation of the rate at which data is sent from the Unreal Engine simulator to the simulation table's motion controller, which is limited by the screen refresh rate at approximately 60 Hz.

#### Conclusion

This validation showed the ability of the physical simulation table to match the simulated roll and pitch angles gathered from Unreal Engine. The validation showed that for low-frequency, high-amplitude motion, the two systems have the ability to operate in sync. It does, however, give cause for addressing the high-frequency, high-amplitude motion that could potentially be lost due to low data transmission frequency limited by Unreal Engine or due to the simulation table's motion controller damping out the motion. In order to add some semblance of higher-frequency road noise to the system, Gaussian random z-direction vibration was added to the motion signal as a ratio of the current speed to the top speed to control the amplitude of the road noise.

Future iterations of the ATV simulator could visit this data transmission issue by using a head-mounted display with a faster, 120 Hz refresh rate, or by utilizing a projection screen with a high refresh rate. Such head-mounted displays are not available at this time. Additionally, adding individual actuators to each tire would allow for the study of response of the ATV to impacts into individual wheels.

## Chapter 4: Characterization of Subject Perception and Simulator Sickness

### Introduction

The simulator's ability to convince the subject to believe he or she was riding an ATV was crucial to reducing simulator sickness during testing. Simulator sickness is a common problem among simulators trying to recreate motion and imagery simultaneously. It is a result of a slight lag between the motion simulation and the visual simulation that can result in a desynchronizing of the visual perception and the vestibular perception (Brooks, et al., 2010). To reduce this sickness, numerous inputs were adjusted iteratively by asking experienced ATV riders to comment on their experience using the ATV simulator. These iterative tests were performed prior to subject testing, and all subjects experienced the same simulator condition. Additionally, a survey and test of the Oculus Rift head-mounted display was conducted in order to explore future directions using head-mounted displays instead of traditional projection systems.

### Methodology

In order to make a more realistic simulator, numerous aspects of the simulator were adjusted as we received input from experienced ATV operators. The key aspects that were adjusted include: steering sensitivity, braking sensitivity, throttle sensitivity, amplitude of road noise, and direction of road noise. Each of these were adjusted in an iterative process that allowed for fine-tuning of the simulator. Steering sensitivity, braking sensitivity, and throttle sensitivity were adjusted by adjusting a ratio that was multiplied to the raw steering input, and the road noise was adjusted by expanding the bound of the random noise generator coded into the simulator. Additionally, the direction of the random accelerations was controlled to find which combination provided the best recreation of road noise.

A survey was conducted during subject testing after subjects were asked to freely travel around a contained map while using the Oculus Rift head-mounted display. Subjects were told that they could stop using the head-mounted display at any time after beginning the trial and were timed to test their tolerance for the display. Five subjects were then asked to take a wellness survey identifying if they had experienced discomfort, nausea, eye soreness, or a host of other mild symptoms.



## Results

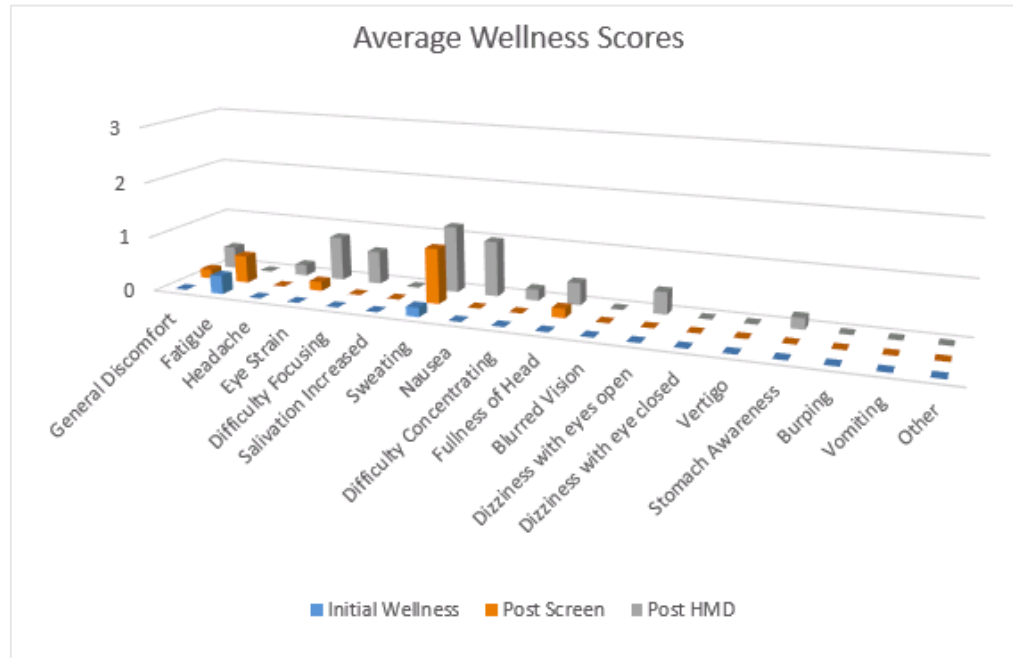


Figure 13: Average wellness scores from each survey taken throughout the experiment. Subject 3 did not report results for the Post HMD survey due to a system failure.

## Discussion

By looking at the average wellness scores across the subject population, we are able to identify trends regarding how the simulator and the head-mounted display affected the subjects. In order to get an overview of how each system affected the subjects, wellness surveys were administered at the beginning of the test, after loss-of-control testing was performed, and after head-mounted display testing was performed. During testing, the simulator consistently crashed while performing head-mounted display testing during trials with subject 3. This turned out to be an issue with lack of memory available on the C: drive because Unreal Engine builds a temporary cache on the disk while the program runs. For this reason, subject 3 was not included in the wellness scores for “Post HMD.”

In general, most subjects showed no adverse signs on their initial wellness survey. Subject 2 reported being moderately fatigued initially, which resulted in a skewed Post HMD average compared to the two earlier reports. Other wellness metrics showed the adverse effects of the head-mounted display on the subject’s general wellness. Across the population, increased

sweating, slight nausea, and eye strain resulted from the use of the Oculus Rift. This suggests that combining the simulator with the head-mounted display increased the likelihood of simulator sickness, which was not present during testing with a projection screen. Increased sweating was also associated with use of the simulator. This is to be expected, as the simulator requires physical commands from the operator in order to steer and maintain stability.



*Figure 14: A projection screen was used during testing to reduce simulator sickness and improve subject well-being.*

These results bring many insights for future design modifications that will improve the ATV simulator going forward. Increased sweating on the simulator could result in a risk to the subject or the instrumentation. When riding an ATV in the field, wind can help keep the operator cool and dry. In the lab setting, still air can quickly become hot, even with air conditioning on, which can increase the likelihood of subjects sweating. In order to reduce sweating, a fan with speed proportional to the ATV's speed could keep the subject cool and increase the level of immersion in the simulator. Addition of the head-mounted display negatively impacted many factors of the wellness survey. This suggests that with current technology the head-mounted displays, despite improvements, do not yet completely address simulator sickness in more complex simulations. It also suggests that the long-used solution, large projection screens that expand into the peripheral vision, are still the best option for addressing simulator sickness.

## Conclusion

Validation experiments were performed in order to perfect the simulator's performance and to explore future directions for the simulator. The experiments occurred during development, protocol testing, and subject testing. During the protocol, the simulator was tested for how immersive it was for the user. This was a subjective measure, and adjustments were made in an iterative process in order to achieve the best possible result. The main focuses of the iterative process were simulating road noise, engine noise, and control response. Road noise resulted in a solution that included vertical and fore-aft white noise vibration profiles ranging from -5 to 5 m/s<sup>2</sup> amplitude. Engine noise was addressed using a shaker motor rigidly mounted to the chassis of the ATV. After undergoing several trials, the shaker motor was removed after suggestions that it didn't capture the engine vibration correctly. Lastly, during subject testing, a sub-experiment was performed to study the effects of the Oculus Rift head-mounted display. In our study, we found that the head-mounted display had undesirable (Brooks, et al., 2010) effects on subject wellness and generally increased the incidence of simulator sickness in the subject pool. This has supported the idea that an immersive wraparound projection screen is the best choice for future studies at this time.

## Chapter 5: Characterization of Human Instability and Loss of Control

### Introduction

Human instability and loss of control has been lightly studied in the world of engineering and ergonomics. In order to study factors leading to instability and loss-of-control events in a controlled environment, a four-DOF ATV driving simulator was designed and implemented. A loss-of-control event has a large range of definitions, from a slight loss of control where control can be reestablished to a full rollover. In a study by Jennissen et al. (2014), subjects were asked to perform ATV riding tasks on precompiled motion files. The study analyzed the differences in posture between those who actively ride, engaging the whole body, in different dynamic roll and pitch angles. The results showed that the experienced riders in their study compensated for the roll and pitch motions of their motion simulator by deviating their torso angle away from neutral posture in order to keep it vertical with respect to gravity (Jennissen, et al., 2014).

Our simulator has the ability to study a posture similar to that in the past study by Jennissen et al. (2014), but added instrumentation allows us to go beyond simply looking at compensatory posture. The added instrumentation allows us to examine body segment acceleration and angular velocity, as well as reaction forces present between the subject and the machine. Additionally, the simulator is not rigidly attached to the shaker-base, which would allow capturing any event when the ATV tires leave the shaker-base. Considering reaction forces allows for the analysis of how subject coupling with the machine changes as phenomena are exerted on the body. Additionally, it allows us to look at how forces are applied on the machine as subjects perform compensatory postures during dynamic motion of the simulator. Using the ATV simulator to produce situations that could potentially lead to loss of control, the metrics previously mentioned were analyzed to characterize the biomechanical aspects of loss-of-control events.

## Methodology

### Data Collection Systems

Numerous systems were used to help characterize the loss of control experienced while riding an ATV and analyzing how a rider compensates for the loss of control. These systems included an MVN Xsens markerless motion capture suit, MVN MTw inertial measurement units, a five-camera Vicon Motion Capture system, and 48 Tekscan FlexiForce force sensors. Each of these systems has an important role in characterizing the biomechanical aspects of loss-of-control events.

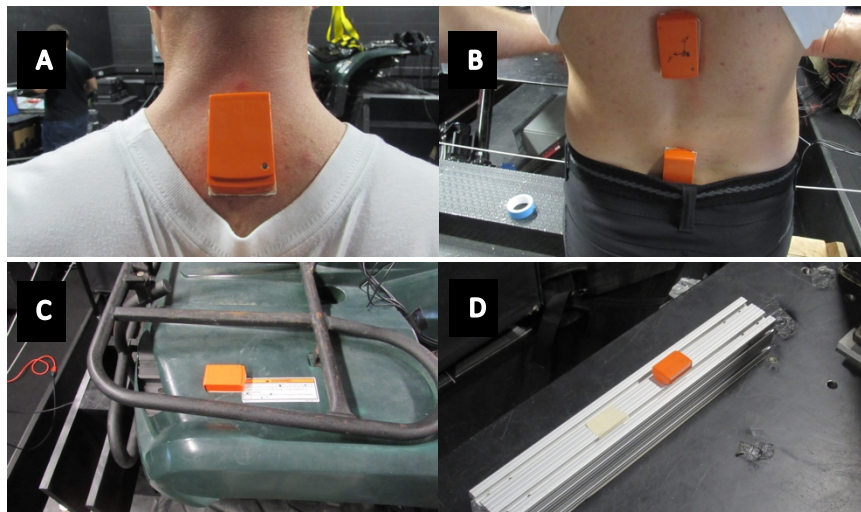


Figure 15: Placement of MVN MTw IMU sensors. (A) C7 (B) T12 and S1 (C) ATV (D) Simulation Table. Not Pictured: Head Sensor Mounted to Helmet.

### *Inertial-Based Motion Capture*

Four MVN MTw inertial measurement units were placed on each subject on the head, the C7 vertebrae, the T12 vertebrae, and the L1 vertebrae, as shown in Figure 15. Additionally, one MTw IMU was rigidly fixed to the frame of the ATV, and another was rigidly fixed to an aluminum block, which was in turn rigidly fixed to the motion simulation table. The aluminum block was used to separate the IMU from the steel platform of the simulation table. This was necessary because IMUs are sensitive to magnetic fields, like the ones generated by ferromagnetic materials. The IMUs measured angular velocity and acceleration at each of the body segments that had a sensor fixed to it. Each sensor was placed at a common axis on the body, so that compensation for drift could be performed. A similar compensation was performed for each sensor fixed to the simulation system. Peak moments of acceleration and angular velocity were

considered to be signifiers for potential loss of control of the simulator. At the five peak moments, frames 1.5 seconds before and after were selected to analyze the IMU metrics throughout the potential loss of control.

#### *Marker-Based Motion Capture*

The Vicon Motion Capture system was utilized to capture the postures of the subjects throughout their trials. Twenty-three motion capture markers were placed on each subject on landmarks that were necessary for rebuilding the upper body of the subject. A list of these landmarks can be found in Appendix E. Additionally, markers were placed on the the ATV's frame in order to give a reference frame for the subject's motion. Subject postures were then analyzed at moments before, during, and after peak accelerations and angular velocities sensed by the inertial measurement units. Five frames were selected to analyze how the subject biomechanically responded to potential losses of control and compensated to regain control of the ATV. The joint angles of the wrist, elbow, shoulder, clavicle, C7/T1, T12/L1, and L5/S1 and the orientation of the head were considered for the analysis of motion data.

#### *Force Sensors*

Forty-eight Tekscan FlexiForce force sensors were placed on the simulator in order to measure reaction forces between the subject and the ATV. The FlexiForce sensors were calibrated to measure forces between zero and 100 pounds in a linear manner. Calibration was performed by applying a uniaxial load using an MTS compression protocol, as shown in Figure 16.



*Figure 16: An MTS machine was used with a compression protocol to load the force sensors. Not pictured, pucks were used in final calibration to concentrate the load on each sensor. Sensors were tuned during maximum compression.*

Sensors were first conditioned by performing cyclical loading to the sensors up to two times the maximum calibrated load. Sensors were tuned to read 5 volts at 100 pounds of compression. Data were recorded multiple times to test for consistency of reading. Those plots can be seen in the appendix. After placing the sensors, many of which were on curved surfaces, baseline voltages were recorded, and the signals were detrended.

The location of each sensor on the ATV simulator can be seen in Figures 17 and 18. A unique capability of Tekscan's flexible sensors is that they maintain their linearity even when curved. The sensors were distributed on the handlebars, saddle, foot, and between the thighs to detect numerous types of compensation occurring during testing. Similar to the other two metrics, forces were analyzed before, during, and after moments of peak acceleration and angular velocity in order to analyze the subject's interaction as they approached loss of control and during recovery from the loss of control.



*Figure 17: Location of each of the 48 force sensors placed on the ATV. The 8 sensors placed under the handlebars are not pictured.*



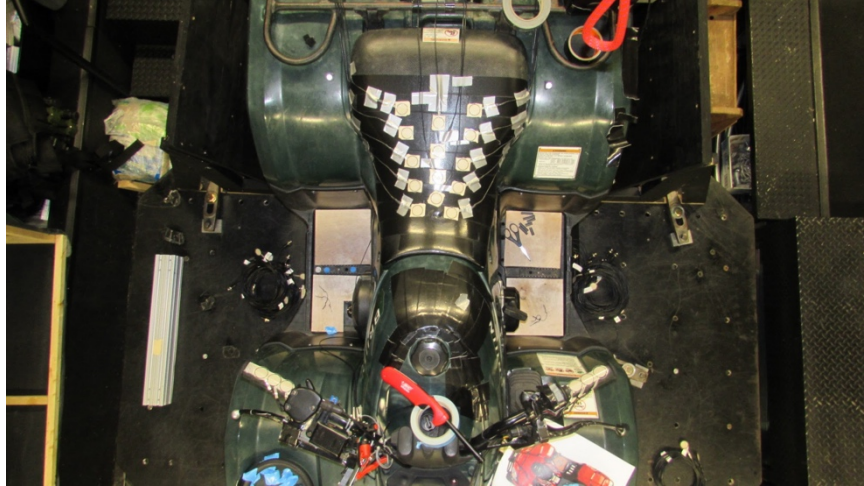


*Figure 18: Tekscan FlexiForce sensors placed on ATV simulator. Double-sided tape was used to adhere the sensors to the simulator. The sensors' linear behavior was consistent even when bent, allowing placement on a variety of surfaces.*

## Data Processing

Due to technical issues, the data from the optical motion capture system were not used. Data from the IMU sensors and FlexiForce force sensors were processed in Matlab. The IMUs contain an accelerometer and a gyroscope, both of which were utilized. Acceleration and angular velocity data were filtered through a 30 Hz low-pass Butterworth filter. Acceleration data (Figure 19a) was then analyzed by inspecting the acceleration of individual sensors relative to the acceleration of the simulation table. The magnitude of the relative acceleration in the X, Y, and Z directions (Figure 19b) was then taken over the entire time series. Angular velocities were also analyzed as a magnitude value of the pitch, roll, and yaw rotations.

Thirty-two force sensors were utilized to identify forces on the handlebars, foot wells, seat, and saddle. Each of these force signals was filtered through a 30 Hz Butterworth filter as well. The signals were then run through their respective calibration curves, seen in the appendix, to convert them to force values from voltage. Force values were summed across the sensors in their respective areas. This resulted in a total of seven sums: Left Hand, Right Hand, Left Foot, Right Foot, Left Saddle, Right Saddle, and Seat. Due to uncertainty regarding whether or not the resulting quantitative values were accurate, force data was scaled on to a zero to one scale, normalized for the maximum force for each trial. This was considered to depict qualitative trends in force input.



These data were further analyzed to identify moments that appeared to show loss of control or instability in the operator. This was done by analyzing the forces and accelerations and analyzing the frames 1.5 seconds before and after the event. Analyzing such events granted insight into how the operator responded to sudden accelerations and regained control after instability.

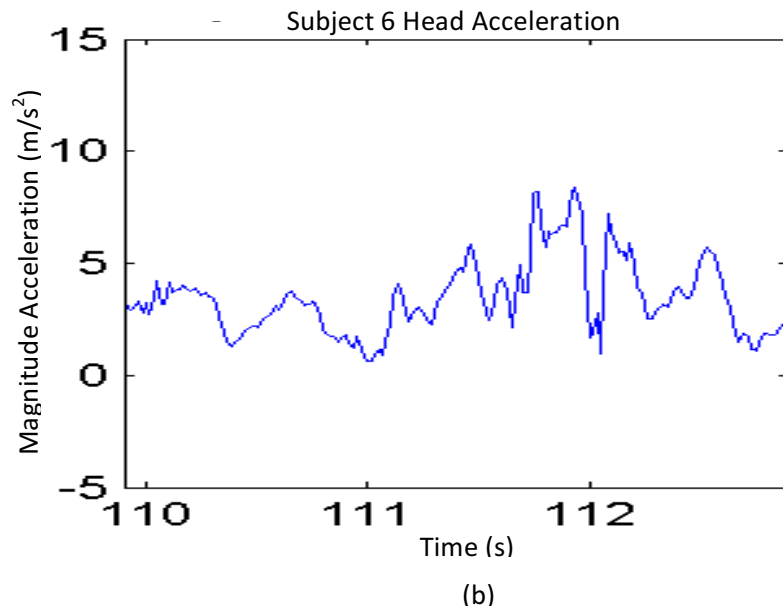
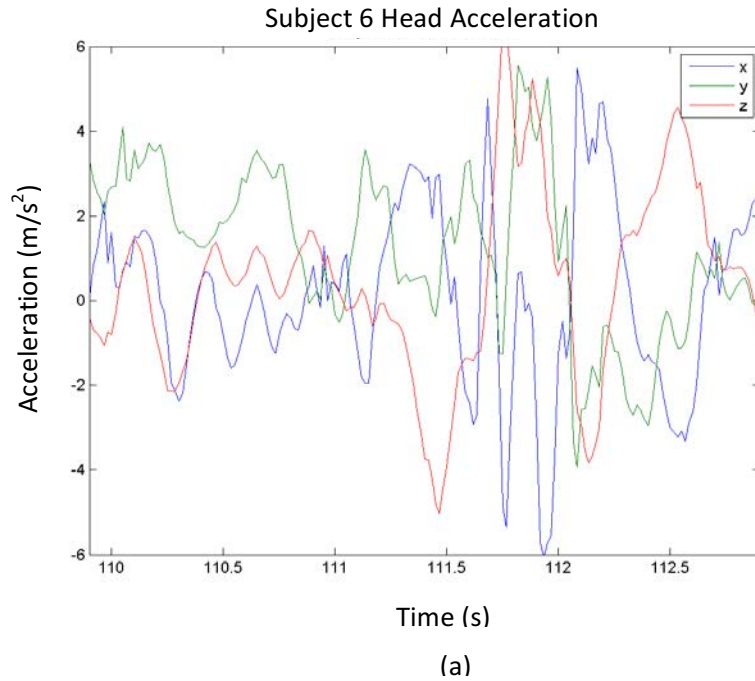
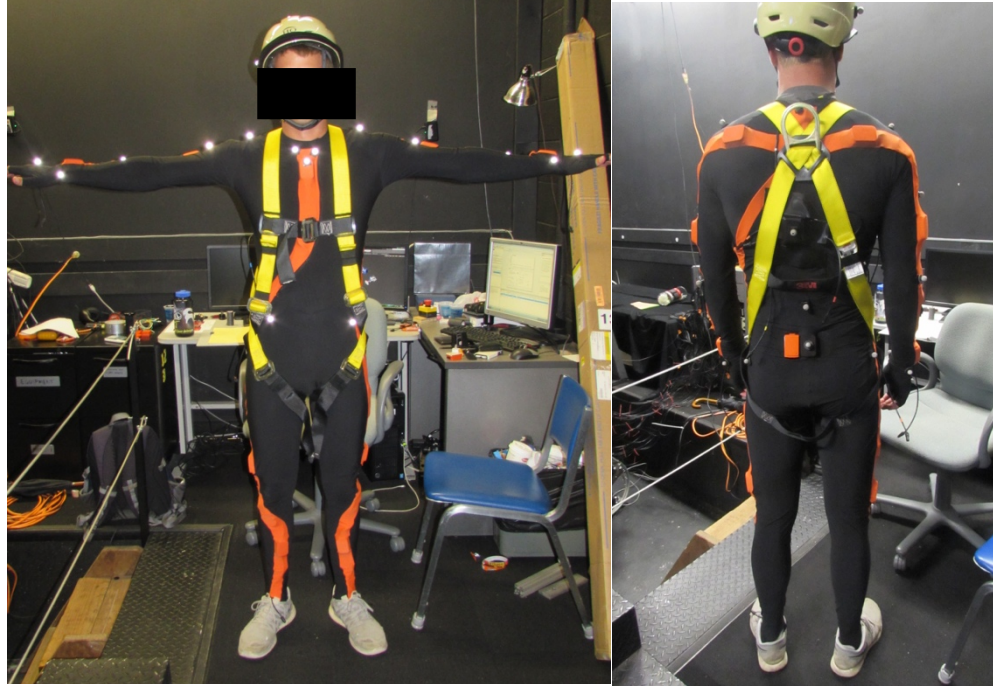


Figure 19: Comparison of component accelerations (a) and magnitude acceleration (b).

## Experimental Protocol

Six male subjects voluntarily participated in our study in accordance with the Institutional Review Board and were compensated for their ability to complete certain numbers of trials, pending their desire to continue the trials. Written informed consent was obtained from each subject prior to testing. The university's Institutional Review Board approved the study. The average age was 24.5, the average height was 176 cm, and the average weight was 178.5. All subjects had a long history of riding ATVs, at least 100 hours of riding experience with an average of 245 hours after removing an outlier of 2500 hours, and were considered competent riders. Participants were required to take a field survey, found in the appendix, to gauge whether or not they had traits suggesting they may have Attention Deficit Disorder (ADD) or Attention Deficit/Hyperactivity Disorder (ADHD), as we required a subject pool that did not have those traits.

Once it was deemed that the subject qualified to participate in the study, their map orders were randomized. A wellness survey, found in Appendix D, was then administered to gauge the subject's initial general wellness, which allowed us to measure the impact of the simulator. Subjects were then given the opportunity to familiarize themselves with the simulator before instrumentation was applied to them. Subjects were given up to five minutes in a controlled map that was separate from the maps used during testing. Once familiarized, the subject was then instrumented with IMUs and motion tracking markers, and experimentation began. A list of the placements of the motion tracking markers and the IMUs can be found in the appendix and can be seen in the figure below.



*Figure 20: Marker placement can be seen on the anterior and posterior of the subject's upper body. Lower-body markers were not used due to occlusion from the ATV.*

Experimentation included six trials that consisted of three different maps (Figures 21-23) ridden backwards and forwards. These maps required a varying degree of difficulty and skill to traverse the terrain. The three maps included flat terrain, similar to a basin or field; hilly terrain, similar to foot hills; and a mountainous terrain requiring subjects to traverse up and down mountainous ridges. These allowed for a variety of scenarios to observe subjects respond to and offered potential to see near losses of control. Subjects were encouraged to take breaks as necessary between trials to prevent fatigue and simulator sickness.



*Figure 21: Flat map seen from above. This map was considered the least extreme condition and exposed subjects to conditions found on flat terrain. Subjects traversed this map back and forth.*



*Figure 22: "Up and Down" map seen from above. This was considered a moderate-difficulty condition, featuring mild uphill and downhill traverses as well as sloped turns seen primarily in the upper section of the figure. This map was performed both forwards and backwards.*





*Figure 23: "Quick Up and Down" map seen from above. This was considered the most difficult map for subjects to perform. It featured steep, fast ascents and descents as well as tight sloped turns and a hidden deer that subjects were to avoid, as it was expected they would maintain full control of the machine the entire time. This map was performed both forwards and backwards.*

After subjects completed the six loss-of-control trials, they were asked to complete a second wellness survey and another survey related to virtual reality environments and tendency towards sickness while on amusement rides. Subjects then entered a testing phase for gauging the effect of the Oculus Rift head-mounted display on simulator sickness when compared to the large-screen projector used in loss-of-control trials. The subject was asked to operate the simulator while wearing the Oculus Rift for as long as they found tolerable. Time was recorded for how long the subject was able to operate the simulator with the head-mounted display on. They were then asked to complete a final wellness survey to measure the effects of the Oculus Rift head-mounted display on their general wellness. The results and a discussion of this particular sub-experiment are found in Chapter 4.

## Chapter 6: Results and Discussion

### Results

The results from this study yielded time series data for acceleration, angular velocity, forces, and posture. Data for acceleration, angular velocity, and forces are used for this study. Posture data collected using motion capture cameras was not used due to difficulties processing the data. Subjects 1 and 4 were investigated further by examining the component accelerations at each measurement location to identify the acceleration direction of the body with respect to the acceleration direction of the simulator. With regard to component acceleration plots, blue data are x-direction (fore-aft) accelerations, green data are y-direction (side to side) accelerations, and red data are z-direction (up and down) accelerations.

Subject	Trial	Table (s)	ATV (s)	Head (s)	Force (s)
1	1	33.2	33.33	33.45	34.34
2	2	18.05	18.1	18.17	19.08
3	2	34.2	34.23	34.4	35.57
4	3	86.43	86.43	86.6	87.03
6	1	111.4	111.7	111.9	112.1

*Table 1: Response time of the acceleration at the table, ATV, subject's head, and the reaction force for five subjects.*

Table 1 shows the key times that were identified and used in the focus segments for analysis. The table columns "Table," "ATV," and "Head" are times when input and output accelerations were measured by the IMUs. The "Force" column refers to the time when the reaction force took place across the system. The graphs being analyzed before include 1.5 seconds before and 1.5 seconds after the "Table" acceleration time. In Figures 24 through 26, Subject 1 is analyzed in depth. The analysis begins with a look at the magnitude acceleration of each sensor during the focus segment. Normalized force is also visited within the force frames. Lastly, the component accelerations are presented for each sensor throughout the focus segment. This component analysis was performed to note how each segment accelerated with respect to the others. A similar analysis is performed in Figures 30 – 32 for Subject 4, presenting data for magnitude acceleration, normalized force, and component acceleration.

Subject 1

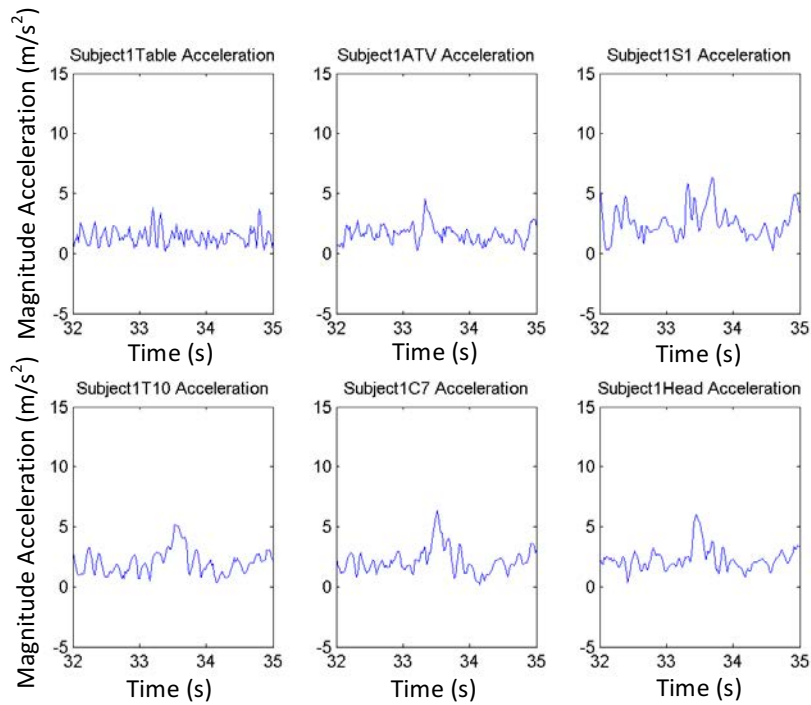


Figure 24: Acceleration at the table, ATV, S1, T10, C7, and the head of Subject 1. The peak acceleration is seen in the center of the plot. It is most evident for body accelerations.

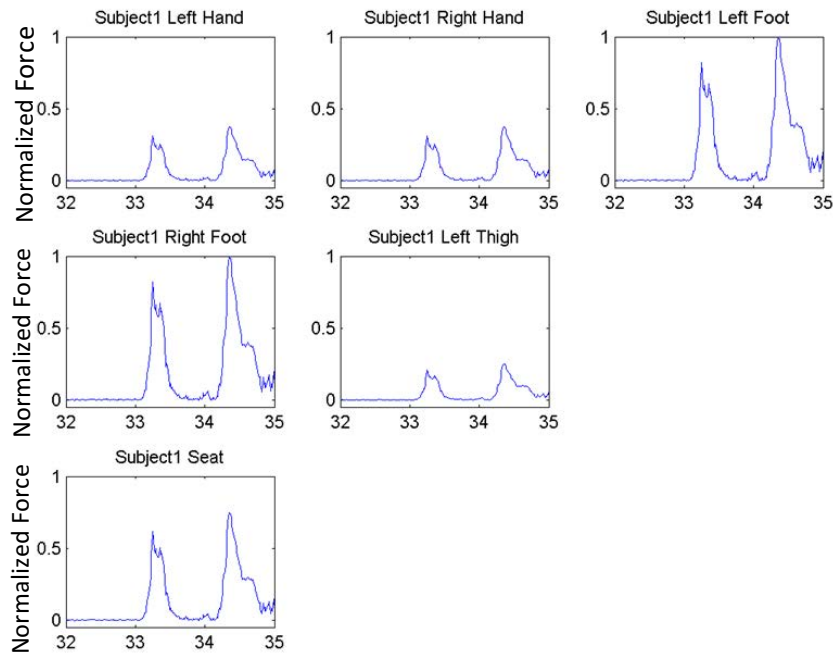


Figure 25: Reaction forces at the left hand, right hand, left foot, right foot, left thigh, and seat for Subject 1. The second peak is identified as the reaction the subject had as a result of instability. Time in seconds is on the x-axis.

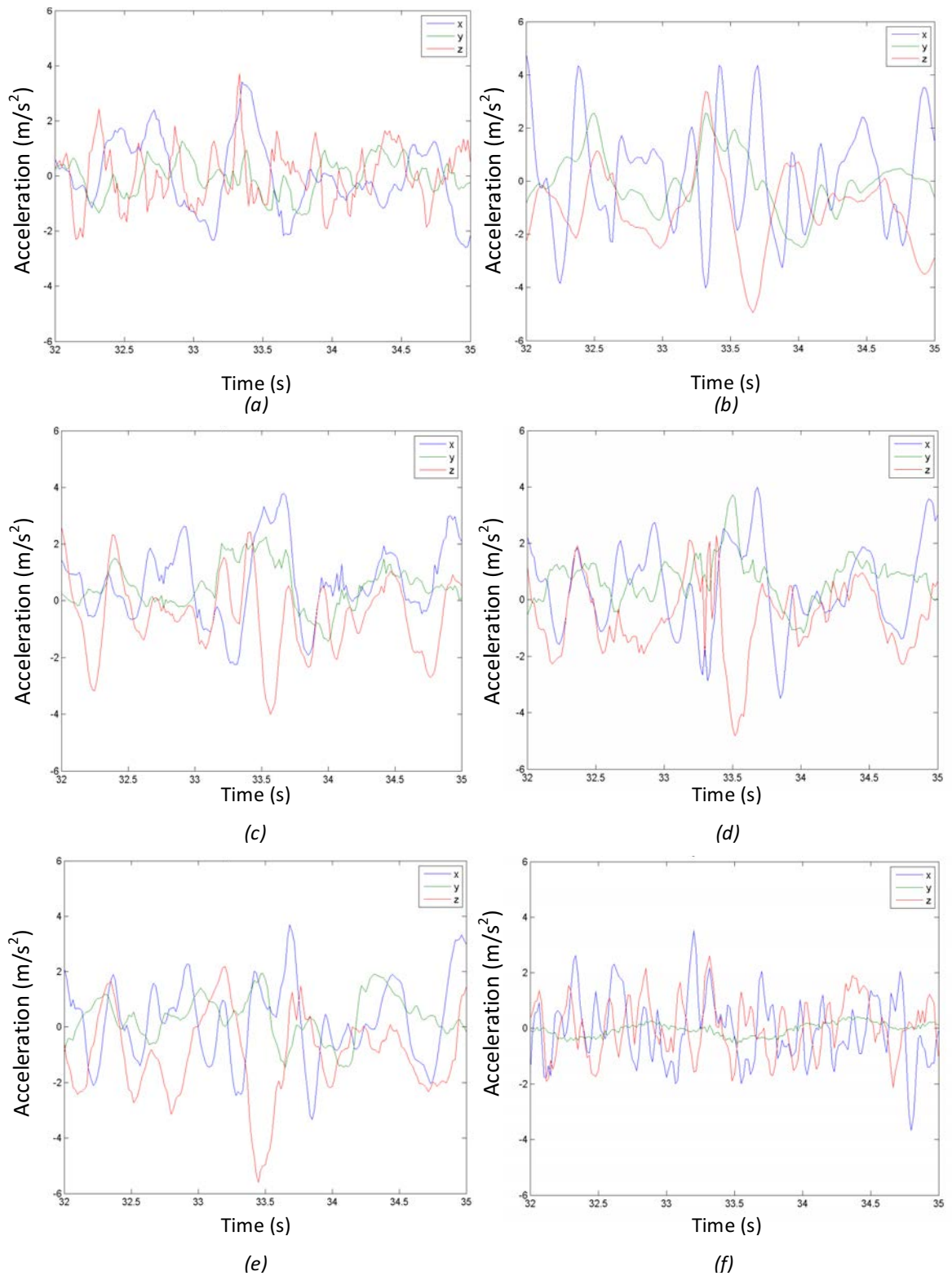


Figure 26: Subject 1's component accelerations during the instability event. Of note is the positive x and z direction accelerations at the input moment in 25 (a) and the resulting positive x and negative z accelerations seen across the rest of the figures.



Subject 2

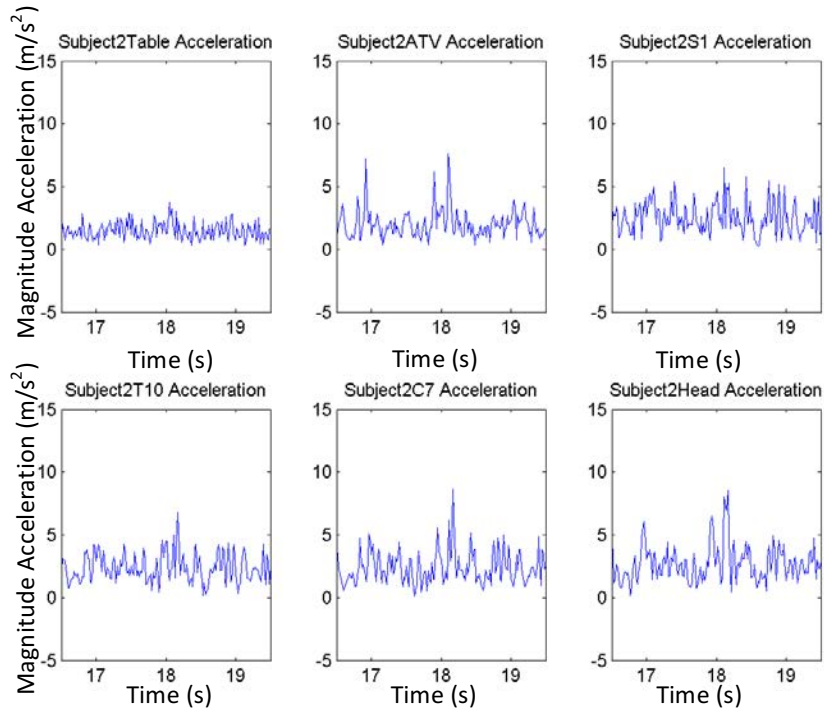


Figure 27: Acceleration at the table, ATV, S1, T10, C7, and the head of Subject 2. The peak acceleration is seen in the center of the plot. It is most evident for body and ATV accelerations.

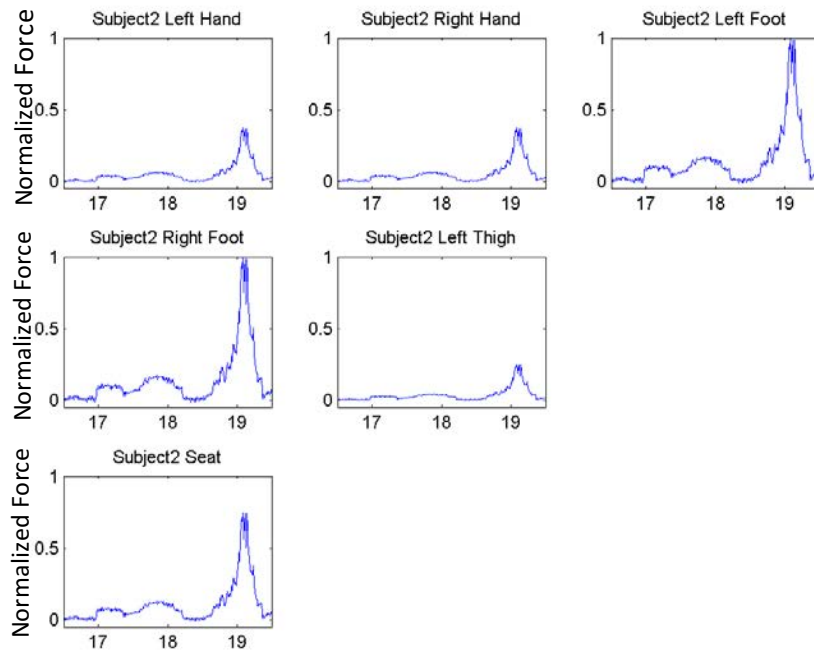


Figure 28: Reaction forces at the left hand, right hand, left foot, right foot, left thigh, and seat for Subject 2. The force reaction is evident at roughly 19 seconds across the system. Time in seconds is on the x-axis.

Subject 3

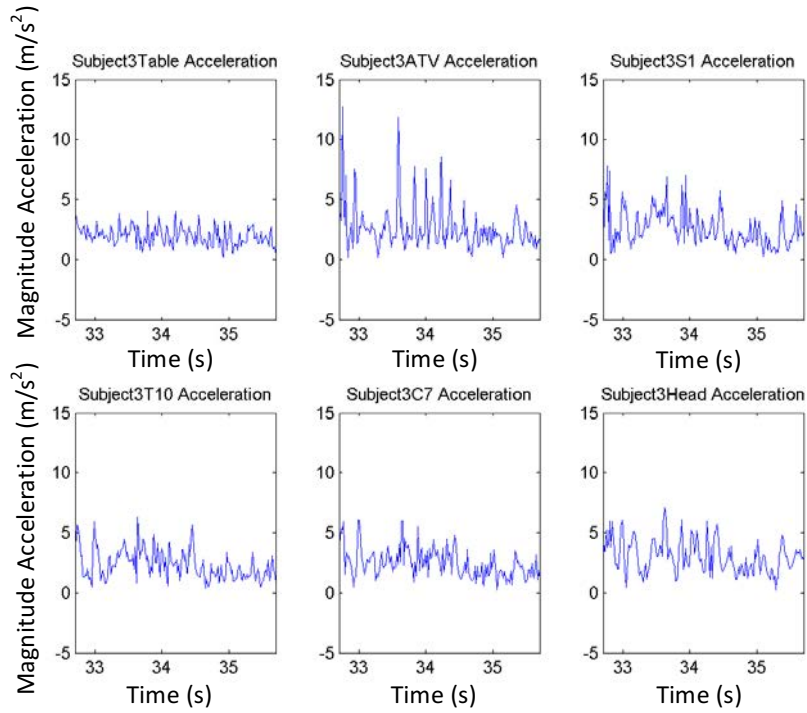


Figure 29: Acceleration at the table, ATV, S1, T10, C7, and the head of Subject 3. The peak acceleration is seen in the center of the plot. It is most evident for body and ATV accelerations.

Subject 4

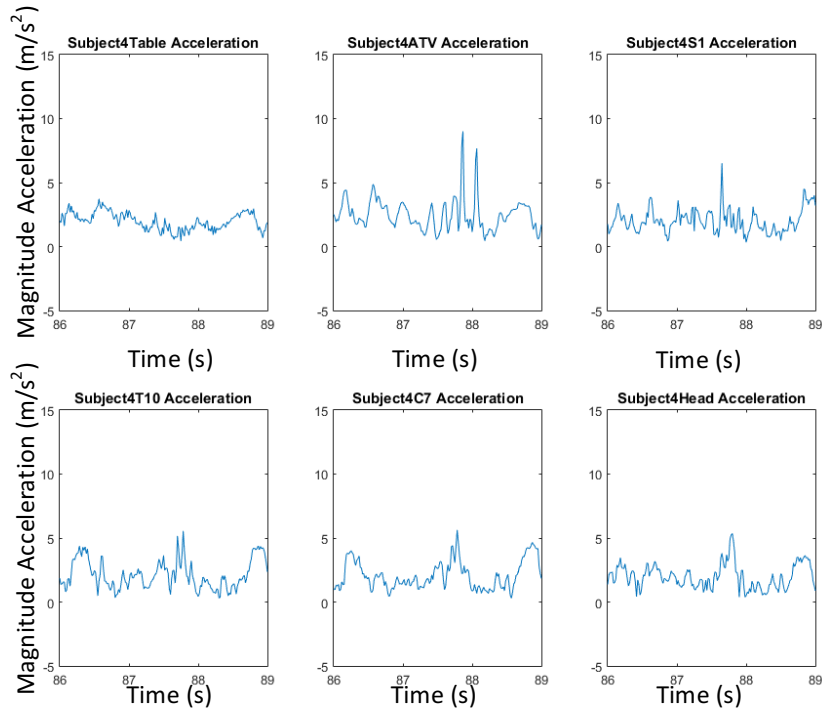


Figure 30: Acceleration at the table, ATV, S1, T10, C7, and the head of Subject 4. The peak acceleration is seen in the center of the plot. It is most evident for body and ATV accelerations.

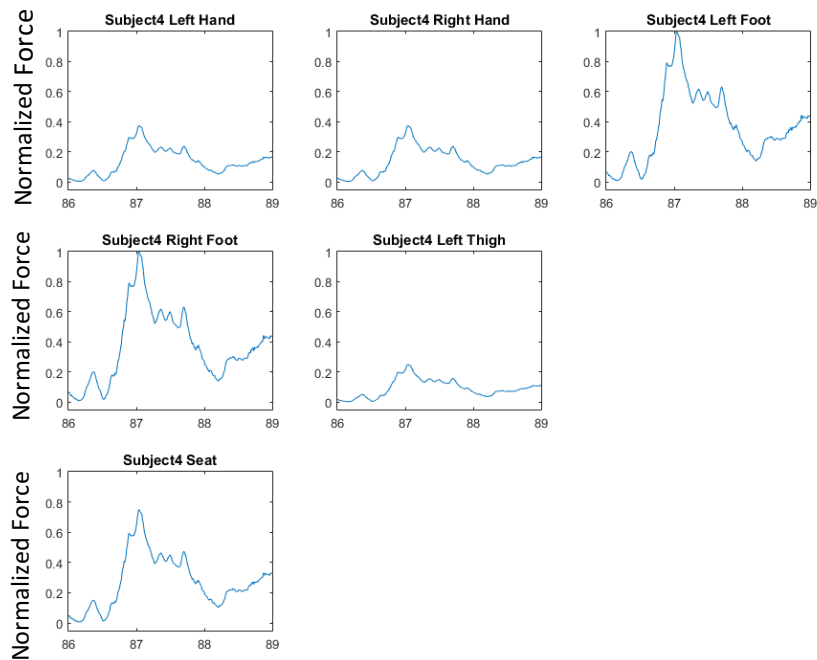


Figure 31: Reaction forces at the left hand, right hand, left foot, right foot, left thigh, and seat for Subject 4. The force reaction is evident at roughly 87 seconds across the system and sustained throughout the instability event. Time in seconds is on the x-axis.

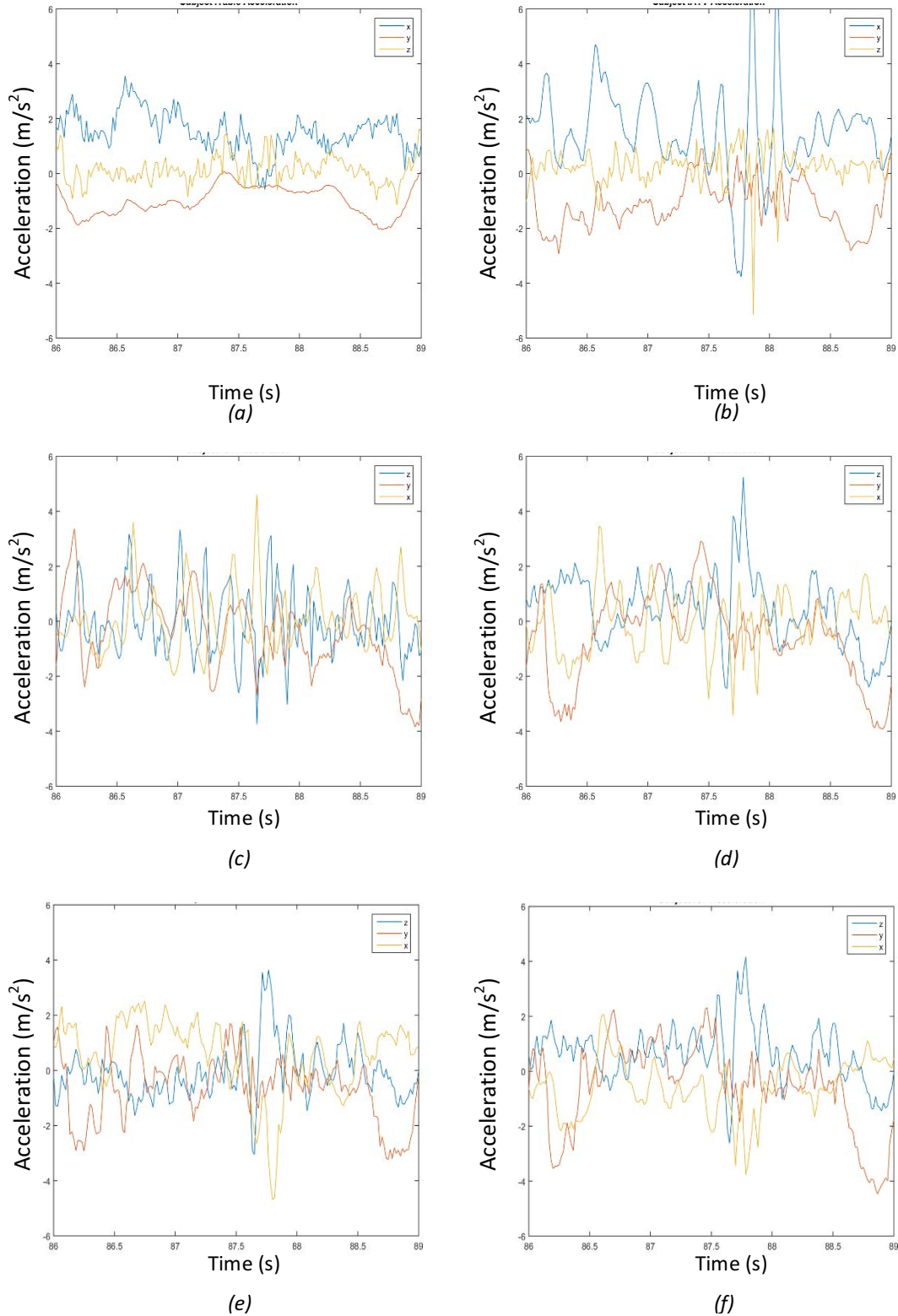


Figure 32: Subject 4's component accelerations during the instability event. S1 and T10 accelerations show an increase relative to the table and ATV with components in the X, Y, and Z directions. Inputs were substantial in the positive X-direction.

Subject 6

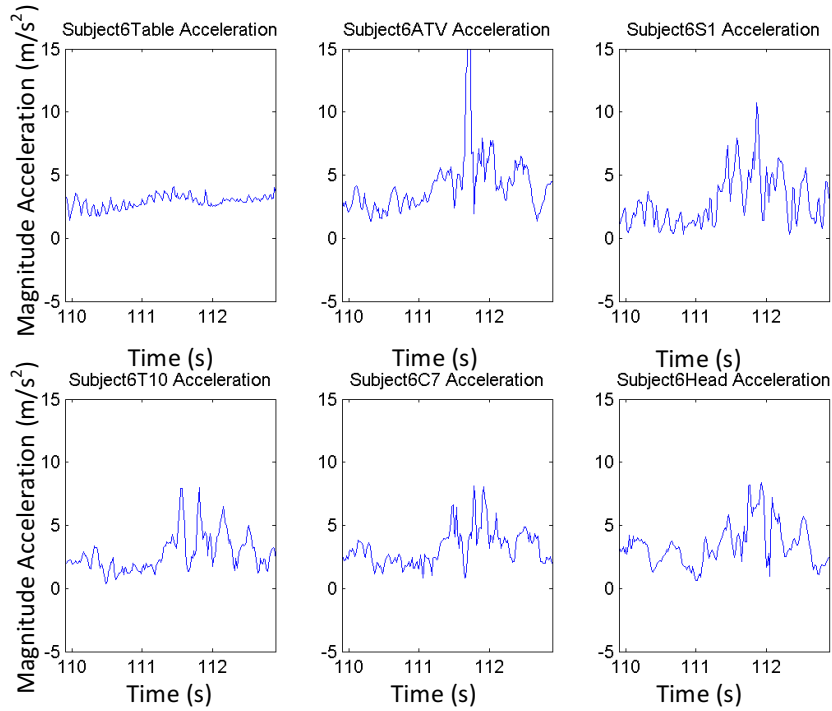


Figure 33: Acceleration at the table, ATV, S1, T10, C7, and the head of Subject 4. The peak acceleration is seen in the center of the plot. It is most evident for body and ATV accelerations.

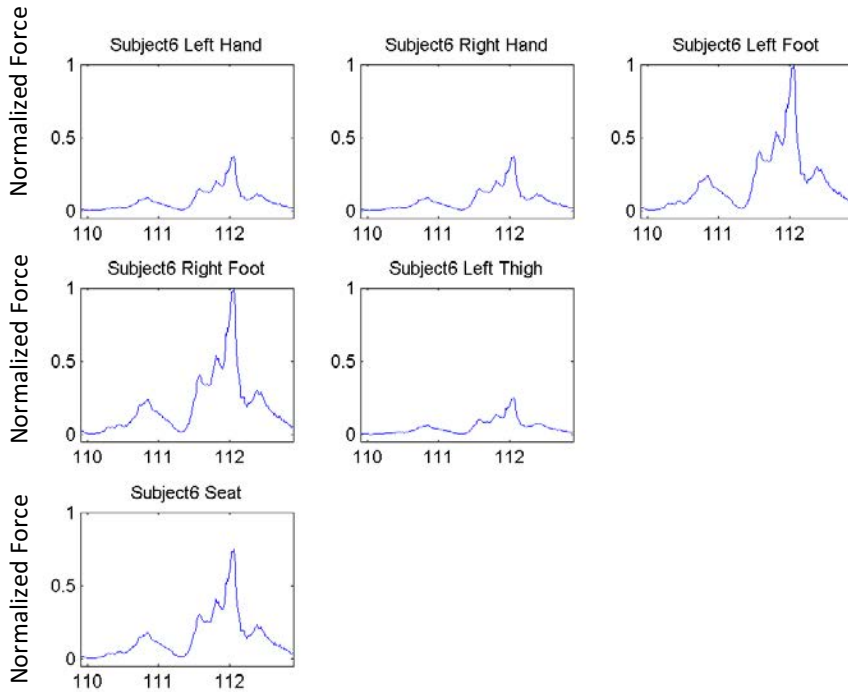


Figure 34: Reaction forces at the left hand, right hand, left foot, right foot, left thigh, and seat for subject 4. The force peak is seen across the system at roughly 112 seconds. Time in seconds is on the x-axis.

## Discussion

The results showed that the ATV simulator could be a useful tool in helping to characterize a potential operator's instability and loss of control during ATV riding. Five samples were selected of so-called "events," or moments where high-magnitude accelerations at the table and high acceleration on the body closely matched with high-magnitude forces measured by the sensing system at different locations where the human has contact with the ATV, such as the handlebars and the foot support. The hypothesis behind the analysis was to identify the time sequences at these events when sudden input accelerations from the table and the ATV resulted in a sudden increase in accelerations and angular velocities in the operator and whether the sudden increase in forces that could be detected by the system were evident following such events. When considering the progression of the "input acceleration, output acceleration, force reaction" chain, it was important to note that certain factors would shift each signal slightly in time. That is to say that the ATV's acceleration would shortly follow the table's acceleration, and the head acceleration would shortly follow the ATV's acceleration, and these acceleration events would be terminated by a sudden increase in the reaction forces at different locations on the ATV. Additionally, it was considered that multiple factors could impact the time that would lead to the resulting reaction forces on the ATV used to stabilize the subject. These factors included, but may not be limited to, reaction time, distractions, tiredness, and disorientation.

One test of the proposed hypothesis is to look to the results from Subject 1 (Table 1) to show the progression in time of acceleration to reaction force. At 33 seconds into the trial, a large acceleration impacted the table and subsequently accelerated the ATV. Soon after, the subject's head accelerated, and roughly one second later, a sudden increase in forces was measured across the ATV system, demonstrating the subjects opposing the acceleration by inducing forces on the ATV to regain stability and control of the machine. Looking further into the components of the accelerations (Figure 31) at the impact moment, the table and ATV experience a strong positive acceleration in the X and Z directions. In response, the subjects' body accelerometers all read strong negative Z-direction and positive X-direction, which may suggest a major change in posture or global position. By the time the subject applied strong forces upon the ATV, the acceleration and angular velocity readings had subsided, showing that control of the machine had been reestablished.

Subject 4's results similarly showed evidence of the subject becoming unstable and then regaining stability. However, Subject 4 regained stability within half a second, which is twice as fast as Subject 1 was able to. At 86.43 seconds, a sudden acceleration occurred as shown by the magnitude plot. Looking to the component accelerations, there were accelerations in the positive x-direction and negative z-direction. At 86.6 seconds, the acceleration was transferred to the head of the subject moving in the negative x-direction and negative z-direction. At 87.03 seconds into the trial, forces across the system spiked, and the accelerations returned to normal. This was a consistent case across subjects as can be seen by the variety of selected frames. Full files for all subjects can be found in the appendix.

This cycle of sudden input acceleration, output acceleration, instability, reaction, and reestablishment of stability is key to identifying an operator's capacity to safely operate an ATV, whether it is occupationally or recreationally. In the case of this study, most subjects reported no fatigue or other initial wellness issues. Additionally, none of the subjects showed signs of ADD or ADHD. These measures are of note because any of the wellness metrics or a potential for distraction could have led to a higher risk of instability or loss of control as reaction times to input increase.

This could be especially important when applied to the case of agricultural workers. Work shifts in agriculture can often last long periods of time or occur at unusual hours. Fatigue and tiredness could result from these conditions and put workers at risk for loss of control or instability, which puts a worker at risk for occupational injury. Additionally, non-ATV-related work in agriculture could cause fatigue and sweating. Sweating could reduce the strength of the linkage between the operator and the machine. In a high-input acceleration situation, this could lead the hands to slip and expose the operator to a potential for injury.

Situations such as those listed in the previous paragraph are examples of future directions for study using this ATV simulator that could assist with gaining insight into loss of control under many conditions without putting subjects at significant risk as could result from a live field study of operating ATVs in sub-peak conditions. These conditions are derived from both occupational and recreational situations that could pose risks to operators. In sub-peak conditions, studies relating to occupational risk could analyze the effect of fatigue from work, fatigue from ATV operation, tiredness, or sweating. In recreational settings, drunkenness, distracted operating, and operation of an improperly sized ATV are prospects for future work. Additionally, medical

conditions could be studied for their impact on the risk of instability in operators from both parties. The data in the results section and in the appendix serve as a baseline for the studies listed above.

Future studies could also take advantage of new technologies and sensors. In this study, a five-camera motion capture system was used. Due to the small number of cameras, capabilities were limited by factors such as small capture space and noisy raw data. Motion capture data would be useful to analyze how the body physically changes posture before, during, and after instability events and the regaining of stability. Electromyography (EMG) sensors could also yield useful data as to muscle activation and muscle fatigue, which could give insight into methods used for regaining stability and the effect of fatigue on reaction time and stabilization ability. Lastly, small load cells that could be integrated into the ATV's components would permit comparison between subjects not just within a trial for each subject's abilities.

## Chapter 7: Conclusion

Operating all-terrain vehicles injures and kills many people every year, whether it is in occupational or recreational settings. Despite the statistics, little work has been done to understand what the causes leading to instability and loss of control are. Field research surveys have been performed to paint a picture of the frequency with which loss of control impacts agricultural workers. Due to the nature of studying loss of control, it is no surprise that few to no field studies have been performed since it could potentially lead to subject injury. Thus, lab studies are an effective way to study loss of control amongst ATV operators without placing them at risk of injury. Once again, few studies had been performed in controlled lab settings to study operator loss of control. The one study found during the literature review was a lab-controlled study analyzing the effects of active riding (Jennissen, et al., 2014). This study used a predetermined simulation file and an ATV that was stripped of its suspension system.

To assist in answering the question of what factors lead to loss of control and instability among ATV operators in a safe, controlled lab setting, a homebrew ATV simulator was developed. The simulator allowed for the subject to traverse numerous terrains at their own pace and with their own methodologies. Subjects all were experienced, in peak condition, reported having no wellness or health issues, and passed a screening for ADD and ADHD. Collection of data for



acceleration, angular velocity, force, and posture were recorded and analyzed for instability events in the file that could lead to key frames for analysis.

A cycle was identified occurring across numerous subjects and scenarios that was used to identify when a subject may have been experiencing a loss of control or a moment of instability. The cycle included:

- 1) A sudden, large input acceleration from the simulation table and ATV.
- 2) The subject showed transmission of the acceleration. This resultant acceleration in the subject was often larger.
- 3) A measured force input across the system, which was considered to be a reaction to the acceleration.

The cycle was then analyzed at the component levels to analyze the subject's reaction motion to the table's reaction motion to identify how certain inputs yielded certain outputs. We identified that, during instability events, peak forces were delayed from the input, as may be expected, and that these reactions varied by as much as .5 seconds. These results in healthy, experienced ATV riders serve as a baseline for future studies into operators in sub-peak conditions such as exhaustion, fatigue, tiredness, and other conditions listed in the discussion.

## Chapter 8: Future Work

Future work is needed to use the ATV simulator to test people under different conditions such as fatigue, medication, age, and gender. These studies would focus on the subject's response time to input and the magnitude of the resulting reaction forces under different terrain conditions. Updated sensing sources could be useful for such tests, including a more traditional, reliable force-sensing system or an updated motion capture system. New data sources could also be useful in studying the subject's reaction to input while operating the simulator; one example is EMG to measure muscle activity.

Future work could also include characterizing system components to identify whether the results of the work in this thesis are related to physical characteristics of the system, including the resonance of the ATV's suspension and tires and the human resonance. Identification of these characteristics could shine a light on any fundamental issues affecting the human-machine interface.

## References

- Brooks, J., Goodenough, R., Crisler, M., Klein, N., Alley, R., Koon, B., . . . Wills, R. (2010, May). Simulator Sickness during Driving Simulation Studies. *Accident Analysis and Prevention*, 42(3), 788-796.
- Carman, A. B., Gillespie, S., Jones, K., Mackay, J., Wallis, G., & Milosavljevic, S. (2010). All terrain vehicle loss of control events in agriculture: Contribution of pitch, roll and velocity. *Ergonomics*, 53(1), 18-29.
- Jennissen, C. A., DeShaw, J., Meusch, J. C., Denning, G. M., McGehee, D. V., & Rahmatalla, S. F. (2014). Dynamic Response of Experienced All-Terrain Vehicle Operators to Simulated Unexpected Terrain Changes. *Proceedings of the Human Factors and Ergonomics Society 58th Annual Meeting*, (pp. 1889-1893).
- Milosavljevic, S., McBride, D. I., Bagheri, N., Vasiljev, R. M., Carman, A. B., Rehn, B., & Moore, D. (2011). Factors associated with quad bike loss of control events in agriculture. *International Journal of Industrial Ergonomics*, 317-321.
- Scarborough, N. (2015). *Number of People Living in Household that own an ATV (All-Terrain Vehicle)*. Retrieved from Statista: <http://www.statista.com/statistics/228874/people-living-in-households-that-own-an-atv-all-terrain-vehicle-usa/>
- Scarborough, N. (2015). *People living in households that plan on buying an ATV (All-Terrain Vehicle)*. Retrieved from Statista: <http://www.statista.com/statistics/228847/people-living-in-households-that-plan-on-buying-an-atv-all-terrain-vehicle-usa/>
- Topping, J., & Garland, S. (2015). *2013 Annual Report of ATV-Related Deaths and Injuries*. Consumer Product Safety Commission. Bethesda: US Consumer Product Safety Commission.

## Appendices

### Appendix A: Force Calibration Figures

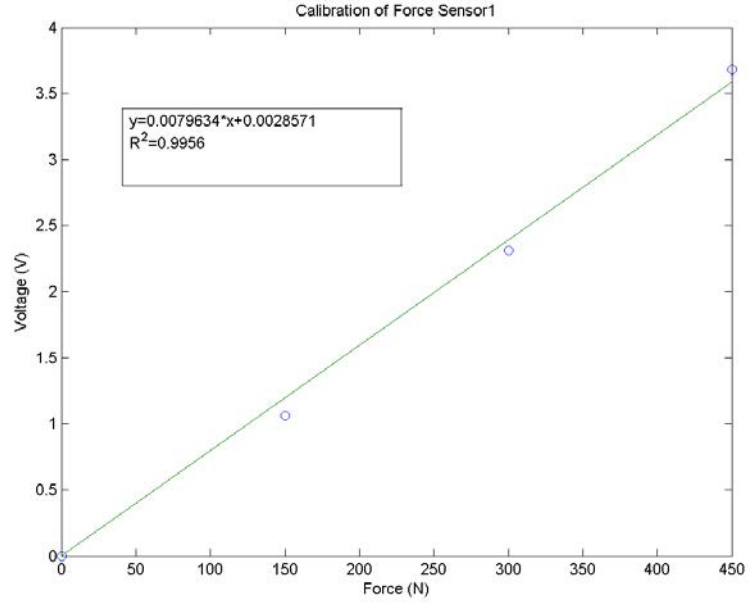


Figure A. 1: Force calibration of FlexiForce sensor. The equation is used to convert voltage to force, and high  $R^2$  value assists with assigning confidence to that value.

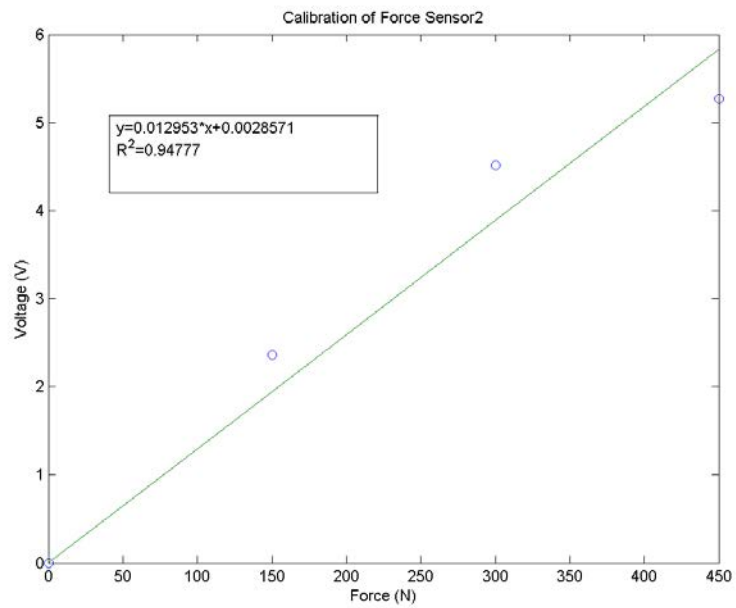


Figure A. 2: Force calibration of FlexiForce sensor. The equation is used to convert voltage to force and high  $R^2$  value assists with assigning confidence to that value.

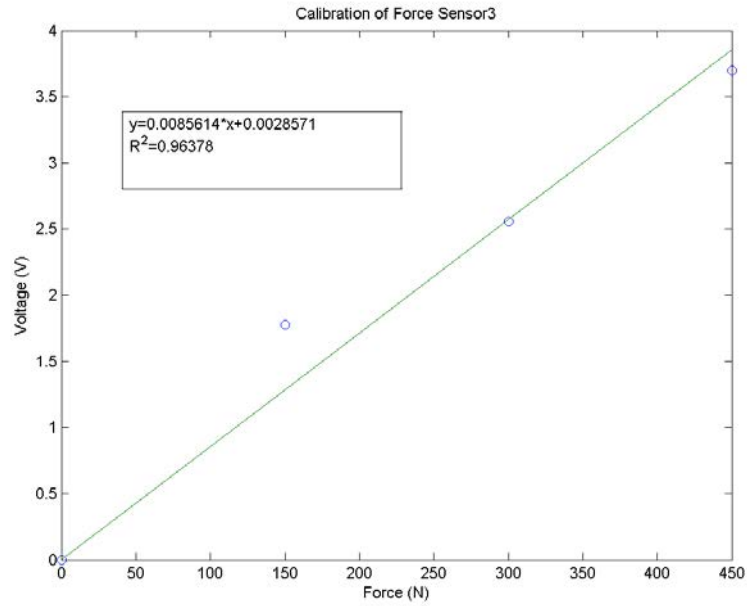


Figure A. 3: Force calibration of FlexiForce sensor. The equation is used to convert voltage to force and high  $R^2$  value assists with assigning confidence to that value.

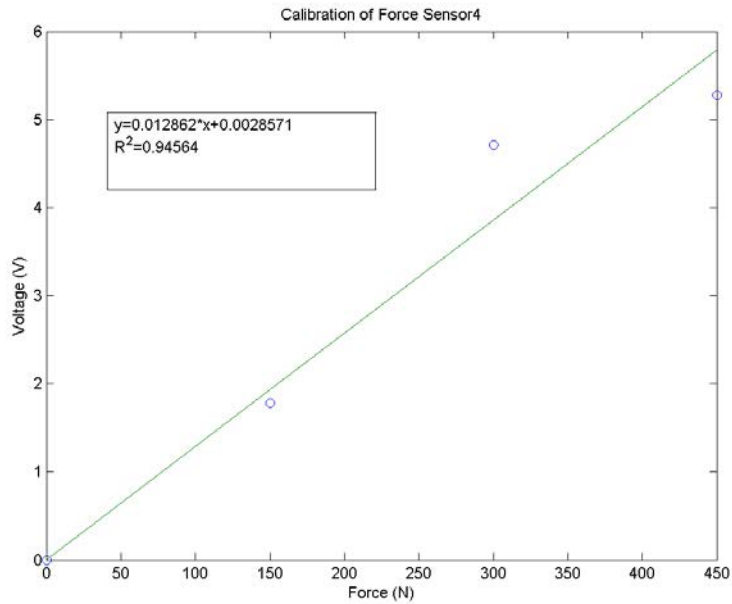


Figure A. 4: Force calibration of FlexiForce sensor. The equation is used to convert voltage to force and high  $R^2$  value assists with assigning confidence to that value.

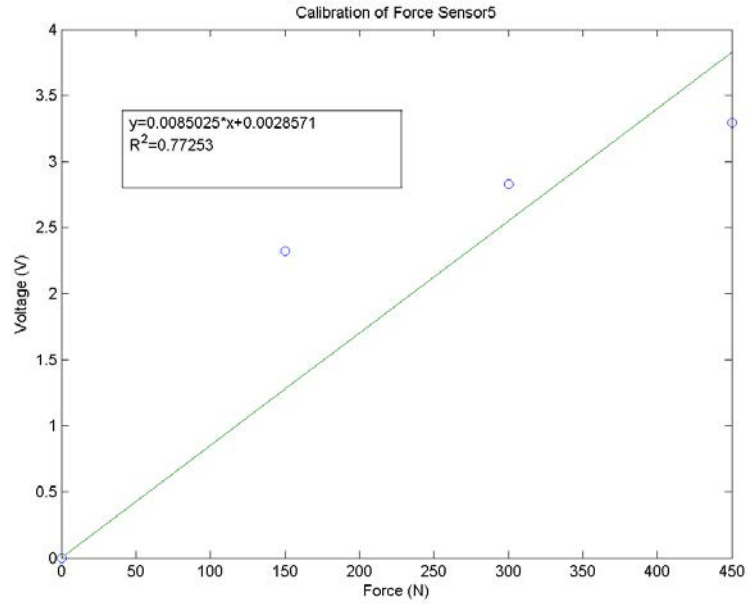


Figure A. 5: Force calibration of FlexiForce sensor. The equation is used to convert voltage to force and high  $R^2$  value assists with assigning confidence to that value.

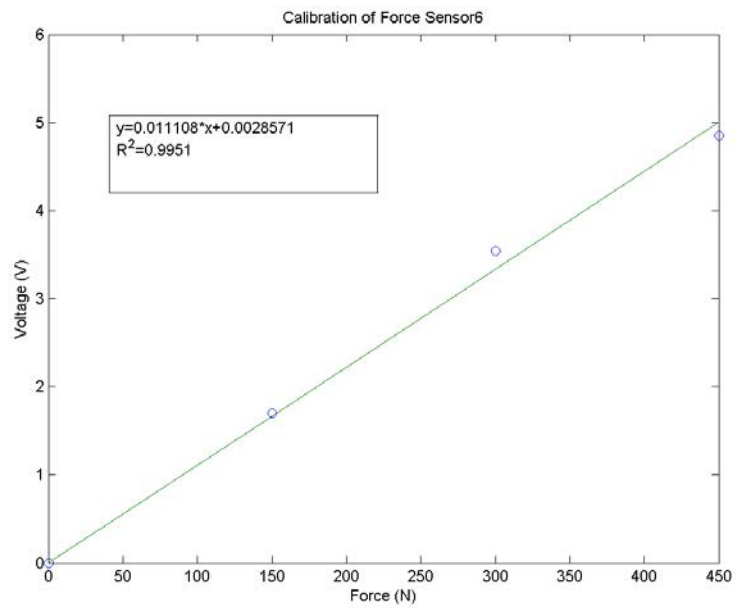


Figure A. 6: Force calibration of FlexiForce sensor. The equation is used to convert voltage to force and high  $R^2$  value assists with assigning confidence to that value.

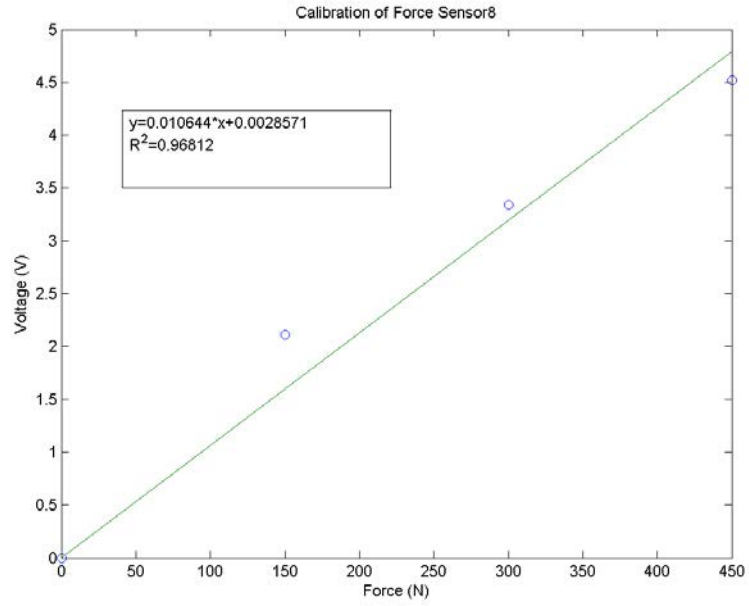


Figure A. 7: Force calibration of FlexiForce sensor. The equation is used to convert voltage to force and high  $R^2$  value assists with assigning confidence to that value.

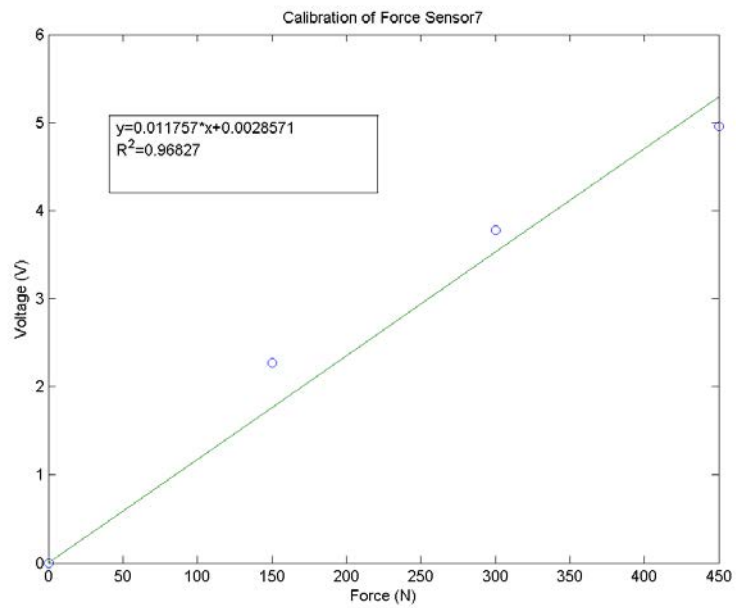


Figure A. 8: Force calibration of FlexiForce sensor. The equation is used to convert voltage to force and high  $R^2$  value assists with assigning confidence to that value.

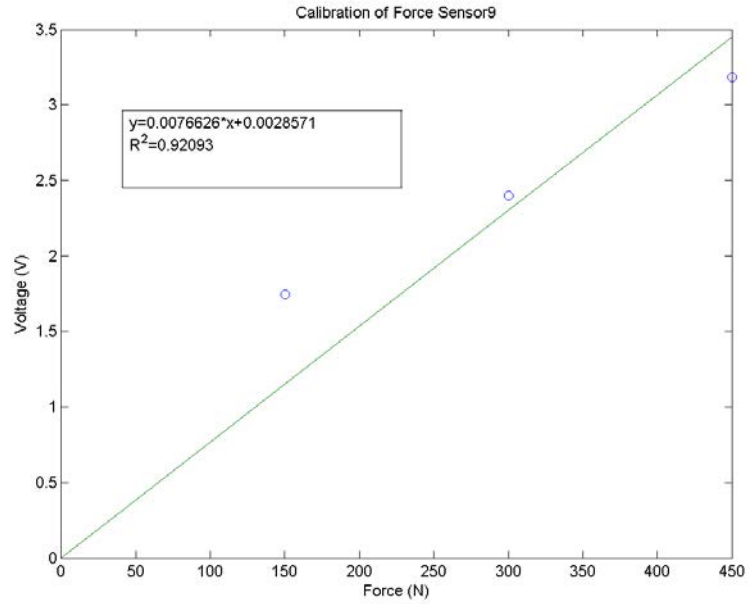


Figure A. 9: Force calibration of FlexiForce sensor. The equation is used to convert voltage to force and high  $R^2$  value assists with assigning confidence to that value.

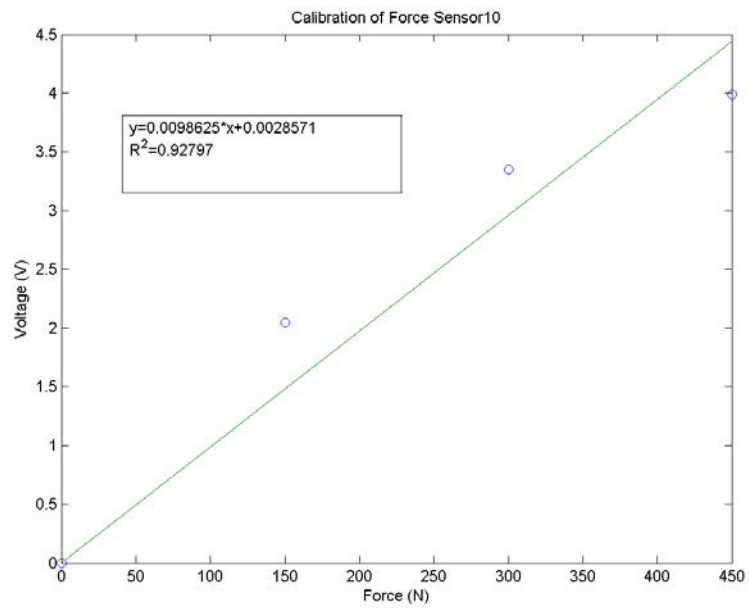


Figure A. 10: Force calibration of FlexiForce sensor. The equation is used to convert voltage to force and high  $R^2$  value assists with assigning confidence to that value.



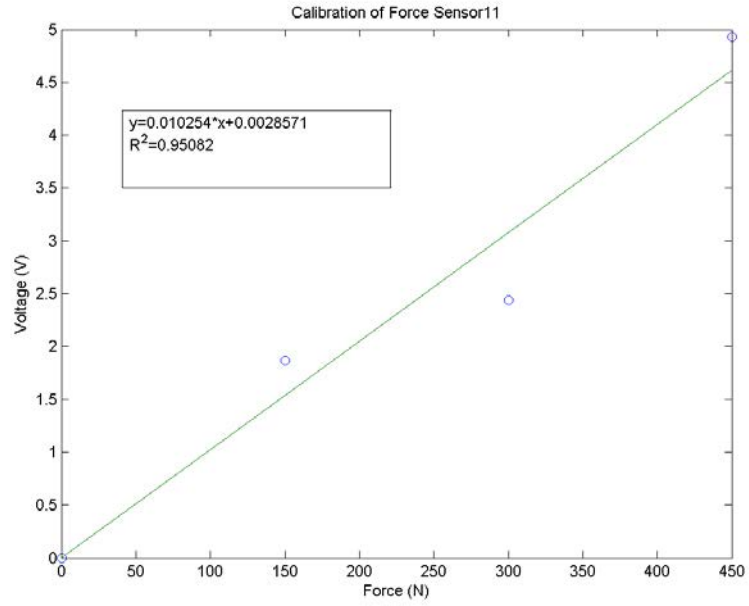


Figure A. 11: Force calibration of FlexiForce sensor. The equation is used to convert voltage to force and high  $R^2$  value assists with assigning confidence to that value.

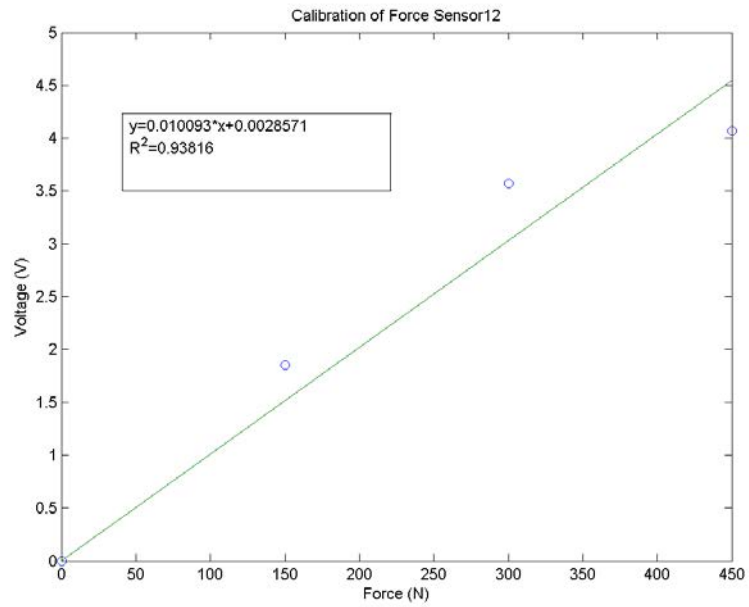


Figure A. 12: Force calibration of FlexiForce sensor. The equation is used to convert voltage to force and high  $R^2$  value assists with assigning confidence to that value.

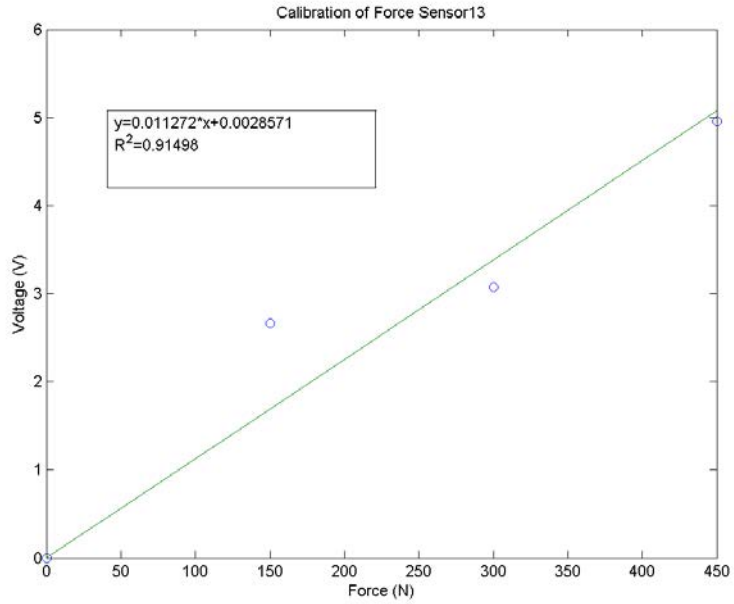


Figure A. 13: Force calibration of FlexiForce sensor. The equation is used to convert voltage to force and high  $R^2$  value assists with assigning confidence to that value.

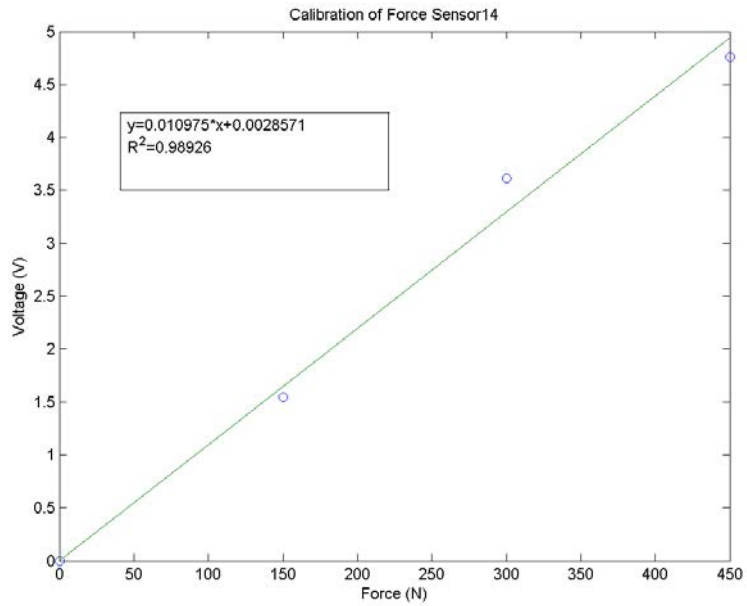


Figure A. 14: Force calibration of FlexiForce sensor. The equation is used to convert voltage to force and high  $R^2$  value assists with assigning confidence to that value.

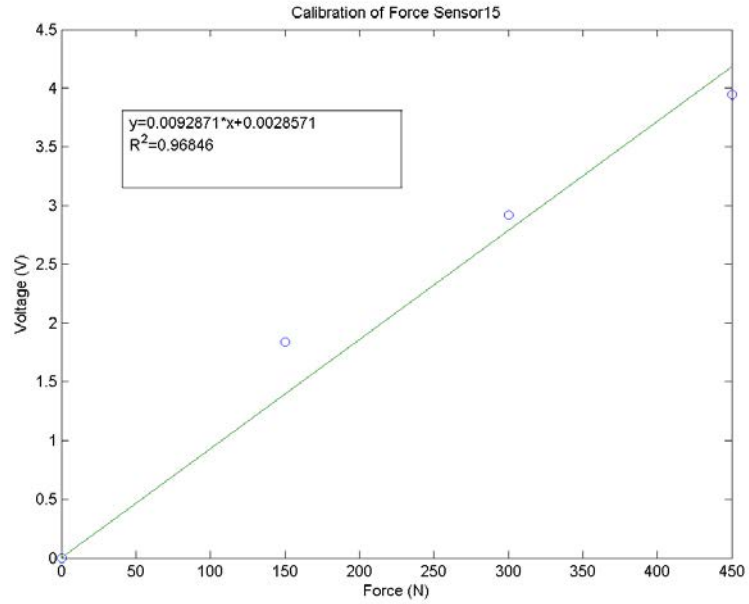


Figure A. 15: Force calibration of FlexiForce sensor. The equation is used to convert voltage to force and high  $R^2$  value assists with assigning confidence to that value.

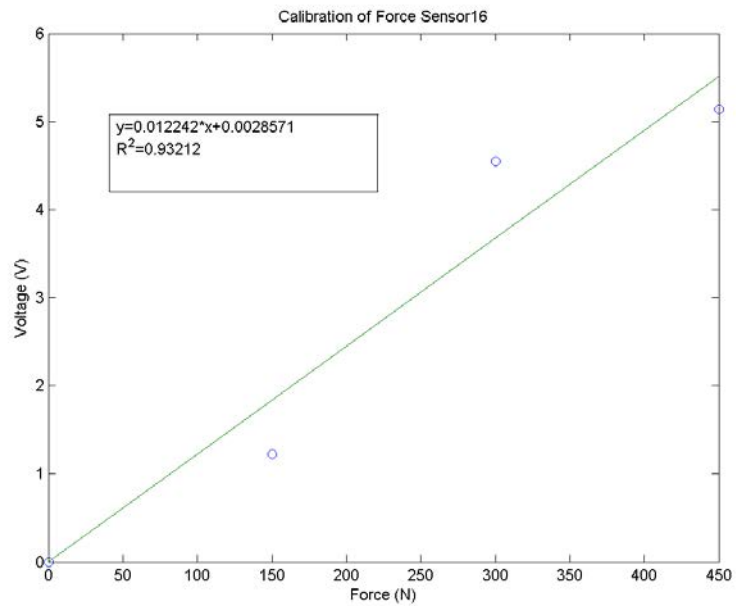


Figure A. 16: Force calibration of FlexiForce sensor. The equation is used to convert voltage to force and high  $R^2$  value assists with assigning confidence to that value.

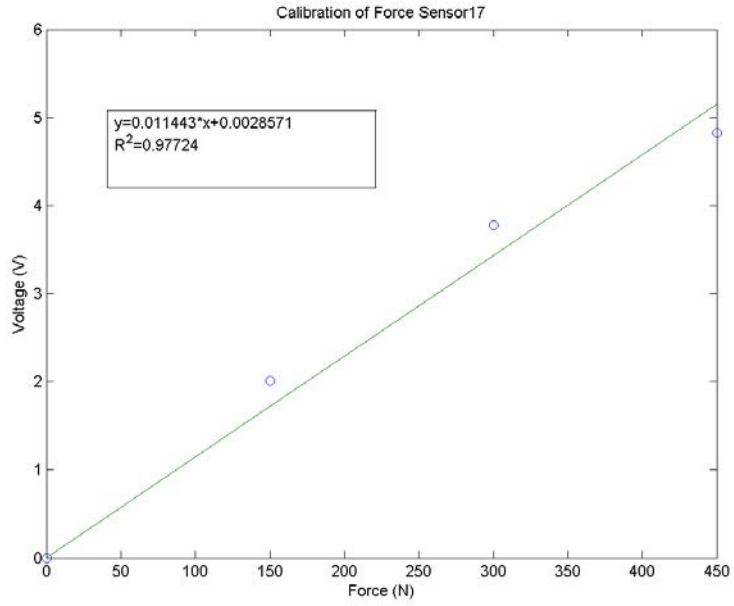


Figure A. 17: Force calibration of FlexiForce sensor. The equation is used to convert voltage to force and high  $R^2$  value assists with assigning confidence to that value.

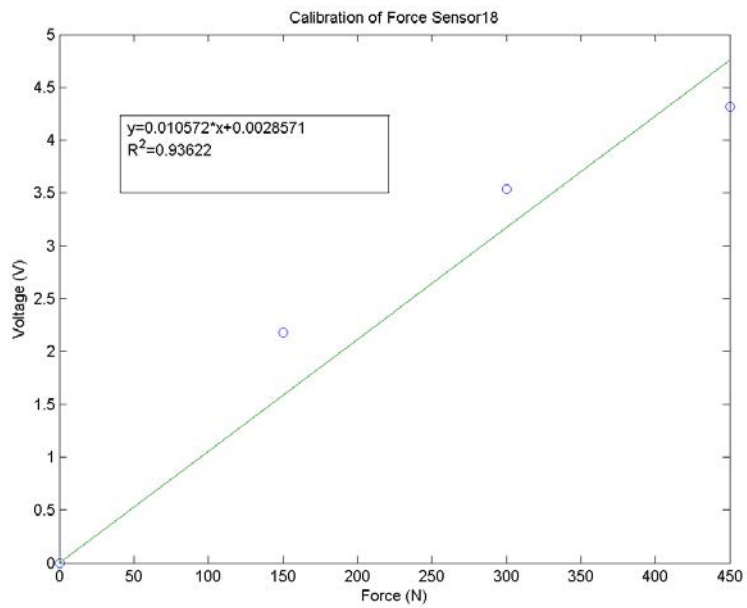


Figure A. 18: Force calibration of FlexiForce sensor. The equation is used to convert voltage to force and high  $R^2$  value assists with assigning confidence to that value.

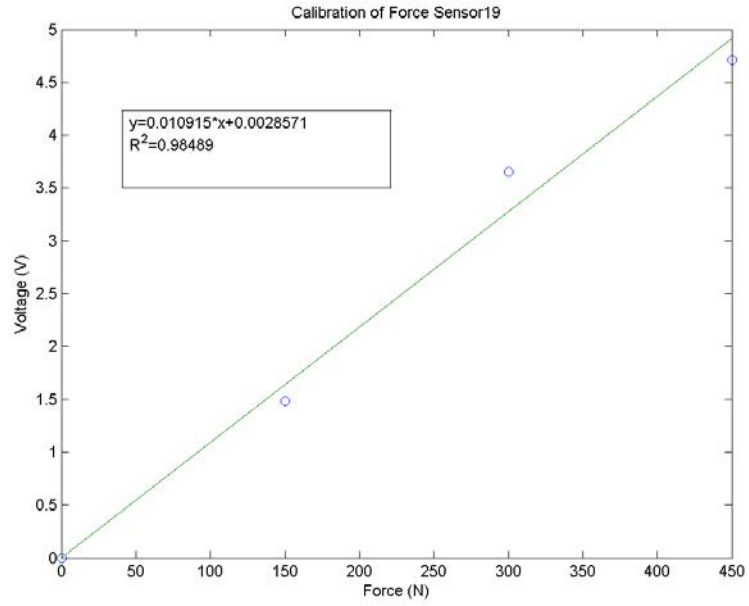


Figure A. 19: Force calibration of FlexiForce sensor. The equation is used to convert voltage to force and high  $R^2$  value assists with assigning confidence to that value.

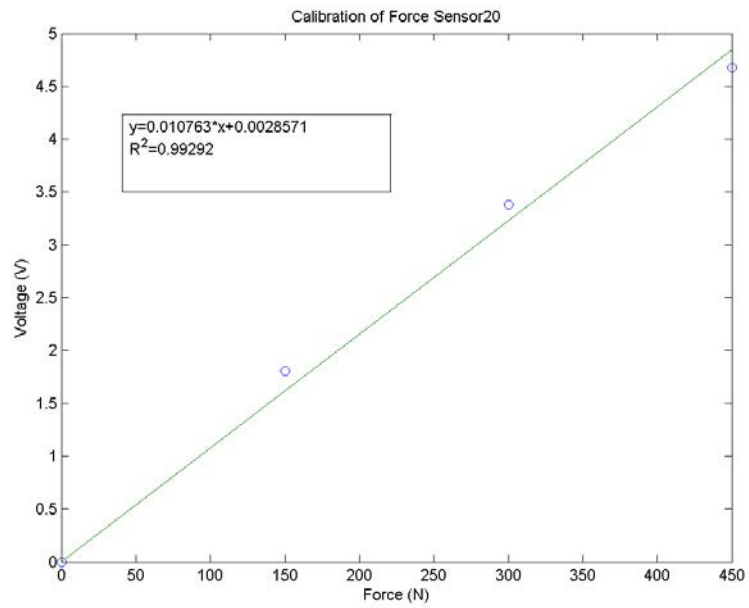


Figure A. 20: Force calibration of FlexiForce sensor. The equation is used to convert voltage to force and high  $R^2$  value assists with assigning confidence to that value.

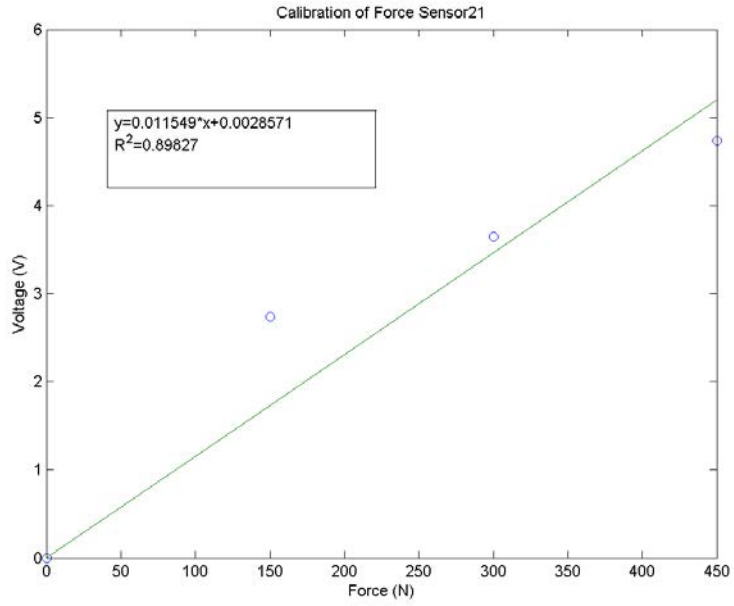


Figure A. 21: Force calibration of FlexiForce sensor. The equation is used to convert voltage to force and high  $R^2$  value assists with assigning confidence to that value.

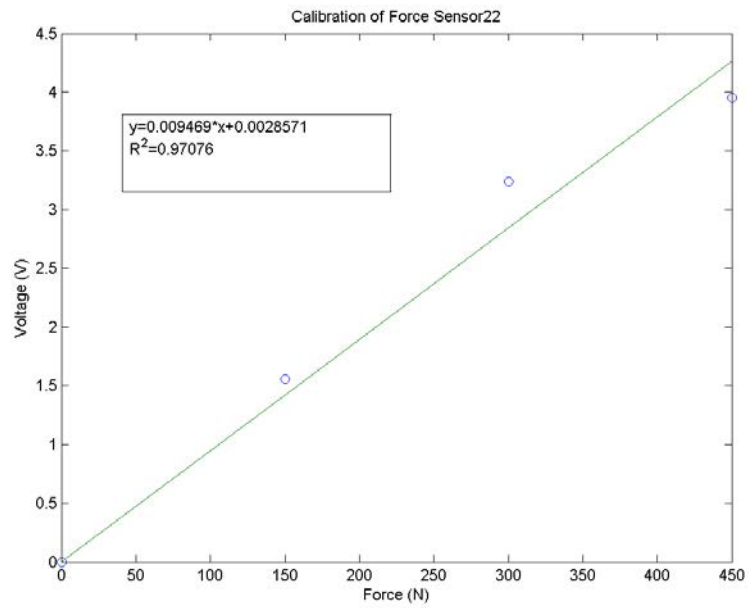


Figure A. 22: Force calibration of FlexiForce sensor. The equation is used to convert voltage to force and high  $R^2$  value assists with assigning confidence to that value.

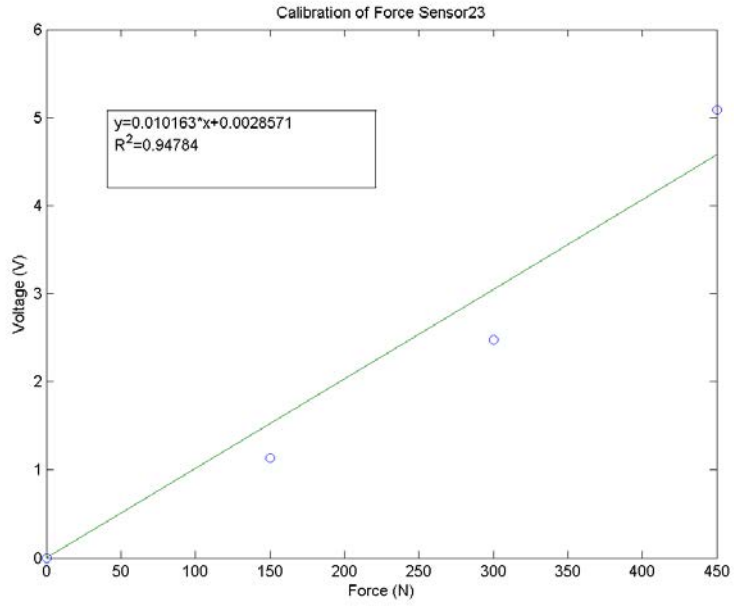


Figure A. 23: Force calibration of FlexiForce sensor. The equation is used to convert voltage to force and high  $R^2$  value assists with assigning confidence to that value.

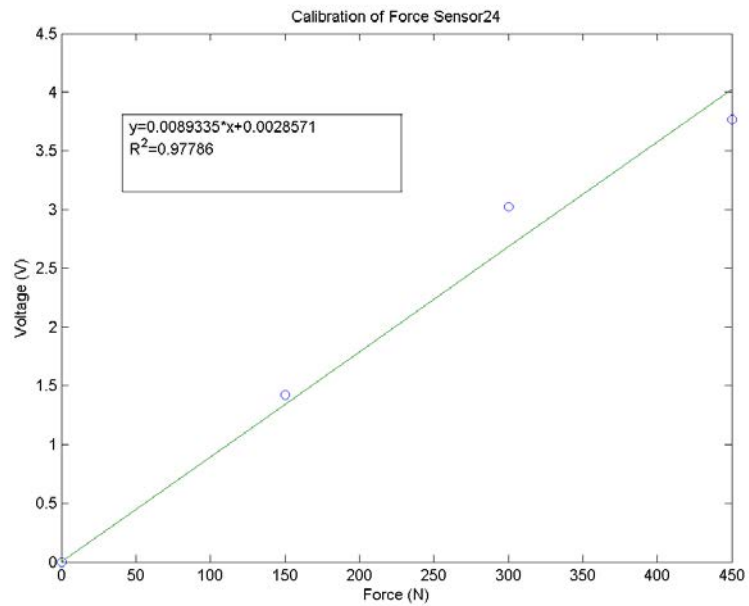


Figure A. 24: Force calibration of FlexiForce sensor. The equation is used to convert voltage to force and high  $R^2$  value assists with assigning confidence to that value.

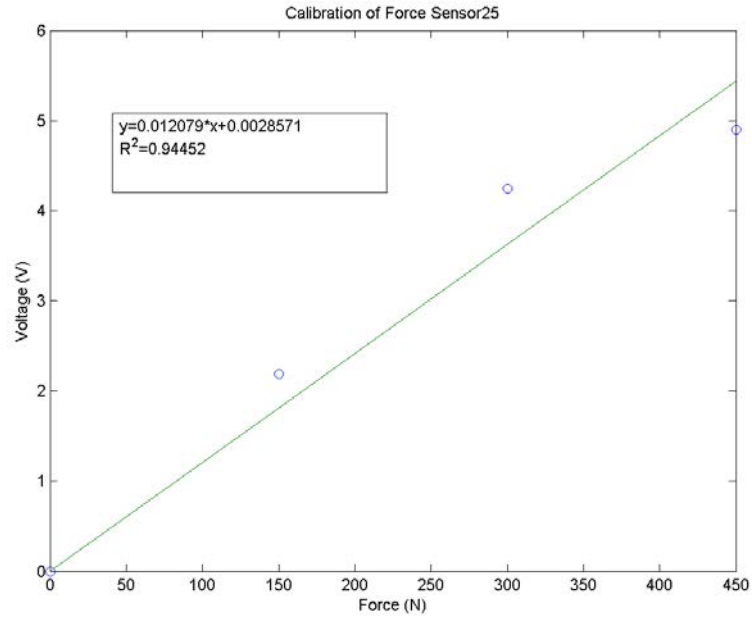


Figure A. 25: Force calibration of FlexiForce sensor. The equation is used to convert voltage to force and high  $R^2$  value assists with assigning confidence to that value.

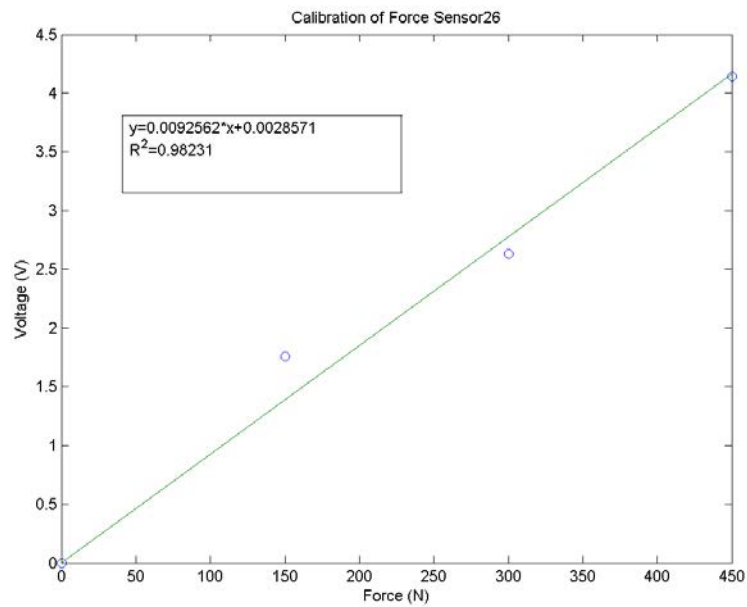


Figure A. 26: Force calibration of FlexiForce sensor. The equation is used to convert voltage to force and high  $R^2$  value assists with assigning confidence to that value.



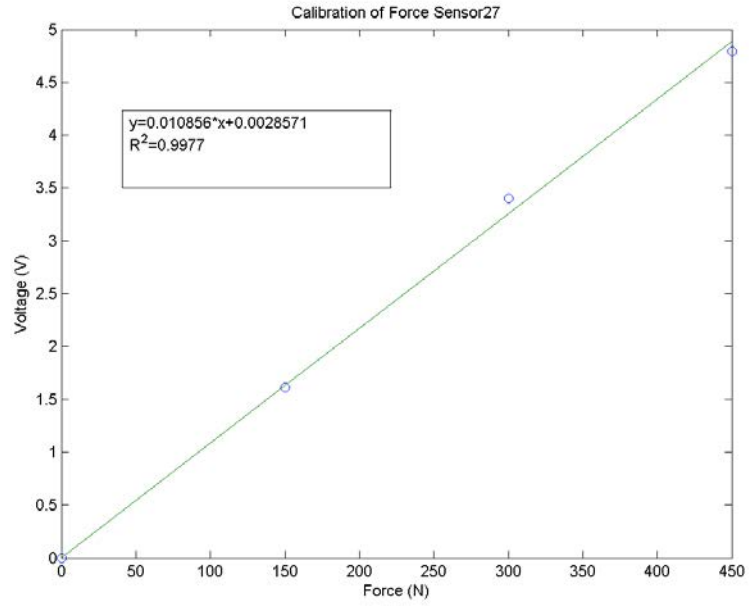


Figure A. 27: Force calibration of FlexiForce sensor. The equation is used to convert voltage to force and high  $R^2$  value assists with assigning confidence to that value.

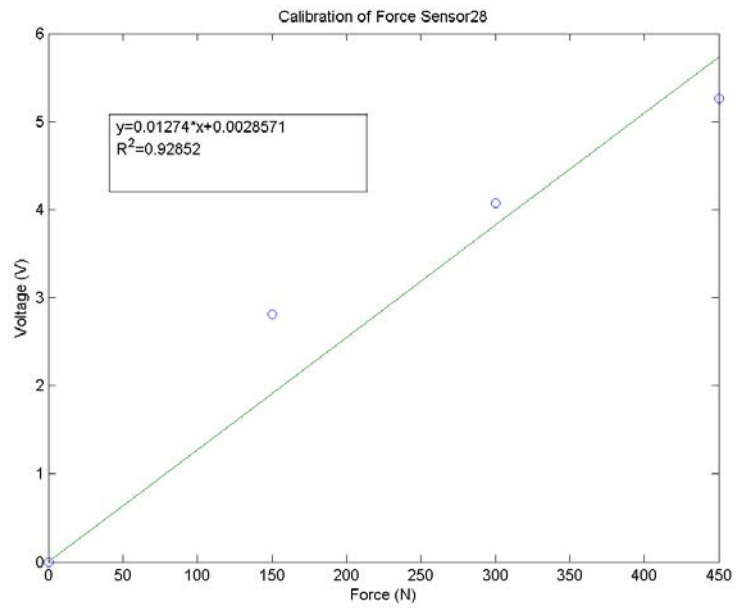


Figure A. 28: Force calibration of FlexiForce sensor. The equation is used to convert voltage to force and high  $R^2$  value assists with assigning confidence to that value.

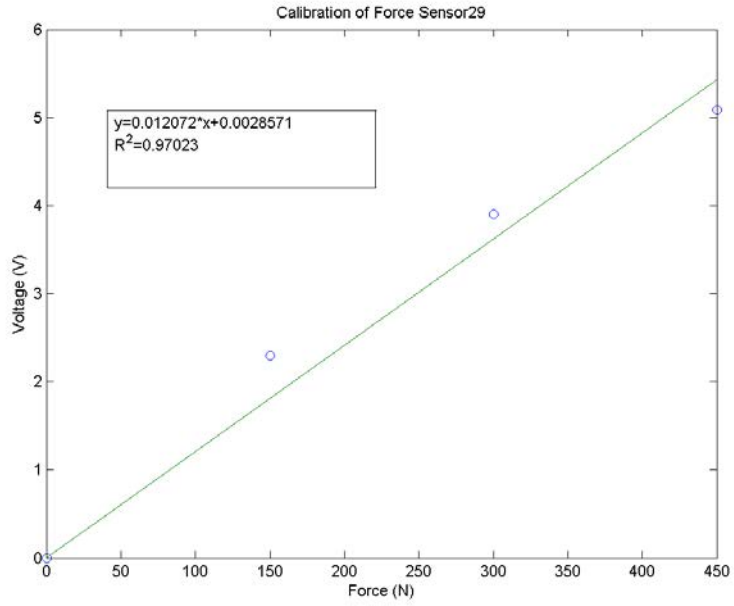


Figure A. 29: Force calibration of FlexiForce sensor. The equation is used to convert voltage to force and high  $R^2$  value assists with assigning confidence to that value.

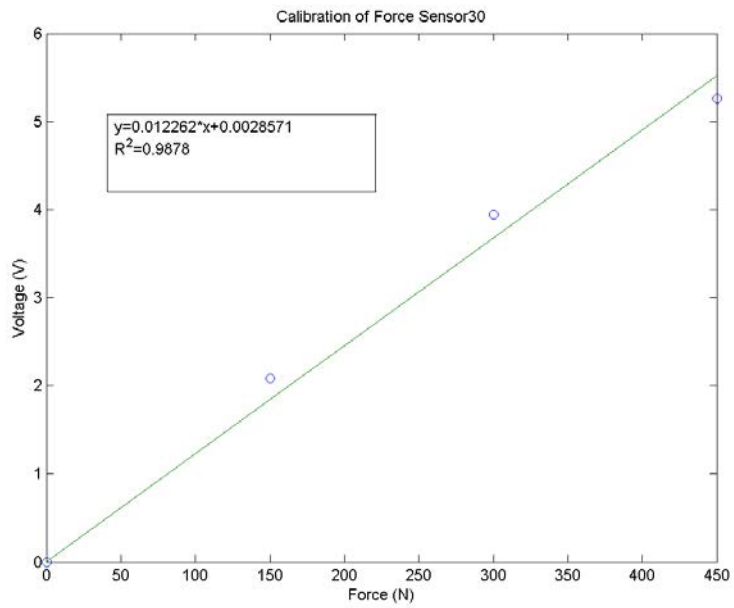


Figure A. 30: Force calibration of FlexiForce sensor. The equation is used to convert voltage to force and high  $R^2$  value assists with assigning confidence to that value.

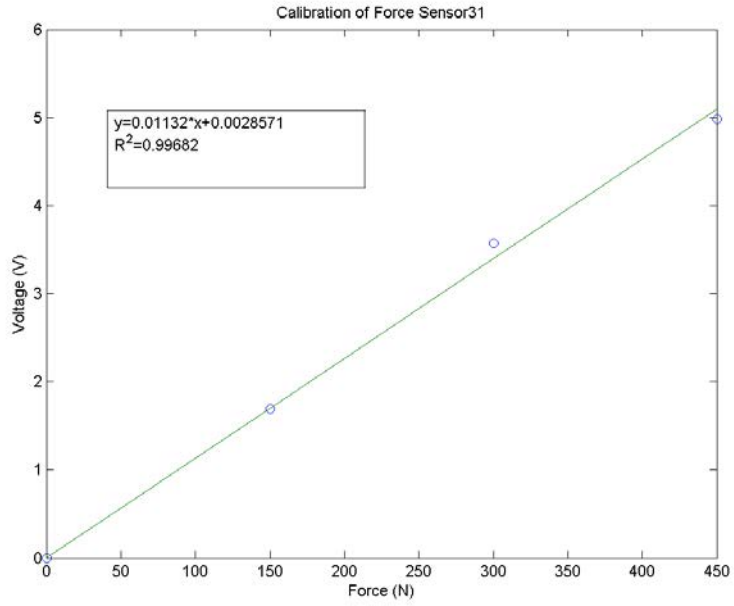


Figure A. 31: Force calibration of FlexiForce sensor. The equation is used to convert voltage to force and high  $R^2$  value assists with assigning confidence to that value.

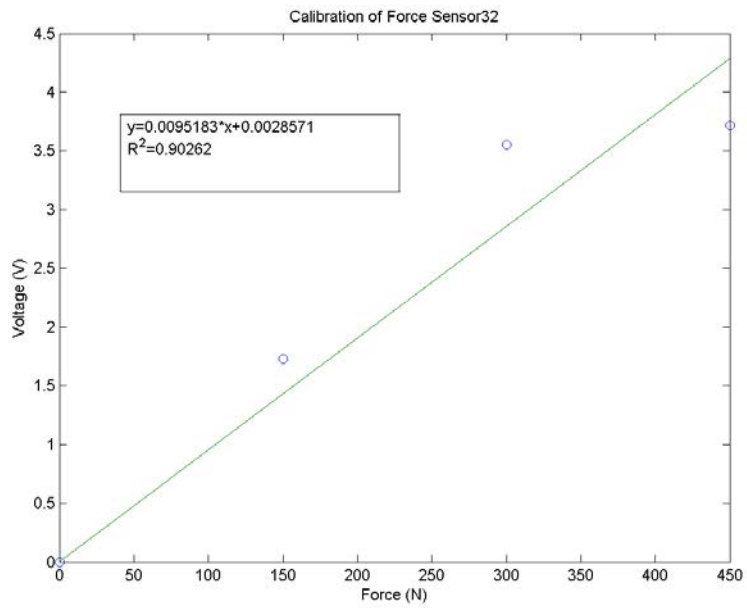


Figure A. 32: Force calibration of FlexiForce sensor. The equation is used to convert voltage to force and high  $R^2$  value assists with assigning confidence to that value.

## Appendix B: Trial Time Series Force Data

### Subject 1

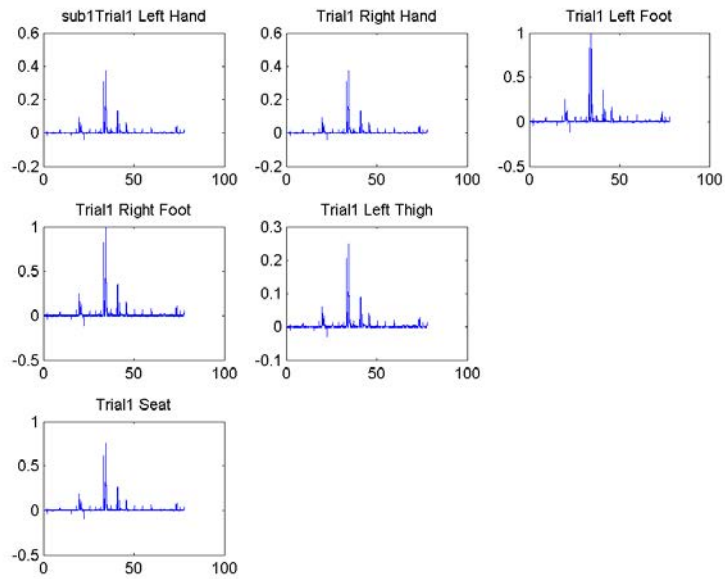


Figure B. 1: Force plots normalized for the peak force across the entire trial and all force sensing areas.

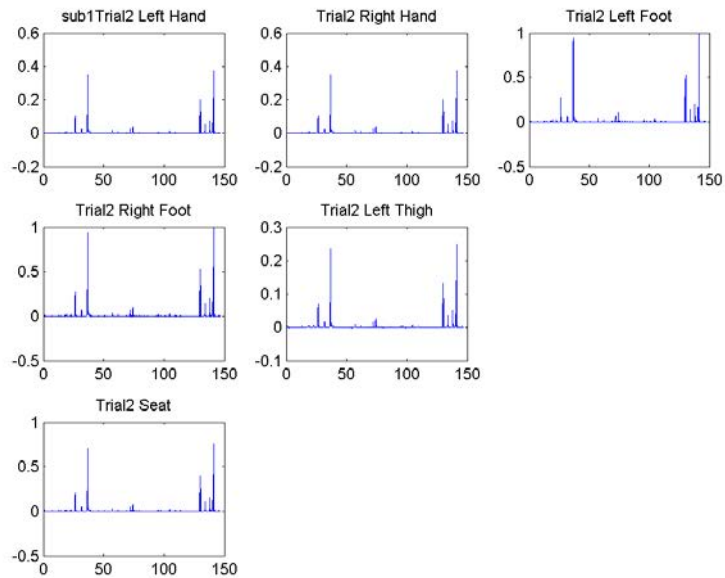


Figure B. 2: Force plots normalized for the peak force across the entire trial and all force sensing areas.

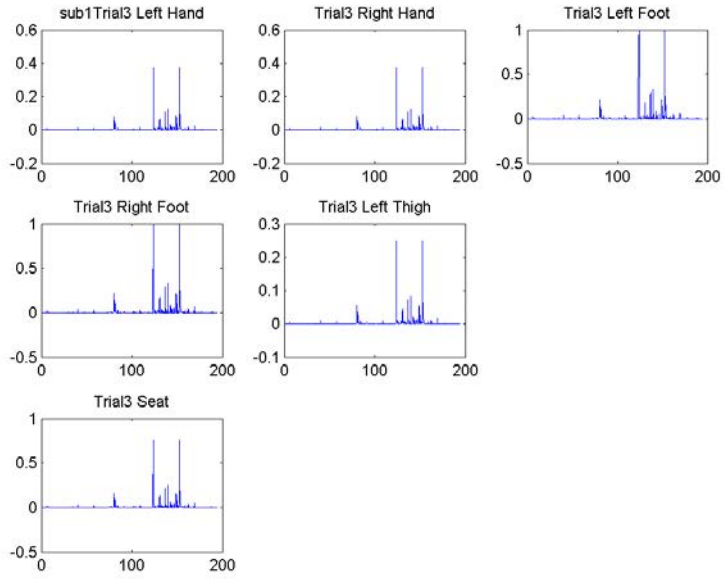


Figure B. 3: Force plots normalized for the peak force across the entire trial and all force sensing areas.

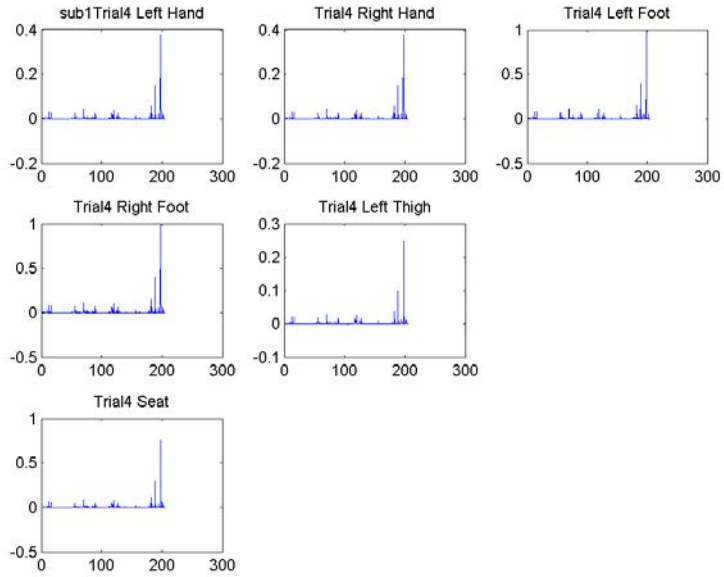


Figure B. 4: Force plots normalized for the peak force across the entire trial and all force sensing areas.

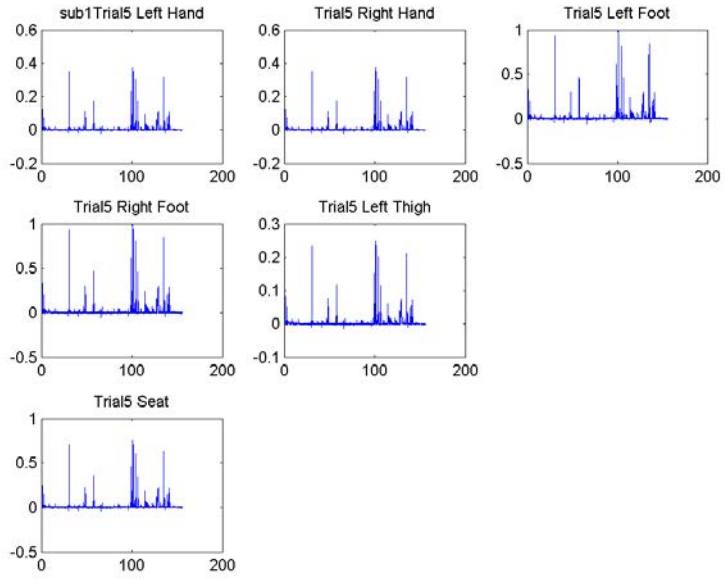


Figure B. 5: Force plots normalized for the peak force across the entire trial and all force sensing areas.

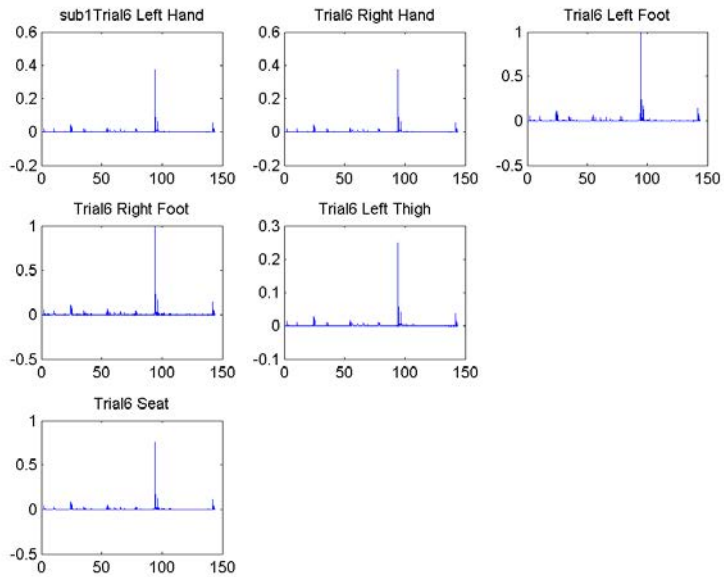


Figure B. 6: Force plots normalized for the peak force across the entire trial and all force sensing areas.

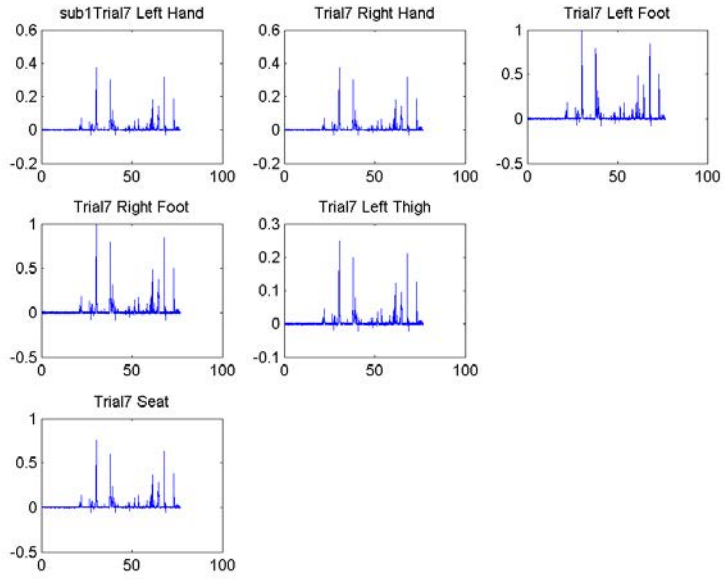


Figure B. 7: Force plots normalized for the peak force across the entire trial and all force sensing areas.

Subject 2

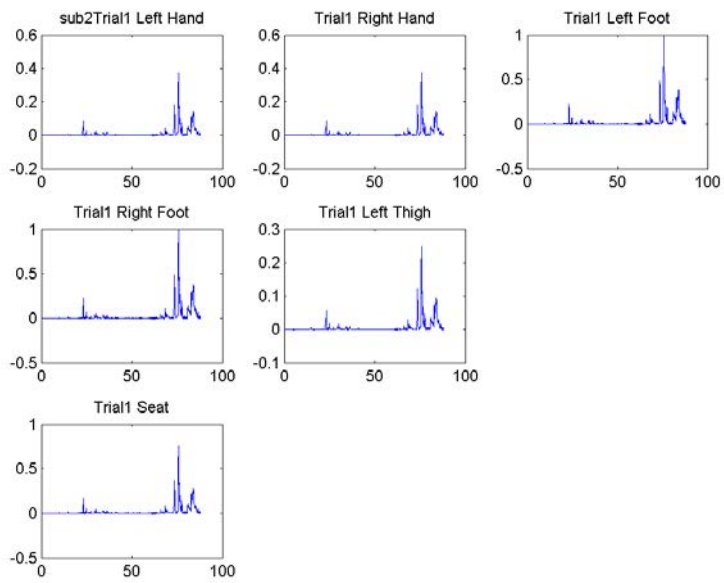


Figure B. 8: Force plots normalized for the peak force across the entire trial and all force sensing areas.

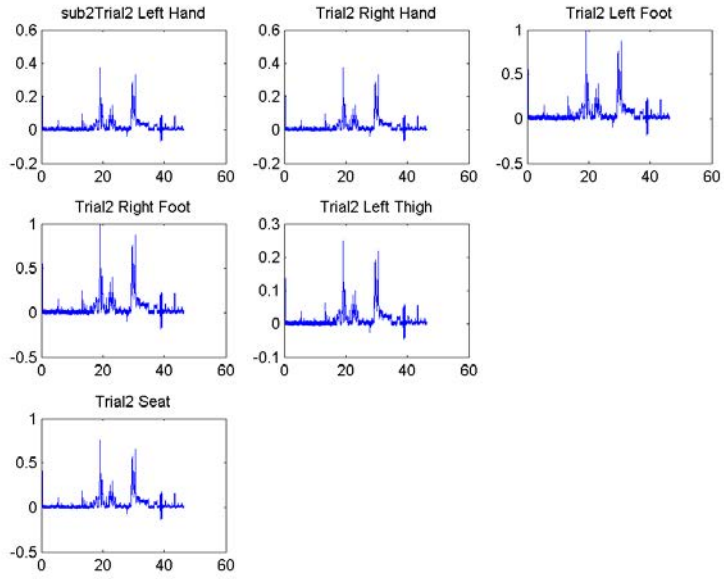


Figure B. 9: Force plots normalized for the peak force across the entire trial and all force sensing areas.

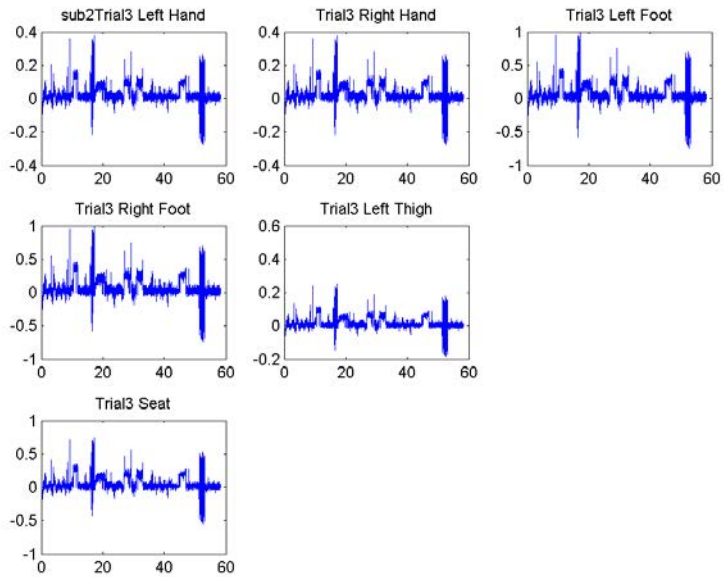


Figure B. 10: Force plots normalized for the peak force across the entire trial and all force sensing areas.



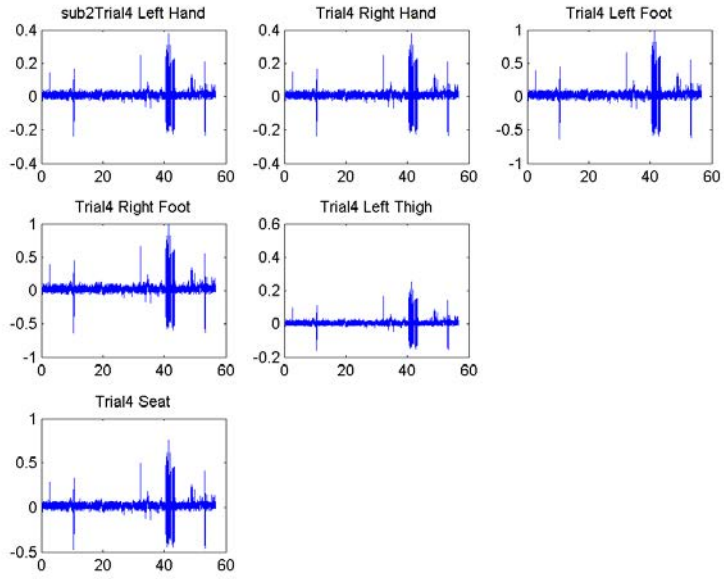


Figure B. 11: Force plots normalized for the peak force across the entire trial and all force sensing areas.

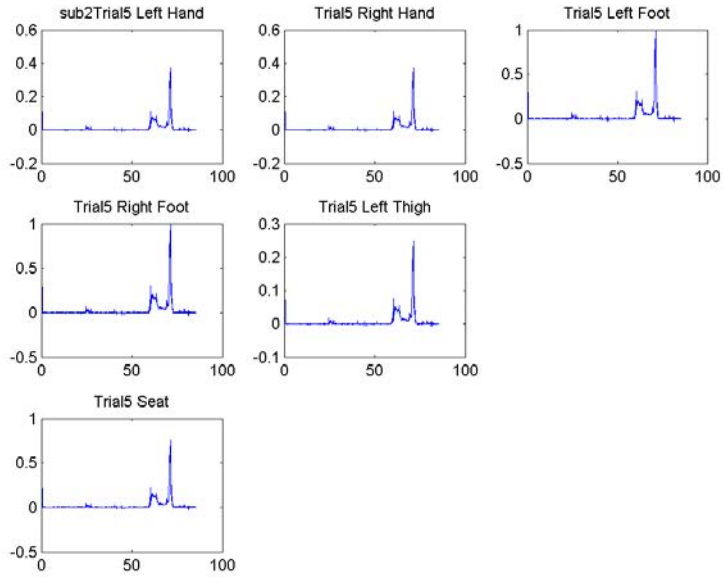


Figure B. 12: Force plots normalized for the peak force across the entire trial and all force sensing areas.

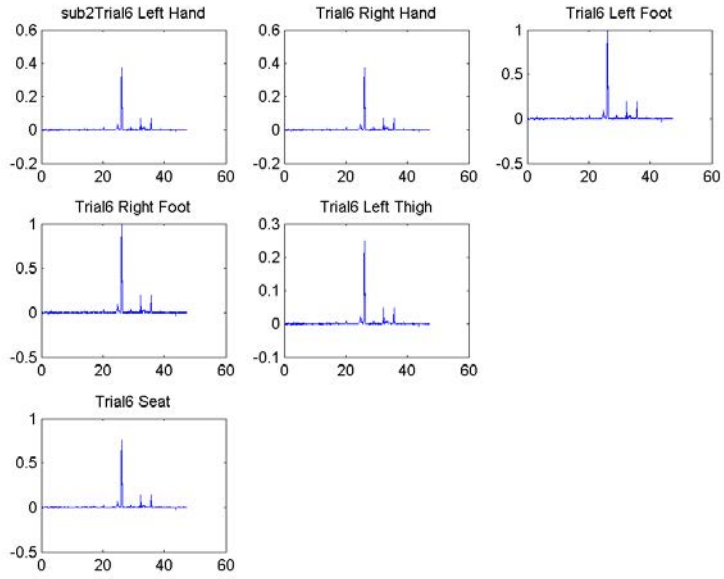


Figure B. 13: Force plots normalized for the peak force across the entire trial and all force sensing areas.

Subject 3

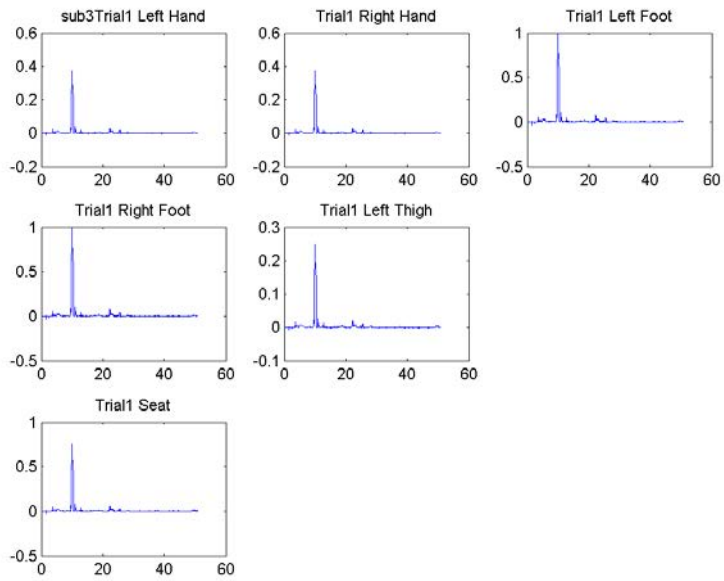


Figure B. 14: Force plots normalized for the peak force across the entire trial and all force sensing areas.

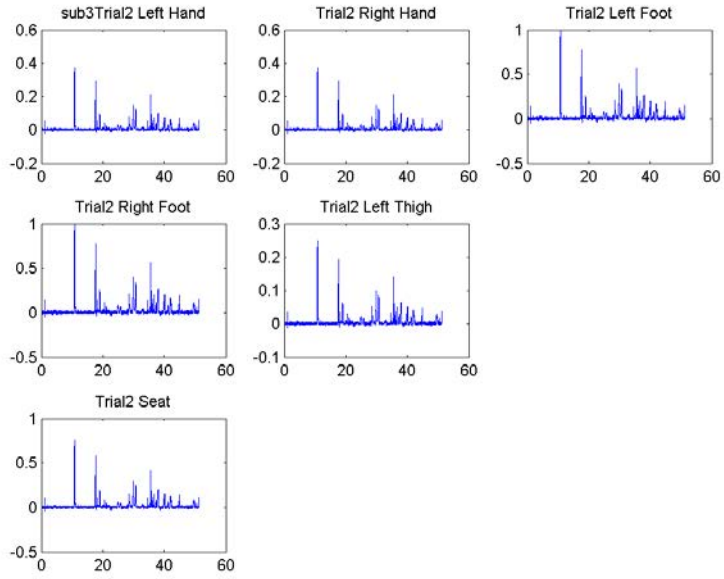


Figure B. 15: Force plots normalized for the peak force across the entire trial and all force sensing areas.

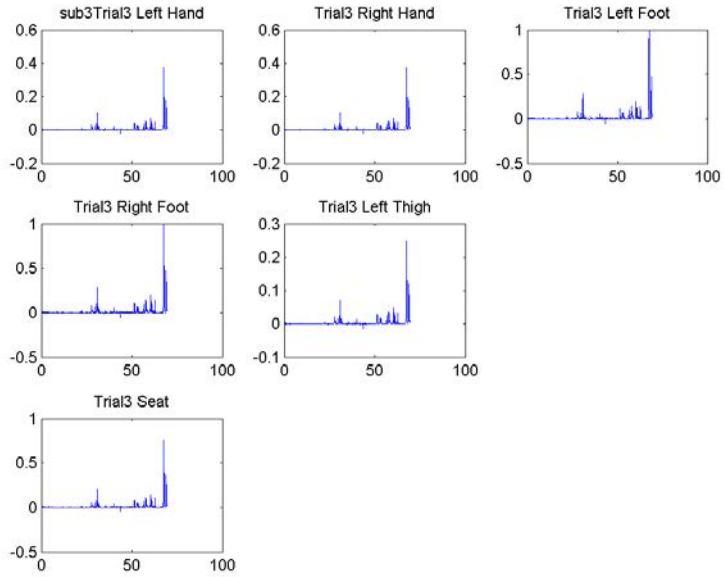


Figure B. 16: Force plots normalized for the peak force across the entire trial and all force sensing areas.

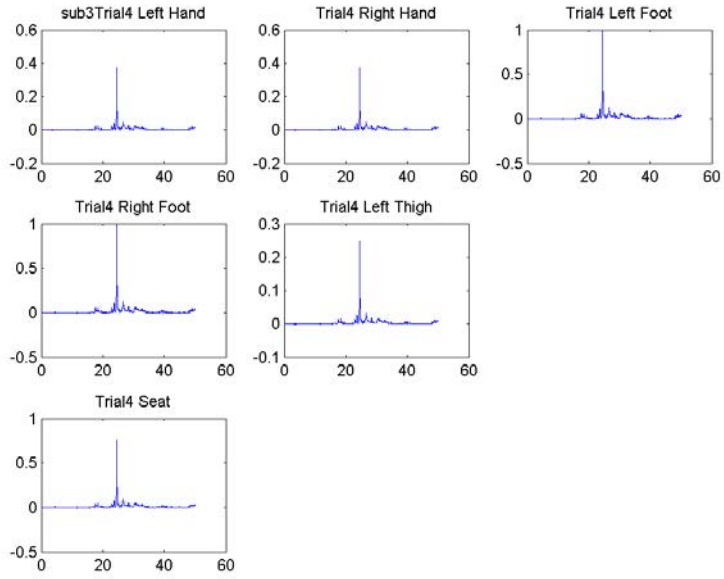


Figure B. 17: Force plots normalized for the peak force across the entire trial and all force sensing areas.

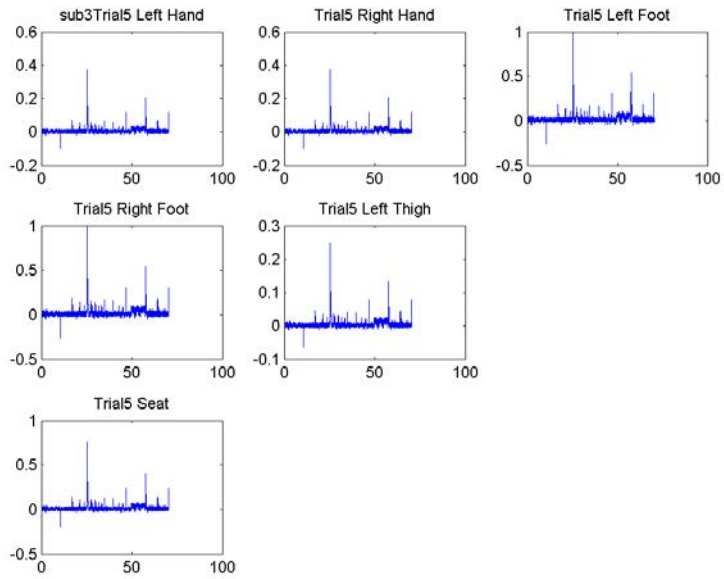


Figure B. 18: Force plots normalized for the peak force across the entire trial and all force sensing areas.

Subject 4

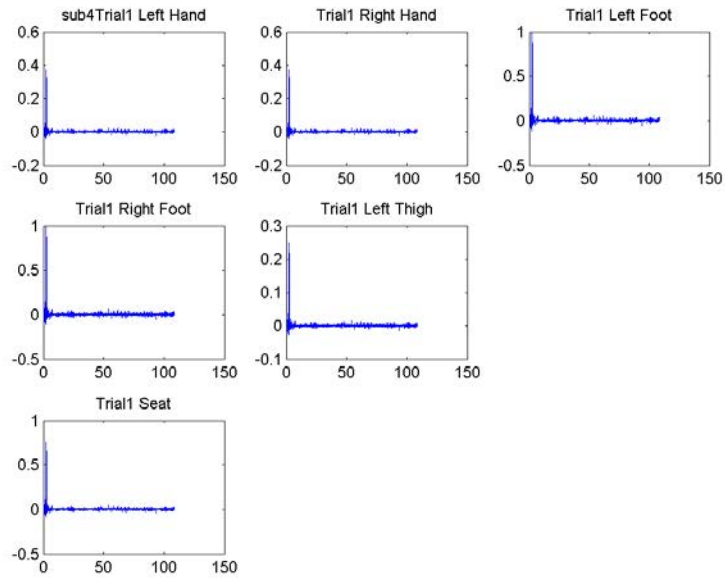


Figure B. 19: Force plots normalized for the peak force across the entire trial and all force sensing areas.

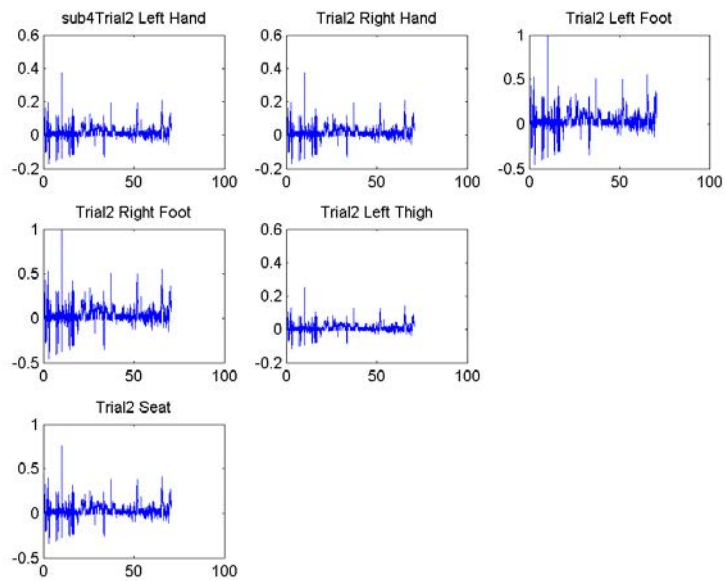


Figure B. 20: Force plots normalized for the peak force across the entire trial and all force sensing areas.

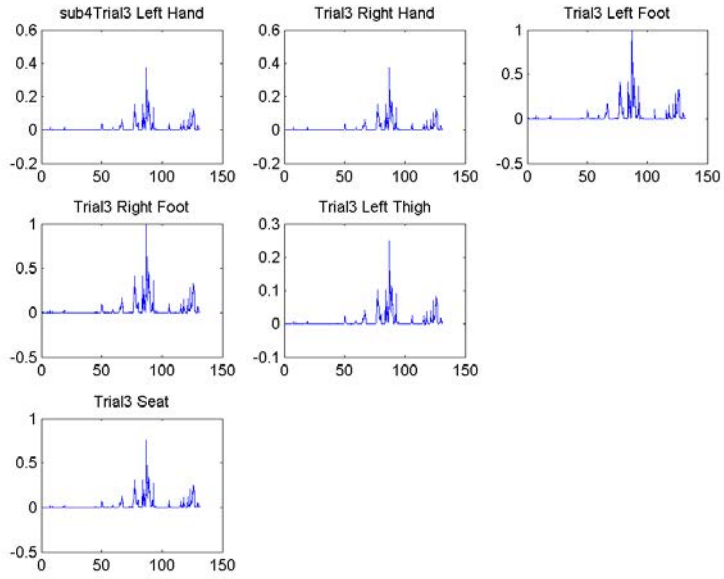


Figure B. 21: Force plots normalized for the peak force across the entire trial and all force sensing areas.

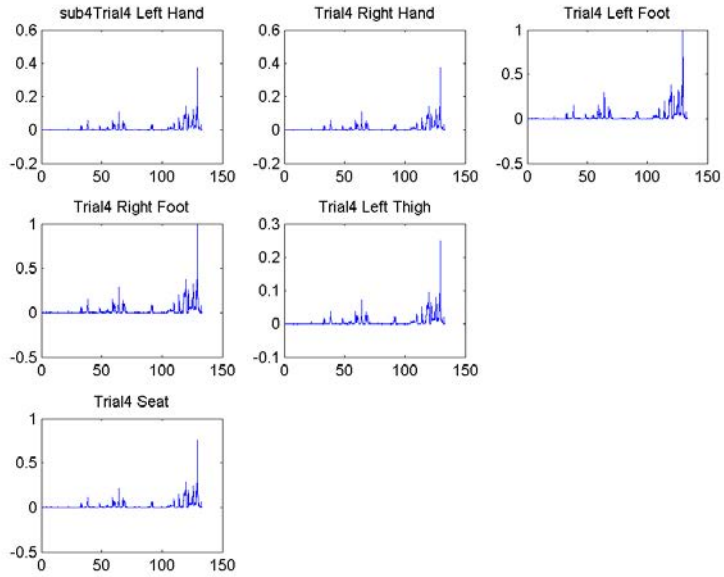


Figure B. 22: Force plots normalized for the peak force across the entire trial and all force sensing areas.

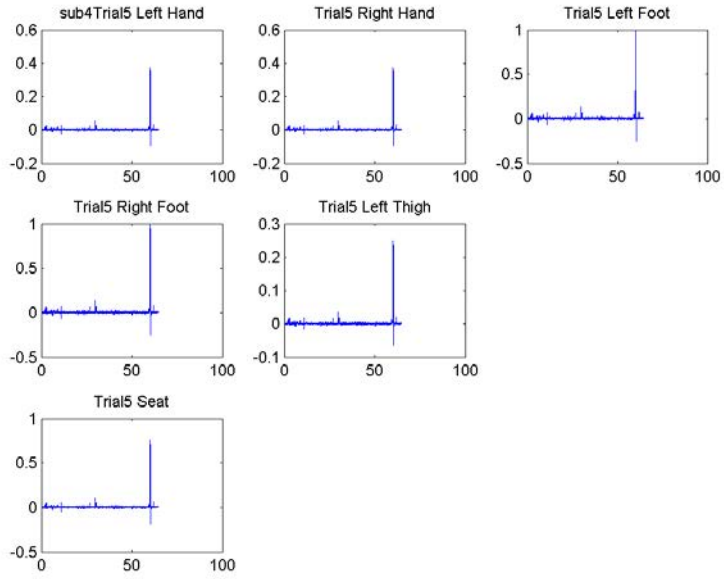


Figure B. 23: Force plots normalized for the peak force across the entire trial and all force sensing areas.

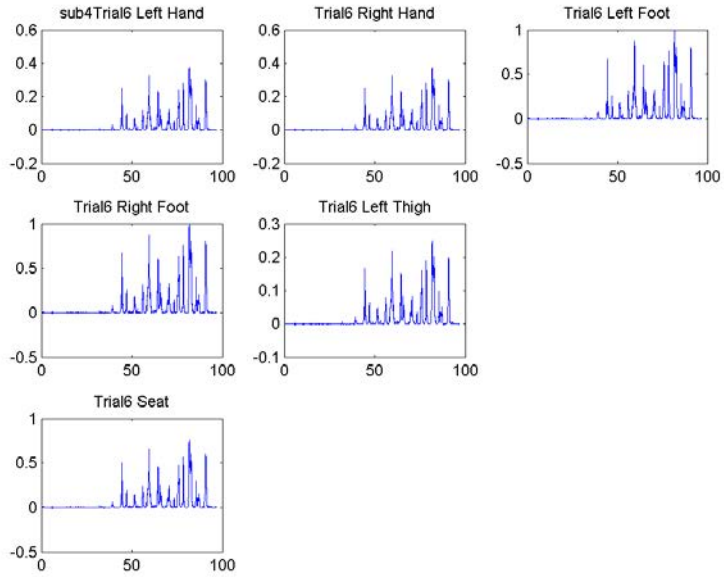


Figure B. 24: Force plots normalized for the peak force across the entire trial and all force sensing areas.

Subject 5

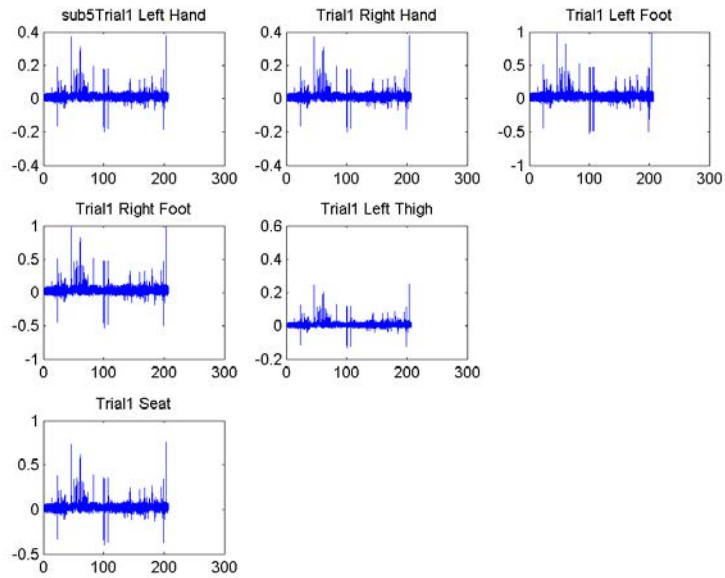


Figure B. 25: Force plots normalized for the peak force across the entire trial and all force sensing areas.

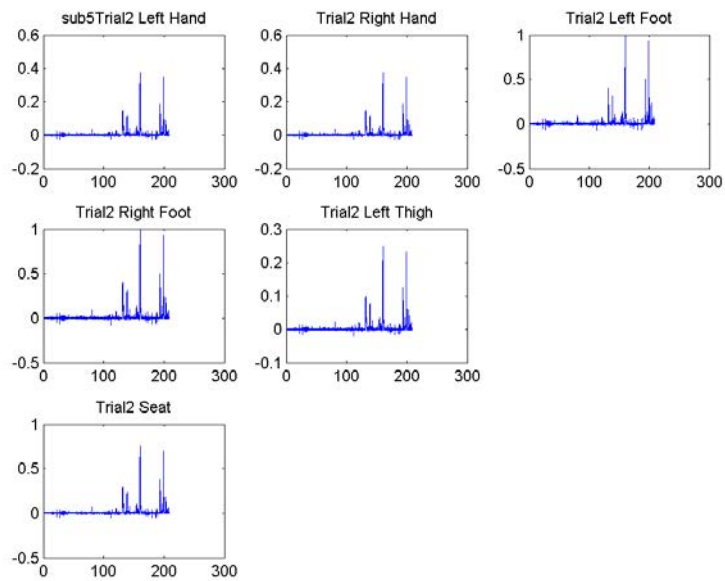


Figure B. 26: Force plots normalized for the peak force across the entire trial and all force sensing areas.



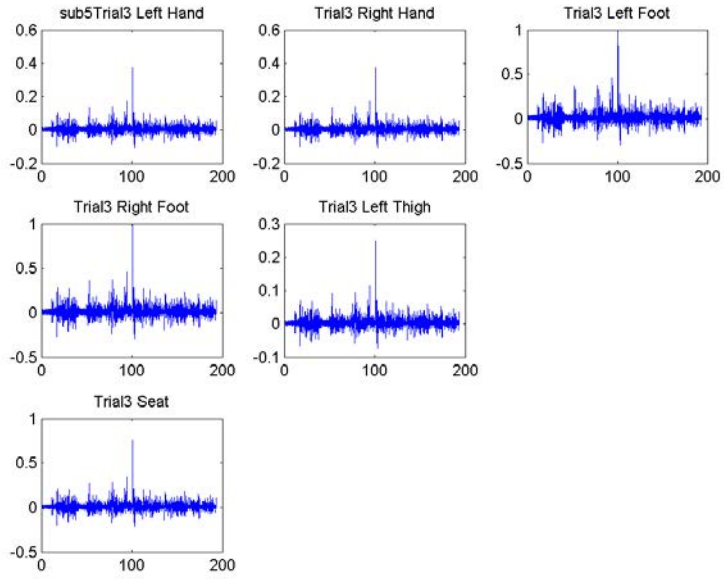


Figure B. 27: Force plots normalized for the peak force across the entire trial and all force sensing areas.

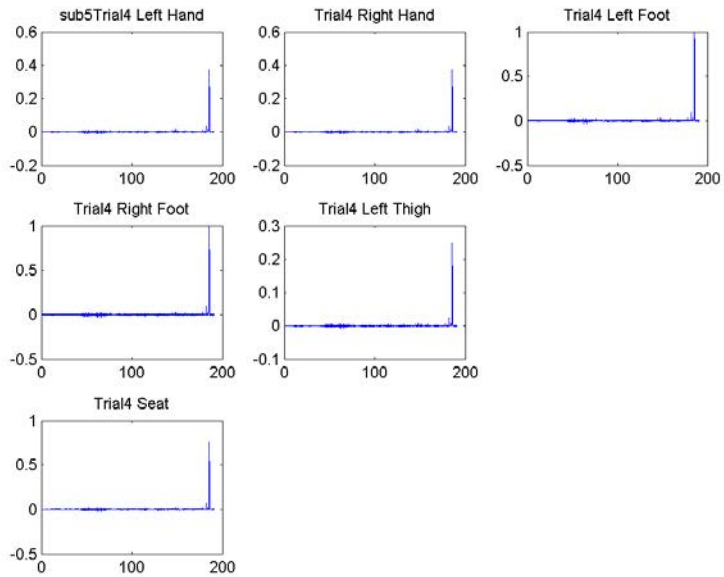


Figure B. 28: Force plots normalized for the peak force across the entire trial and all force sensing areas.

Subject 6

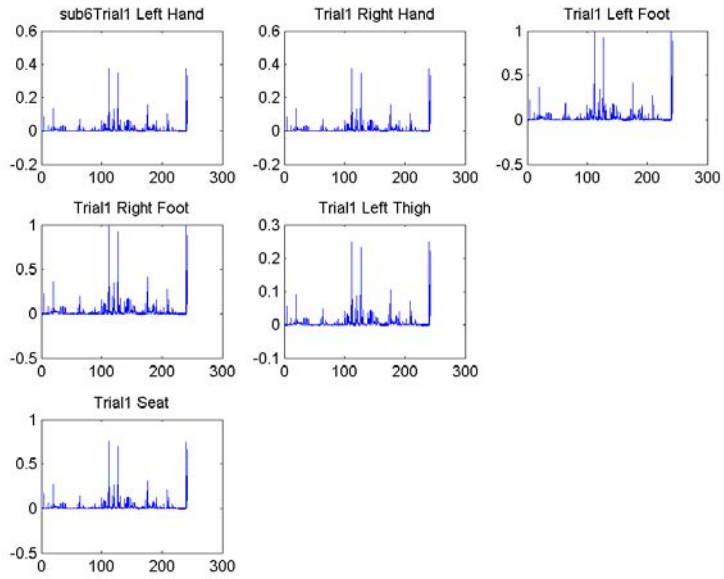


Figure B. 29: Force plots normalized for the peak force across the entire trial and all force sensing areas.

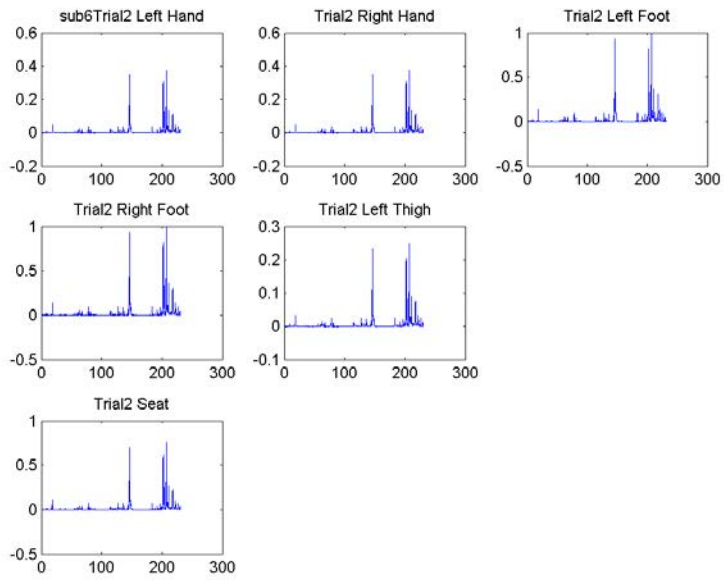


Figure B. 30: Force plots normalized for the peak force across the entire trial and all force sensing areas.

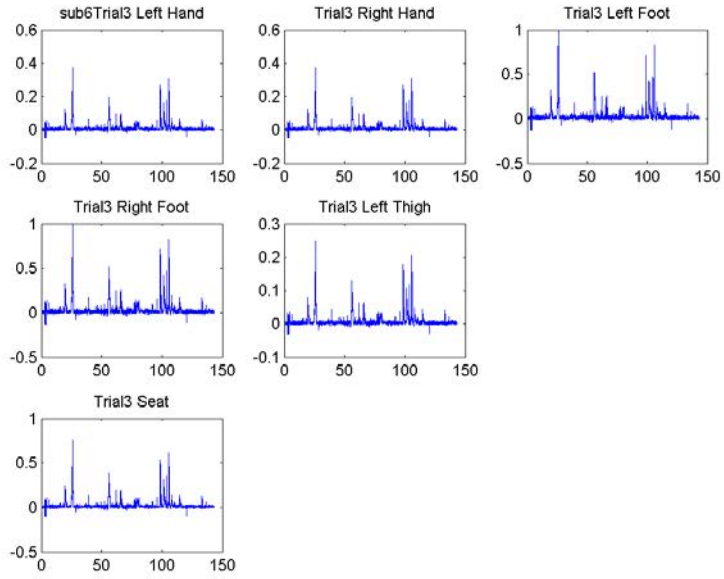


Figure B. 31: Force plots normalized for the peak force across the entire trial and all force sensing areas.

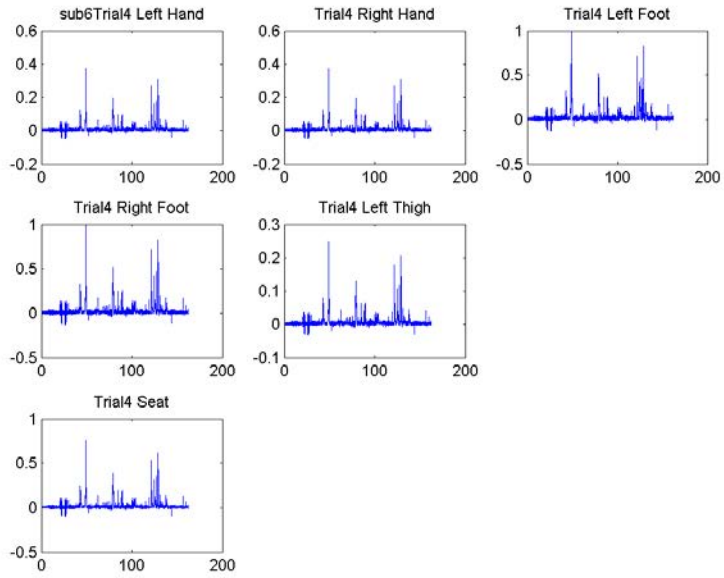


Figure B. 32: Force plots normalized for the peak force across the entire trial and all force sensing areas.

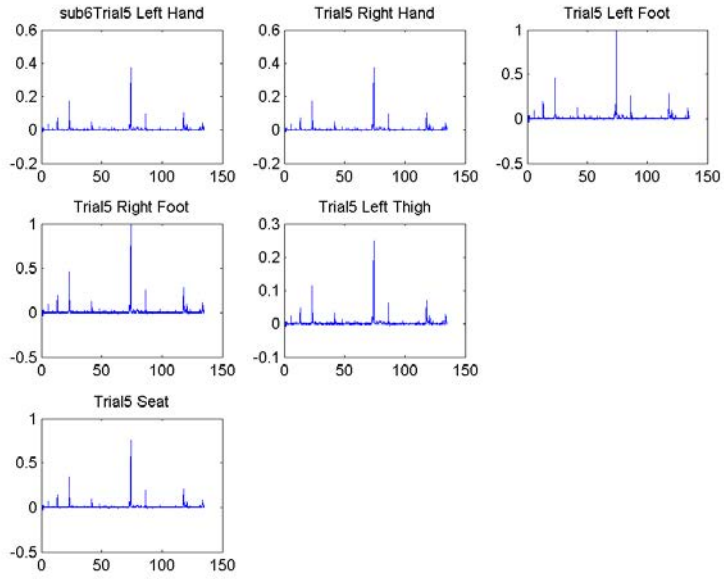


Figure B. 33: Force plots normalized for the peak force across the entire trial and all force sensing areas.

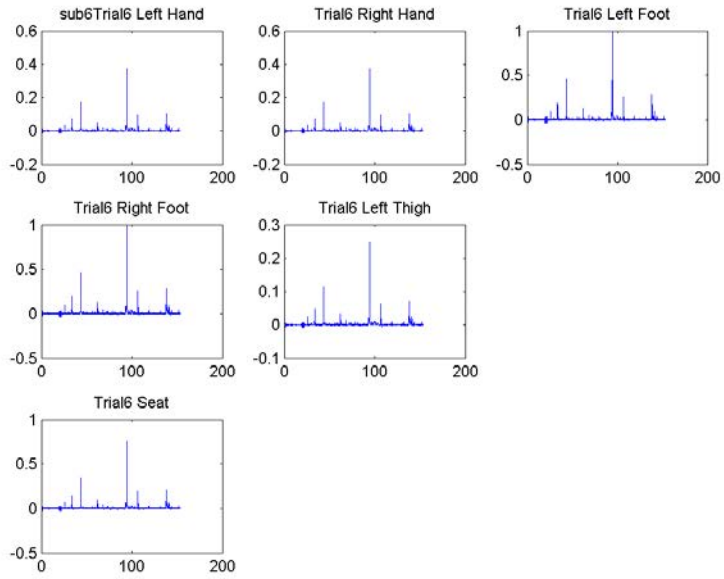


Figure B. 34: Force plots normalized for the peak force across the entire trial and all force sensing areas.

## Appendix C: Trial Time Series Acceleration Data

### Subject 2

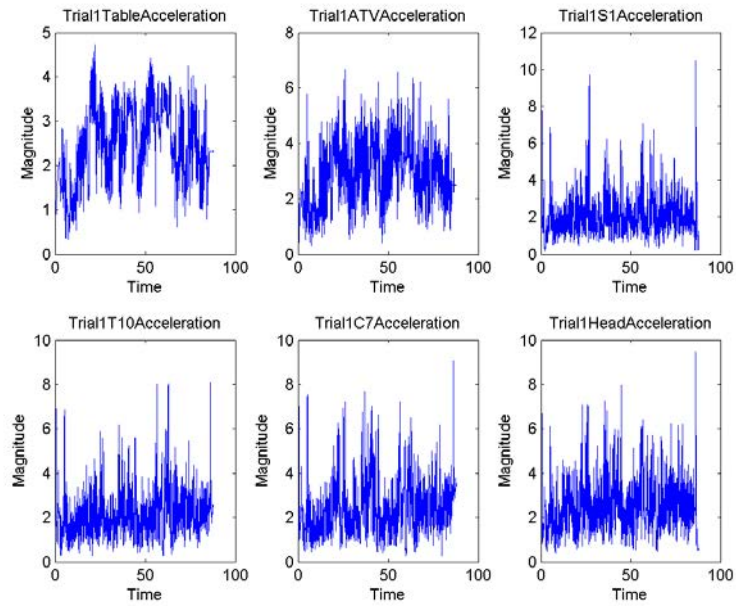


Figure C. 1: Subject 2 Acceleration time series for all sensor locations. Note that Y-axes may vary based on acceleration range.

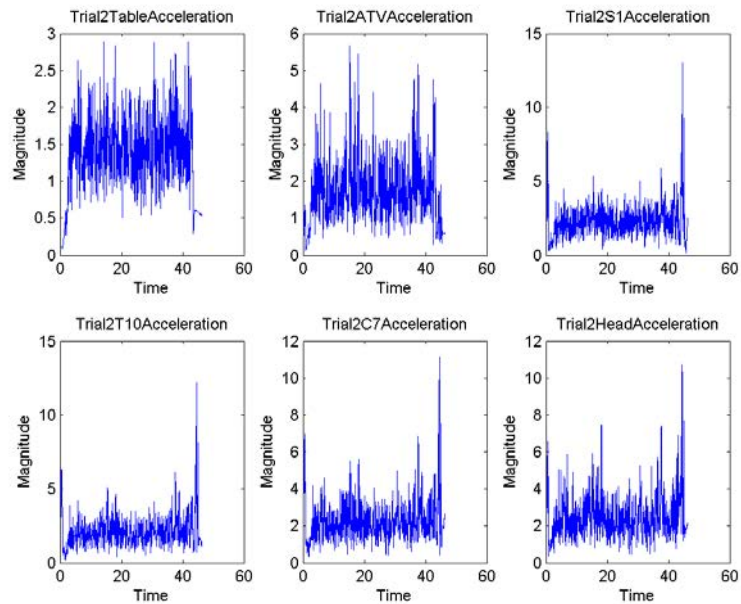


Figure C. 2: Subject 2 Acceleration time series for all sensor locations. Note that Y-axes may vary based on acceleration range.

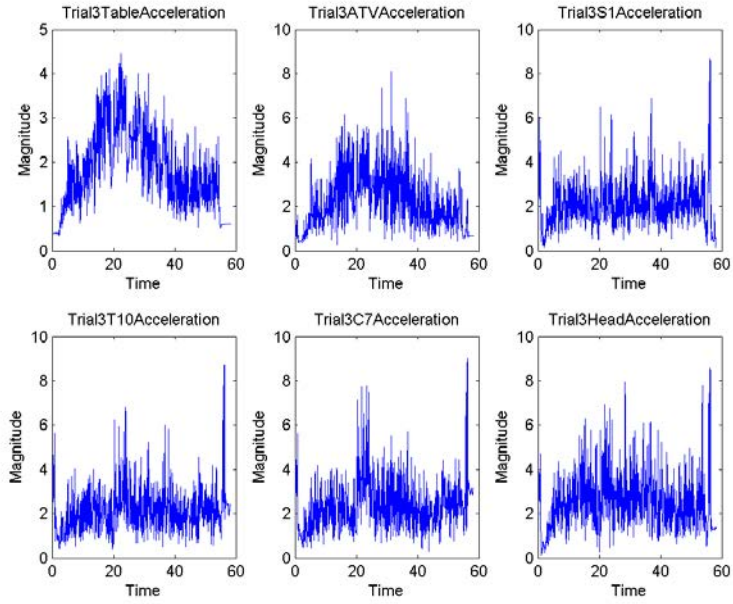


Figure C. 3: Subject 2 Acceleration time series for all sensor locations. Note that Y-axes may vary based on acceleration range.

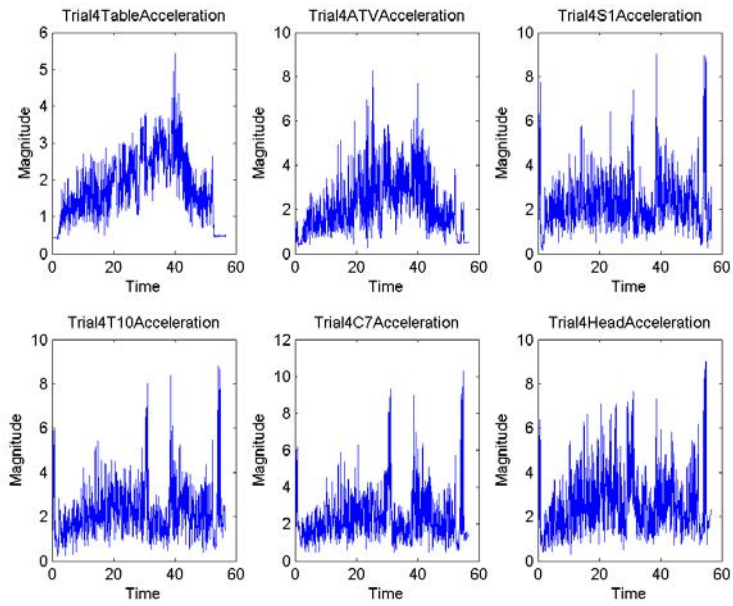


Figure C. 4: Subject 2 Acceleration time series for all sensor locations. Note that Y-axes may vary based on acceleration range.

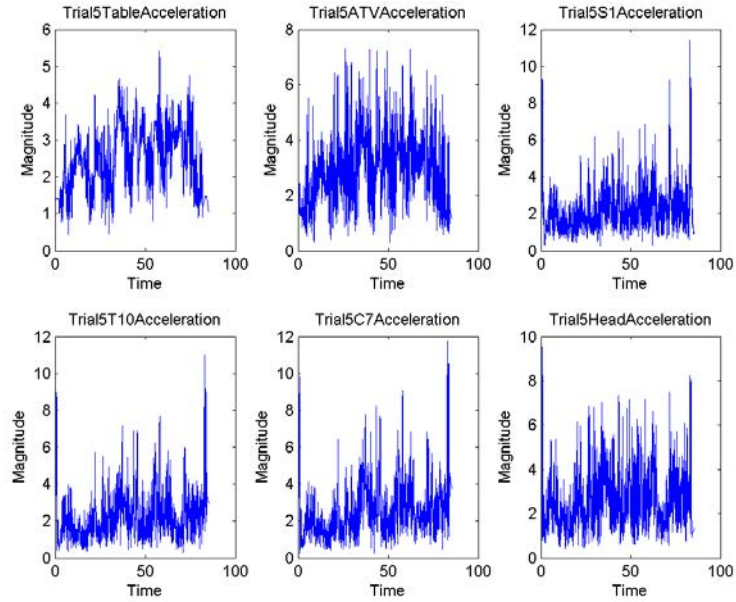


Figure C. 5: Subject 2 Acceleration time series for all sensor locations. Note that Y-axes may vary based on acceleration range.

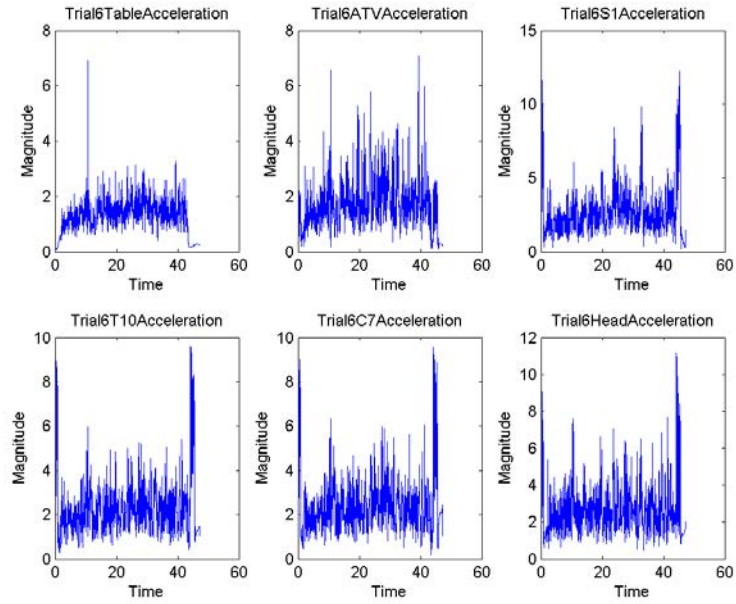


Figure C. 6: Subject 2 Acceleration time series for all sensor locations. Note that Y-axes may vary based on acceleration range.



Subject 3

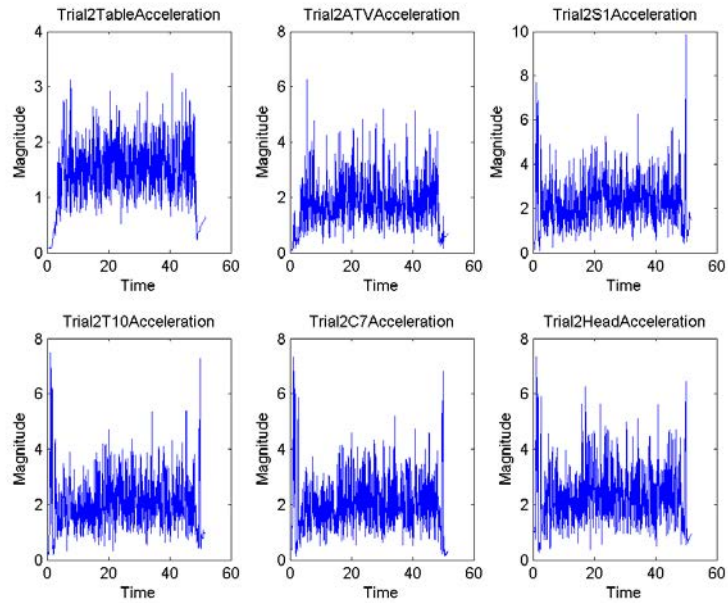


Figure C. 7: Subject 3 Acceleration time series for all sensor locations. Note that Y-axes may vary based on acceleration range.

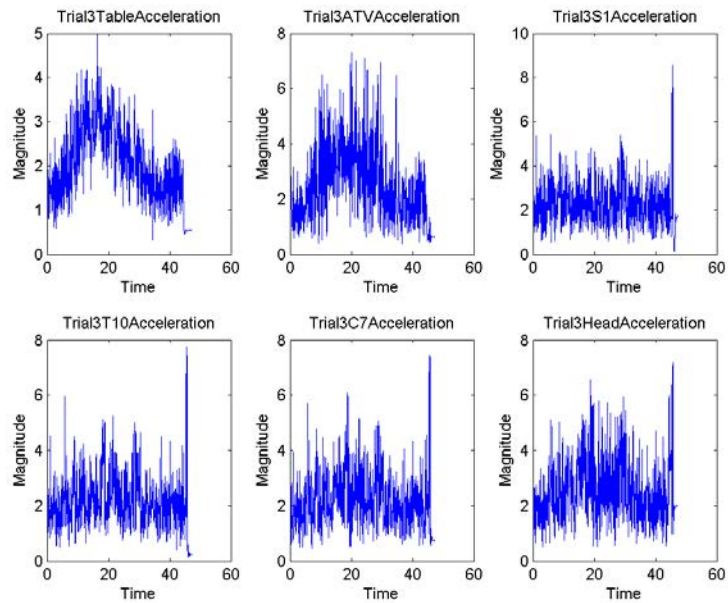


Figure C. 8: Subject 3 Acceleration time series for all sensor locations. Note that Y-axes may vary based on acceleration range.



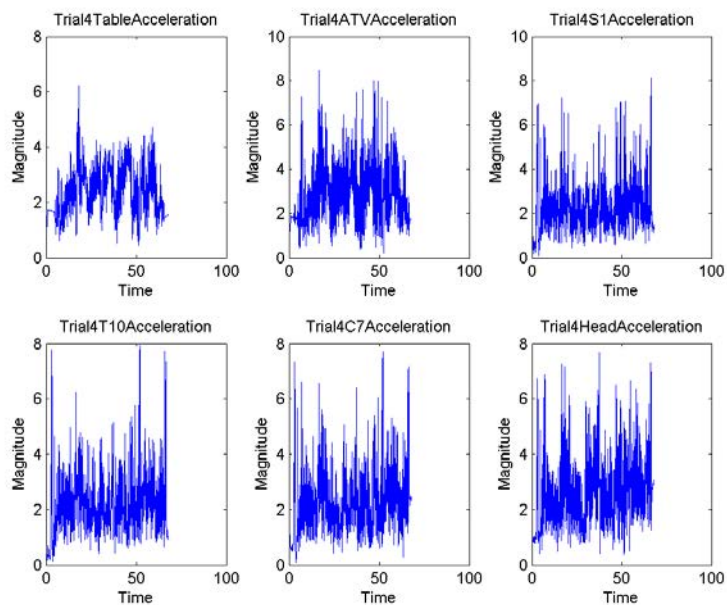


Figure C. 9: Subject 3 Acceleration time series for all sensor locations. Note that Y-axes may vary based on acceleration range.

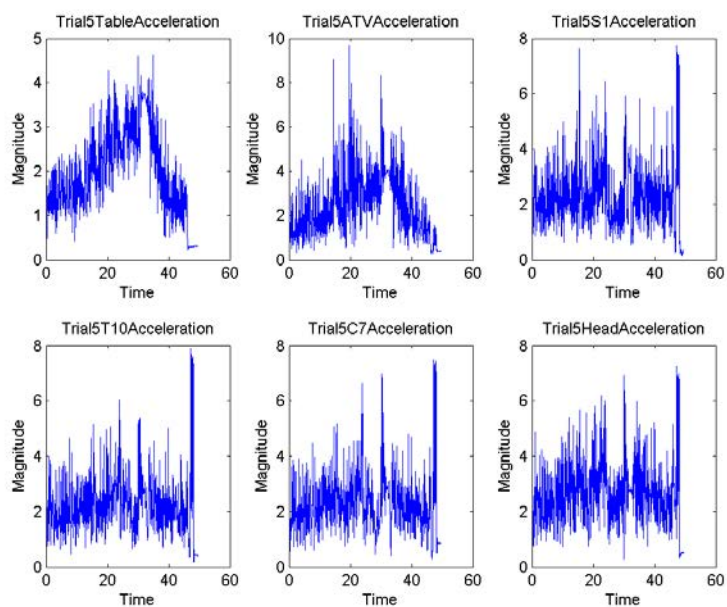


Figure C. 10: Subject 3 Acceleration time series for all sensor locations. Note that Y-axes may vary based on acceleration range.

## Subject 4

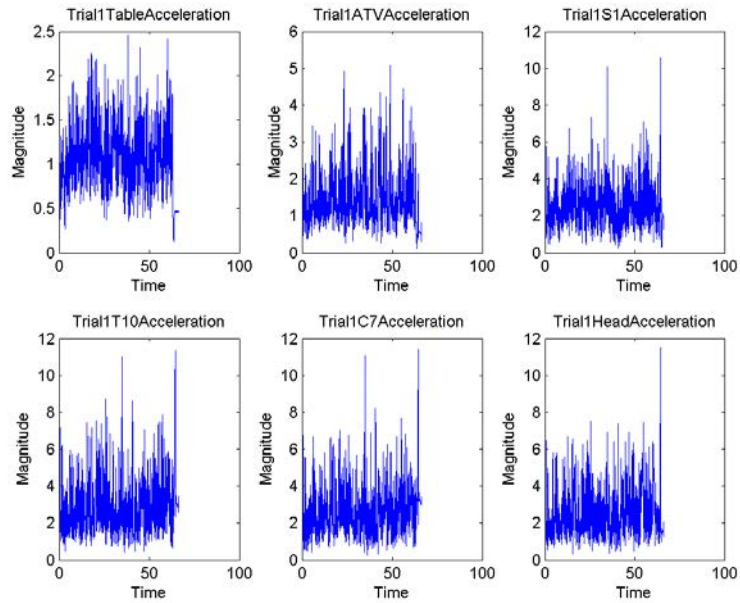


Figure C. 11: Subject 4 Acceleration time series for all sensor locations. Note that Y-axes may vary based on acceleration range.

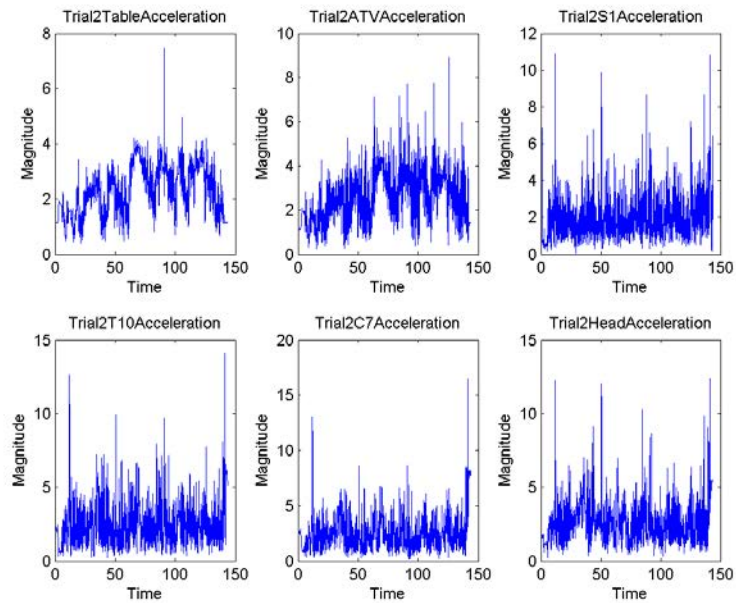


Figure C. 12: Subject 4 Acceleration time series for all sensor locations. Note that Y-axes may vary based on acceleration range.

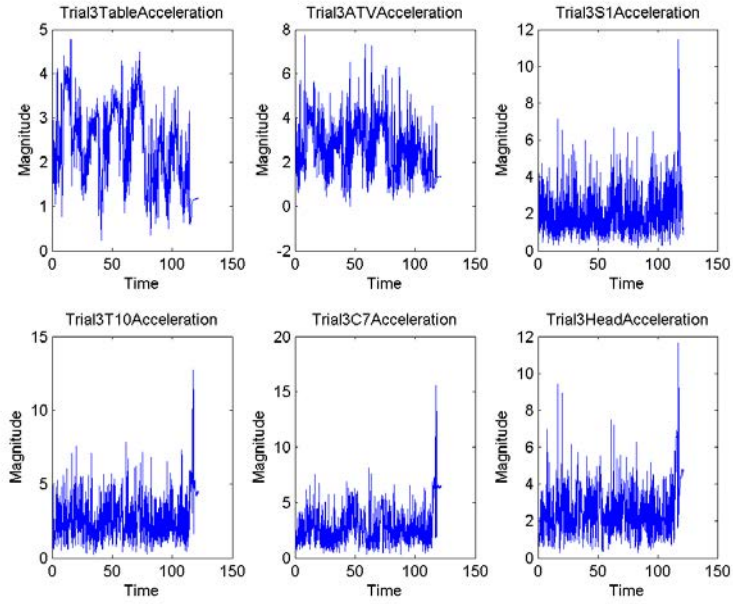


Figure C. 13: Subject 4 Acceleration time series for all sensor locations. Note that Y-axes may vary based on acceleration range.

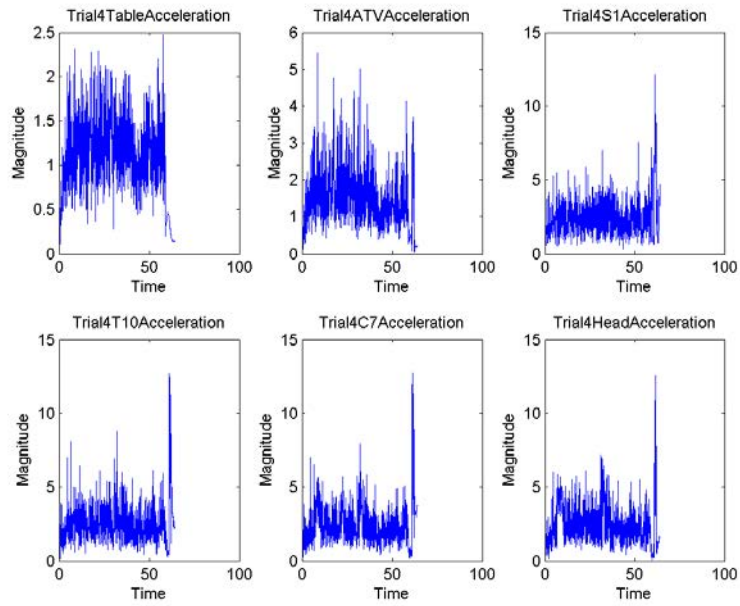


Figure C. 14: Subject 4 Acceleration time series for all sensor locations. Note that Y-axes may vary based on acceleration range.

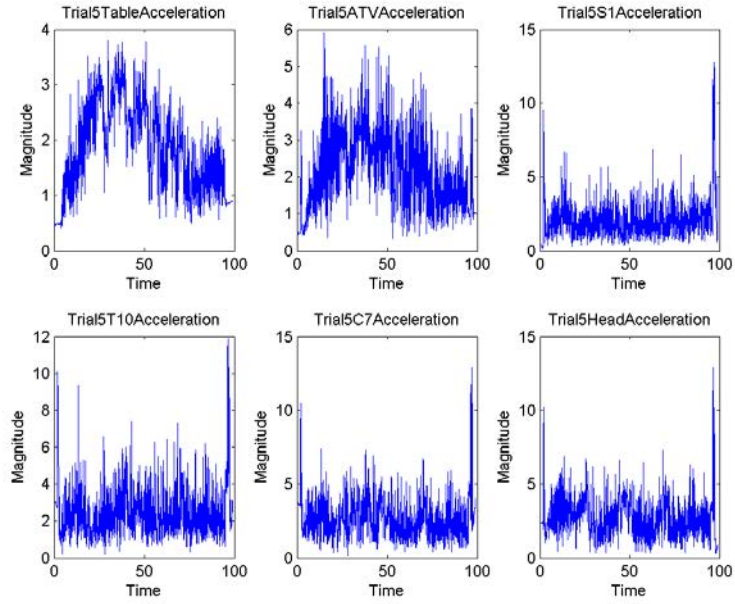


Figure C. 15: Subject 4 Acceleration time series for all sensor locations. Note that Y-axes may vary based on acceleration range.

### Subject 5

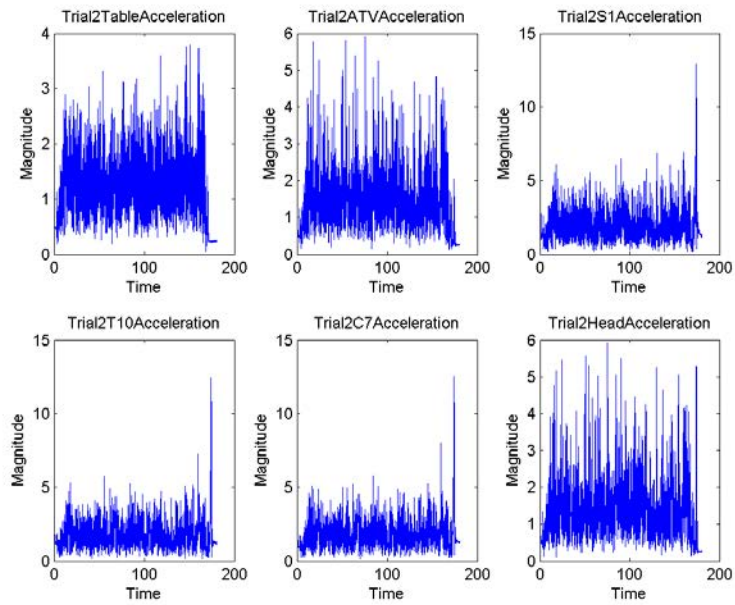


Figure C. 16: Subject 5 Acceleration time series for all sensor locations. Note that Y-axes may vary based on acceleration range.

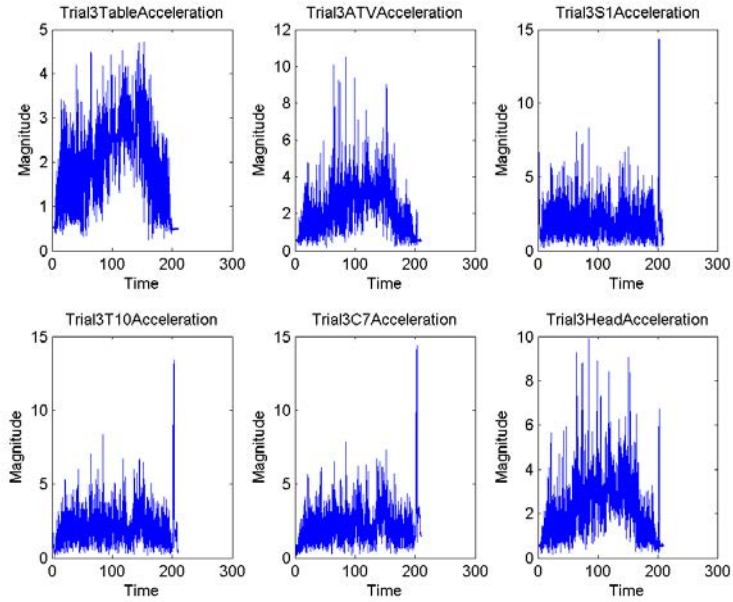


Figure C. 17: Subject 5 Acceleration time series for all sensor locations. Note that Y-axes may vary based on acceleration range.

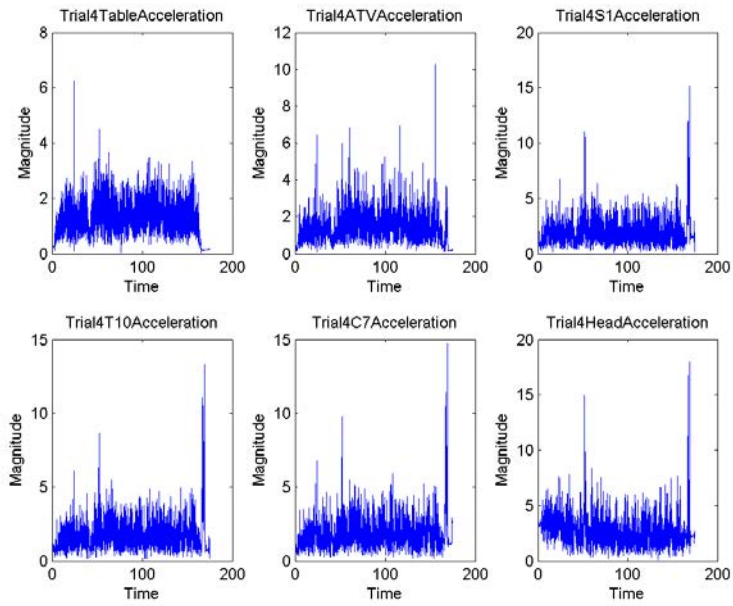


Figure C. 18: Subject 5 Acceleration time series for all sensor locations. Note that Y-axes may vary based on acceleration range.



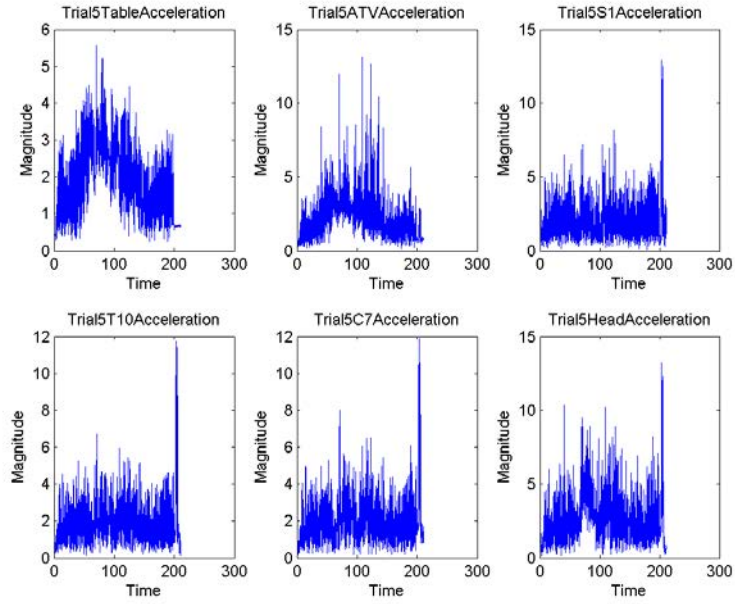


Figure C. 19: Subject 5 Acceleration time series for all sensor locations. Note that Y-axes may vary based on acceleration range.

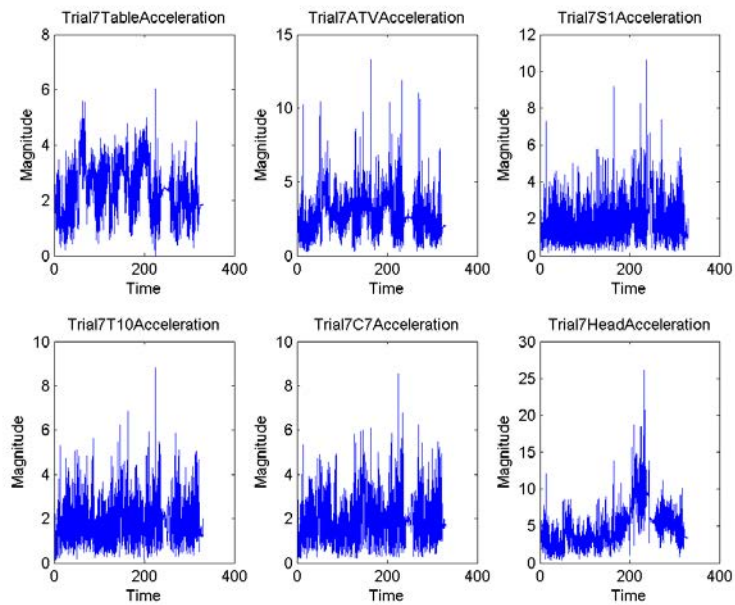


Figure C. 20: Subject 7 Acceleration time series for all sensor locations. Note that Y-axes may vary based on acceleration range.

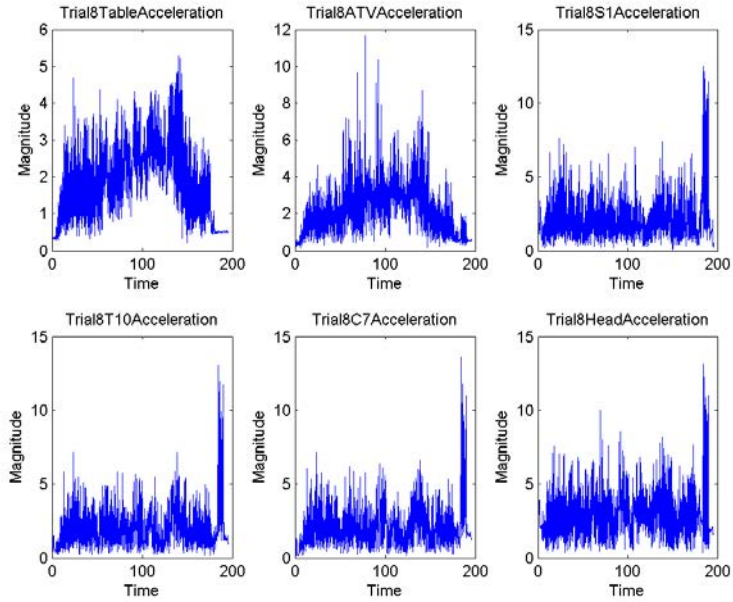


Figure C. 21: Subject 5 Acceleration time series for all sensor locations. Note that Y-axes may vary based on acceleration range.

Subject 6

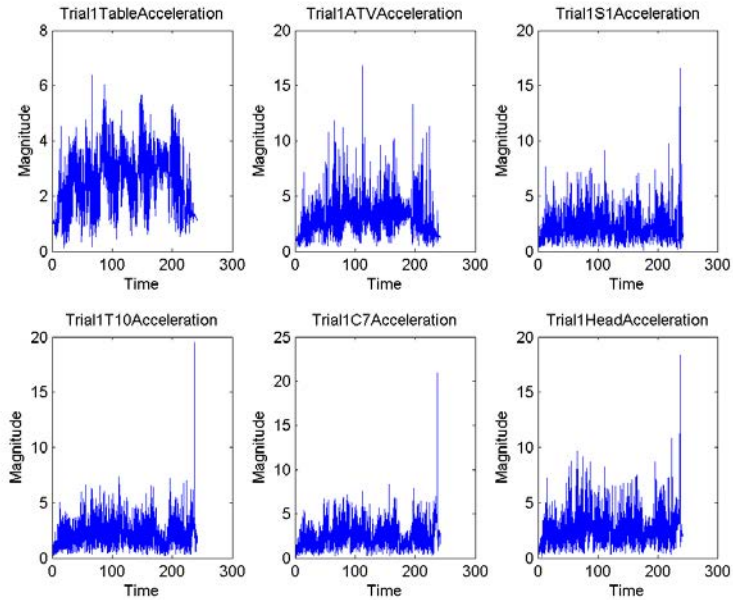


Figure C. 22: Subject 6 Acceleration time series for all sensor locations. Note that Y-axes may vary based on acceleration range.

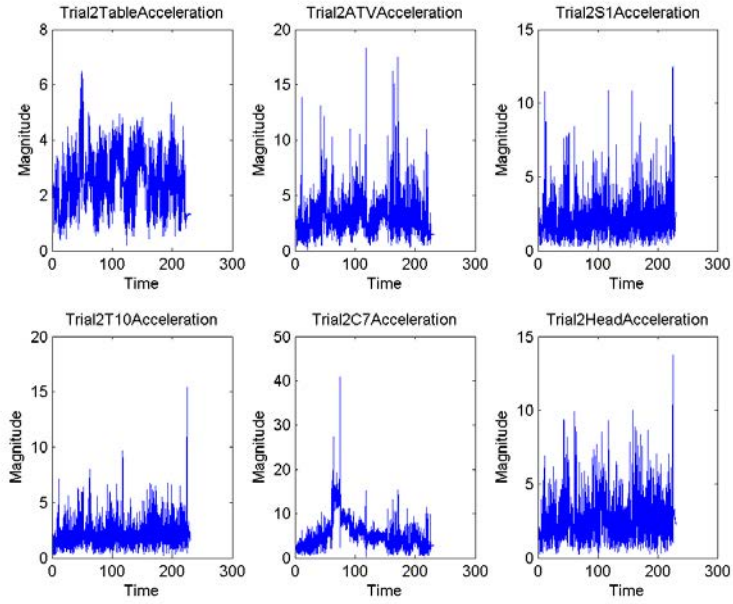


Figure C. 23: Subject 6 Acceleration time series for all sensor locations. Note that Y-axes may vary based on acceleration range.

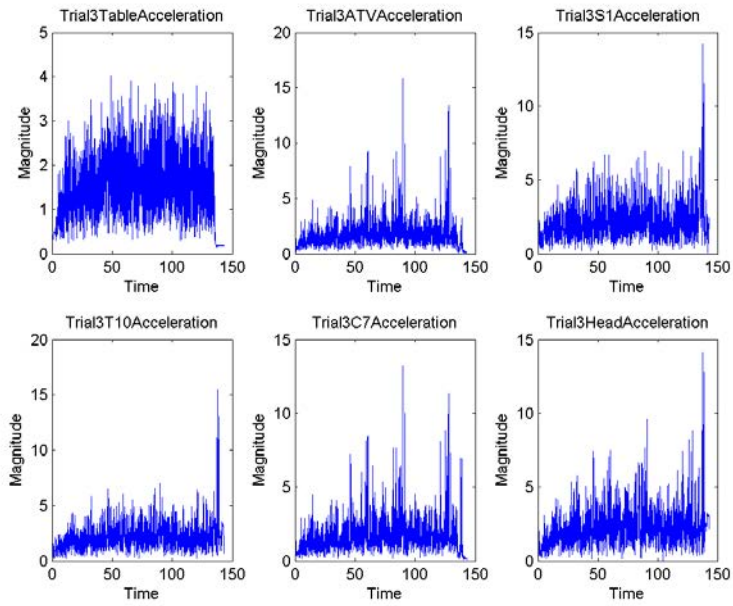


Figure C. 24: Subject 6 Acceleration time series for all sensor locations. Note that Y-axes may vary based on acceleration range.



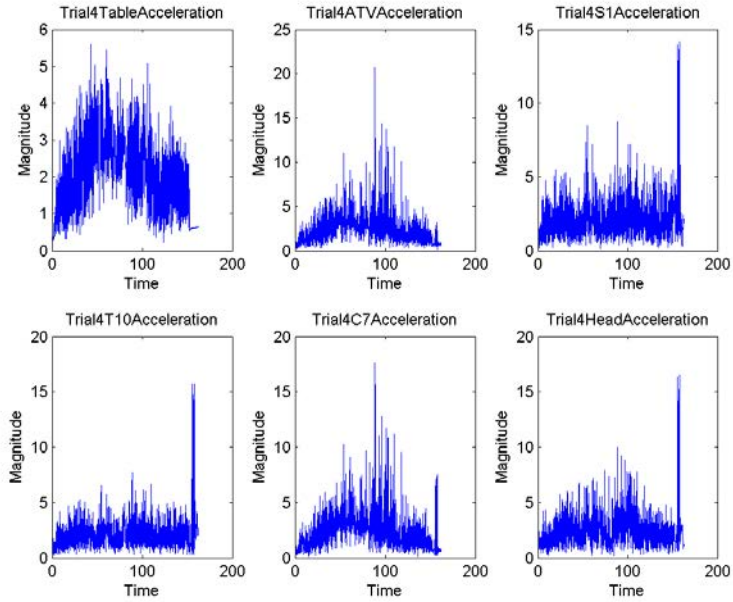


Figure C. 25: Subject 6 Acceleration time series for all sensor locations. Note that Y-axes may vary based on acceleration range.

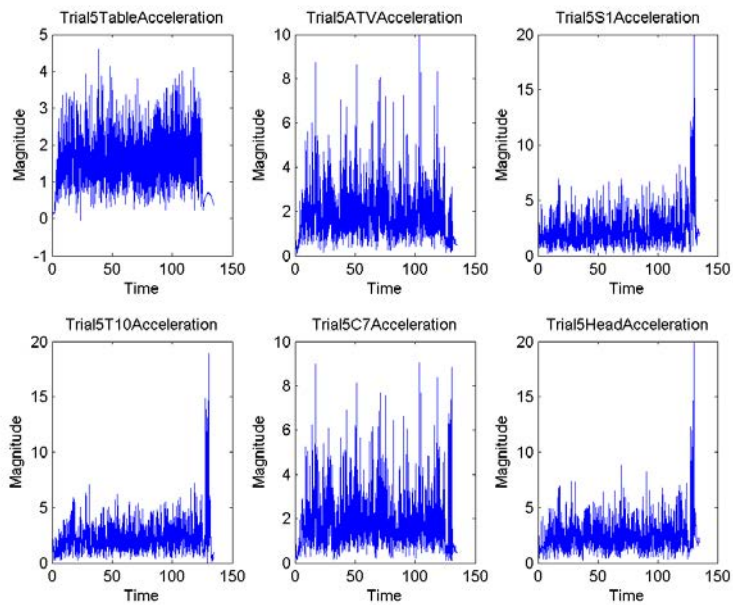


Figure C. 26: Subject 6 Acceleration time series for all sensor locations. Note that Y-axes may vary based on acceleration range.

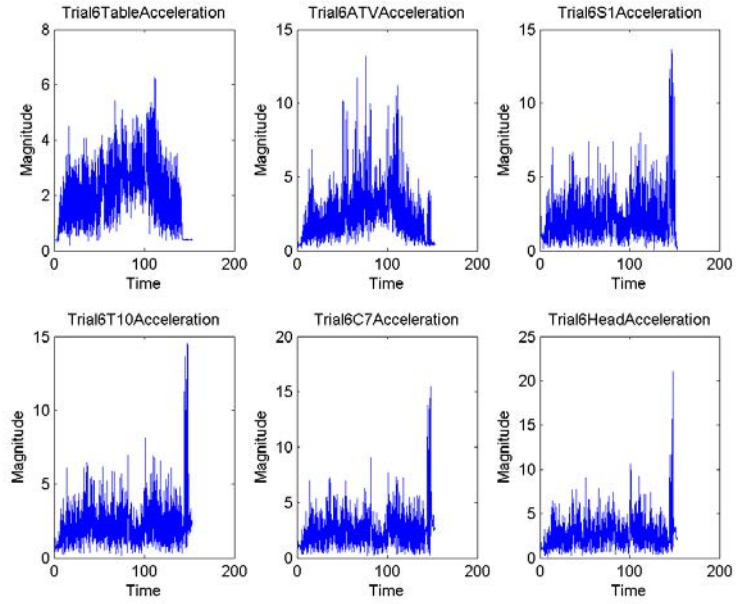


Figure C. 27: Subject 6 Acceleration time series for all sensor locations. Note that Y-axes may vary based on acceleration range.

## Appendix D: Wellness Survey

### WELLNESS SURVEY

#### Directions:

Circle one option for each symptom to indicate whether that symptom applies to you right now.

1. General Discomfort..... None..... Slight..... Moderate..... Severe
2. Fatigue ..... None..... Slight..... Moderate..... Severe
3. Headache ..... None..... Slight..... Moderate..... Severe
4. Eye Strain ..... None..... Slight..... Moderate..... Severe
5. Difficulty Focusing ..... None..... Slight..... Moderate..... Severe
6. Salivation Increased ..... None..... Slight..... Moderate..... Severe
7. Sweating ..... None..... Slight..... Moderate..... Severe
8. Nausea ..... None..... Slight..... Moderate..... Severe
9. Difficulty Concentrating ..... None..... Slight..... Moderate..... Severe
10. \*"Fullness of the Head" ..... None..... Slight..... Moderate..... Severe
11. Blurred Vision ..... None..... Slight..... Moderate..... Severe
12. Dizziness with Eyes Open ..... None..... Slight..... Moderate..... Severe
13. Dizziness with Eyes Closed ... None..... Slight..... Moderate..... Severe
14. \*\*Vertigo .....None..... Slight..... Moderate..... Severe
15. \*\*\*Stomach Awareness .....None..... Slight..... Moderate..... Severe
16. Burping.....None..... Slight..... Moderate..... Severe
17. Vomiting.....None..... Slight..... Moderate..... Severe
18. Other \_\_\_\_\_ .. None..... Slight..... Moderate.....Severe

\* Fullness of the head is an awareness of pressure in the head.

\*\*Vertigo is experienced as loss of orientation with respect to vertical upright.

\*\*\*Stomach awareness is a feeling of discomfort which is just short of nausea

## Appendix E: List of Motion Capture Markers

<b>Motion Capture Marker Locations</b>
<b>Left Shoulder</b>
<b>Right Shoulder</b>
<b>Left Upper Arm</b>
<b>Right Upper Arm</b>
<b>Left Elbow</b>
<b>Right Elbow</b>
<b>Left Lateral Wrist</b>
<b>Left Medial Wrist</b>
<b>Right Lateral Wrist</b>
<b>Right Medial Wrist</b>
<b>Left Hand</b>
<b>Right Hand</b>
<b>Left Clavicle</b>
<b>Right Clavicle</b>
<b>Sternum</b>
<b>Left Posterior Hip</b>
<b>Right Posterior Hip</b>
<b>Left Anterior Hip</b>
<b>Right Anterior Hip</b>
<b>S5</b>
<b>L5</b>
<b>T12</b>
<b>C7</b>
<b>Right Head</b>
<b>Back Head</b>
<b>Top Head</b>

*Table E. 1: Motion Capture Marker Locations. Reflective motion capture markers were attached to landmark locations in order to capture posture and joint angles.*